DISSERTATION

SURFACE AND ANALYTE CAPTURE ANALYSIS OF DNA MICROARRAYS ON MODEL GOLD SURFACES AND COMMERCIAL MICROARRAY SLIDES

Submitted by

Ping Gong

Department of Chemistry

In partial fulfillment of the requirements

For the Degree of Doctor of Philosophy

Colorado State University

Fort Collins, Colorado

Spring 2006

COLORADO STATE UNIVERSITY

February 9, 2006

WE HEREBY RECOMMEND THAT THE DISSERTATION PREPARED UNDER OUR SUPERVISION BY PING GONG ENTITLED SURFACE AND ANALYTE CAPTURE ANALYSIS OF DNA MICROARRAYS ON MODEL GOLD SURFACES AND COMMERCIAL MICROARRAY SLIDES BE ACCEPTED AS FULFILLING IN PART REQUIREMENTS FOR THE DEGREE OF DOCTOR OF PHILOSOPHY.

Committee on Graduate Work

Alan K. Van Orden

Tomislav Rovis

Anthony K. Rappe

Karolin Luger

David W. Grainger/Advisor

Anthony K. Rappe/Department Head/Director

ABSTRACT OF DISSERTATION

SURFACE AND ANALYTE CAPTURE ANALYSIS OF DNA MICROARRAYS ON MODEL GOLD SURFACES AND COMMERCIAL MICROARRAY SLIDES

Nucleic acid microarrays represent a powerful assay tool for large-scale parallel analysis of genome sequences and gene expression in biological and biomedical research. This would imply that DNA microarray assay results are quantitative and reproducible. However, numerous challenges preclude microarray reliability, sensitivity, specificity, direct assay from complex milieu, and direct abundance quantitation required for accurate clinical performance.

The objective of this dissertation research is to provide new insight into the surface chemistry influences on DNA probe environments that affect the efficiency of target capture from solution in order to improve microarray assay performance. To this end, this study is focused on DNA surface and analyte capture analysis of (1) model surfaces with mixed thiol-DNA/mercaptoundecanol (MCU) adlayers on gold, and (2) DNA microarrays on commercial amine-reactive microarraying polymer slides (CodeLink™ and OptArray™). Assay surface reliability, DNA density, hybridization efficiency, and influence of complex milieu (serum dilutions, cell lysate) on hybridization were assessed using X-ray photoelectron spectroscopy (XPS), surface plasmon resonance (SPR), as well as more traditional biological and microarray analysis techniques such as radiometric assay and fluorescence intensity measurements.

Immobilization efficiencies of DNA probes on commercial slides under microarray formats were reproduced using high ionic strength and increased DNA concentrations in macroscopic dimensions to permit analysis with highly sensitive, quantitative surface analytical techniques (e.g., XPS) that are currently incompatible with microarray dimensions. Surface densities of immobilized DNA probes ($2x10^{11}$ ~ $4.4x10^{13}$ probes cm^2) and hybridized DNA targets (and $2x10^{11}$ ~ $8.9x10^{12}$ targets/cm^2) on gold and commercial slides were quantified using sensitive ^{32}P-DNA radiometric measurements. Optimum target hybridization occurred at intermediate probe densities with more upright probe orientation. The more sensitive radiometric results were calibrated with more routine XPS and fluorescence intensity measurements to facilitate future routine DNA density determinations without the use of hazardous radioactive assay. Furthermore, influences of complex milieu and fluorescence dye labels on microarray DNA hybridization were investigated. Serum protein adsorption onto SPR sensor surfaces were found to significantly affect the SPR curve shape, impeding hybridization detection beyond 30% serum, while only minimal effect from complex milieu was observed on the commercial microarray slides.

Ping Gong
Chemistry Department
Colorado State University
Fort Collins, CO 80523
Spring 2006

ACKNOWLEDGEMENTS

I would like to express my sincere gratitude to Prof. David Grainger, my advisor and mentor, without whose guidance, patience and encouragement this work would not have been possible.

I thank Chi-Ying Lee, Dr. Lara Gamble and Prof. David Castner for their enormous collaboration efforts into the DNA/gold model study. Drs. Chad Greef, Mike Lochhead and others at Accelr8 Technology Corporation are greatly appreciated for their generous technical assistance in the microarray experiments. Drs. Anthony Rappe, Tomislav Rovis, Alan Van Orden and Karolin Luger are acknowledged for reviewing and commenting on this dissertation.

My hearty thanks also go out to members of the Grainger research group, Peng Wu, Jim Christie, Marisha Godek, Greg Harbers, Lisa Chamberlain and everybody else who has made this journey through graduate school more enjoyable.

DEDICATION

This dissertation is dedicated to my parents, Jiashu Duan and Wenyan Gong, who have always given me love and support, and let me freely choose my path. Without their encouragement and unfadeable faith in me, I could not have accomplished this.

TABLE OF CONTENTS

Chapter 1 Introduction

This dissertation is written in the "journals-format" style. It is based on two review book chapters (Chapter 2), three journal publications (Chapter 3-5) and two journal manuscripts in preparation (Chapters 6 and 7), each written in a format set by the American Chemical Society. A brief overview of each chapter is presented below.

Chapter 2 is a review of the DNA microarray technology[1,2]: its format, surface fouling considerations as a biomedical diagnostic assay tool, material and analytical chemistry issues involved, and finally analytical methods that have been directed at understanding DNA microarrays. This chapter also introduces the aims of this doctoral research and proposes a set of complementary bioanalytical experiments.

Chapter 3 describes the surface characterization and real time complex milieu hybridization performance of DNA/mercaptoundecanol mixed adlayers formed on gold.[3,4] These adlayers on gold, being compatible with a variety of surface analytical techniques, serve as a model system for better investigating and understanding DNA hybridization at molecular level, and later for comparison with commercial microarraying platforms.

Chapter 4 presents work discussing the reactivity loss of commercial microarray slides over time and a simple regeneration method to solve this problem for improved slide reliability.[5] Maximum slide reactivity is ensured through this regeneration process,

providing a more consistent substrate for DNA probe immobilization as a first step in DNA microarray fabrication and application.

Chapter 5 describes the quantification of surface immobilized microarray DNA probe and hybridized DNA target densities on commercial slides by corroborating three independent surface analytical techniques: fluorescence intensity measurements, XPS and ^{32}P-radiometric assay.[6] Sensitive ^{32}P-DNA radiometric measurements are calibrated with more routine XPS DNA signals, facilitating future routine DNA density determinations without the use of hazardous radioactive assay.

Chapter 6 describes the preliminary research of microarray complex milieu hybridization performance on commercial slides and proposes future work required to complete this complex milieu hybridization study.

Chapter 7 examines the quenching and steric influences of fluorescent cyanine dye labels on microarray DNA hybridization signals.

The objective of this dissertation research is to provide new insight into the surface chemistry influences on DNA probe environments that affect the efficiency of target capture from solution in order to improve microarray assay performance. More specifically, how microarray DNA hybridization is affected by the surface immobilized DNA probe density and orientation, as well as the presence of exotic fluorescent dye labels and complex milieu constituents.

(1) Gong, P.; Grainger, D. W. In *Microarrays: Methods and Protocols (Method in Molecular Biology),* 2nd ed.; Rampal, J. B., Ed.; Humana Press: Totowa, New Jersey, 2006, in press.

(2) Grainger, D. W.; Greef, C. H.; Gong, P.; Lochhead, M. J. In *Microarrays: Methods and Protocols (Method in Molecular Biology),* 2nd ed.; Rampal, J. B., Ed.; Humana Press: Totowa, New Jersey, 2006, in press.

(3) Lee, C.-Y.; Gong, P.; Harbers, G. M.; Grainger, D. W.; Castner, D. G.; Gamble, L. J. *Anal. Chem.* **2006**, *in press*.

(4) Gong, P.; Lee, C.-Y.; Gamble, L. J.; Castner, D. G.; Grainger, D. W. *Anal. Chem.* **2006**, *in press*.

(5) Gong, P.; Grainger, D. W. *Surf. Sci.* **2004**, *570*, 67-77.

(6) Gong, P.; Harbers, G. M.; Grainger, D. W. *Anal. Chem.* **2006**, *in press*.

Chapter 2 A Review of DNA Microarrays: Current Performance, Technical Consideration and Analytical Assessment

This dissertation chapter contains sections from two book chapters in "Microarrays: Methods and Protocols (Methods in Molecular Biology)", Humana Press, 2006 (in press). The chapter titled "Non-Fouling Surfaces: A Review of Principles and Applications for Microarray Capture Assay Designs"[1] was written by Ping Gong and edited by David W. Grainger. The chapter titled "Current Microarray Surface Chemistries"[2] was written by Mike Lochhead and contains sectional contribution from Ping Gong, David Grainger and Chad Greef.

This dissertation chapter is divided into four sections. Section 2.1 provides a brief introduction of the DNA microarray technology, its format, current challenges and potential improvements. Section 2.2 reviews surface fouling considerations in general biomedical diagnostic assays. Materials and analytical chemistry issues involved in DNA microarrays, particularly those that have been reported in the public domain, are systematically reviewed in Section 2.3. Section 2.4 describes analytical methods that have been directed at understanding DNA microarray, the aims of this doctoral research and a set of proposed bioanalytical studies to be performed.

2.1 Introduction to DNA microarrays

2.1.1 DNA microarray format

DNA microarrays are a high-throughput and versatile technology that has promised a revolution in molecular biology.[3-8] By allowing simultaneous analysis of thousands of genes in a massive parallel manner, it provides extensive and valuable information on gene interactions and functions, with potential applications ranging from gene discovery, expression analysis to disease diagnostics and drug discovery. The DNA microarray technique employs the same affinity recognition concept (i.e., complementary binding of two single stranded DNA sequences to form a duplex) as traditional molecular biology methods. While traditional methods are limited to one gene at a time, rendering low throughput and lengthy assay time, microarray technology enables parallel processing of thousands of gene species concurrently by reducing individual assay features to the micron scale (Figure 2.1). This format miniaturization not only

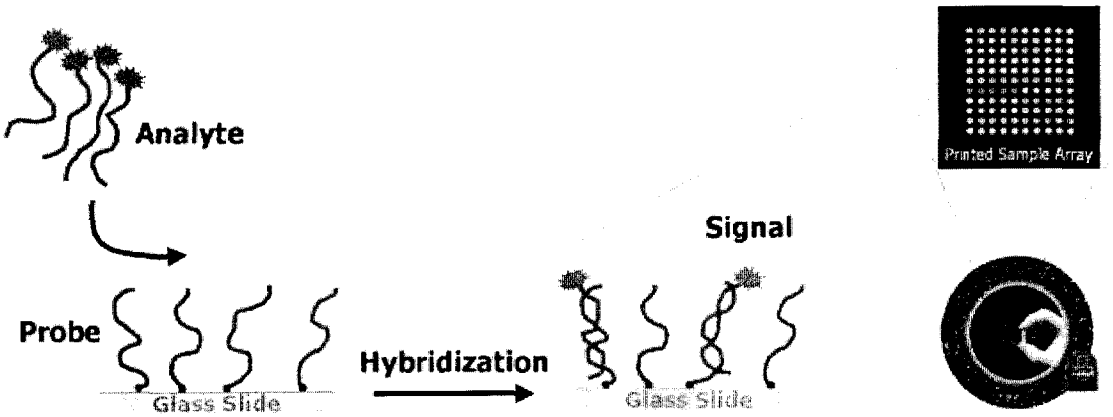

Figure 2.1 DNA microarray at the molecular level

significantly improves assay throughput and reduces sample consumption, but also provides a "whole picture" of gene functions, which was unrealistic to obtain using conventional methods. Additionally, assay miniaturization shows potential in fast kinetics and improved signal-to-noise ratio as proposed in Ekins theory[9,10]. Prospective sensor chip integration with electro/colorimetric sensing components also makes DNA microarrays excellent candidates for point-of-care and field applications.

2.1.2 DNA microarray assay components

A DNA microarray consists of an orderly arrangement of DNA fragments representing the genes of interest (e.g., genes of a certain organism). Each DNA sequence is assigned a specific location on the array, commonly a glass slide, then microscopically spotted to or photolithographically grafted from that location. The primary mission of a DNA microarray is to determine the presence or absence of certain gene species in a biological sample. If the genes of interest are present, it is desirable to determine their abundance in the sample. Furthermore, it is most advantageous if the identity and abundance determination can be performed in field without lengthy and extensive sample pre-treatment.

As schematically shown in Figure 2.2, a complete microarray process starts with

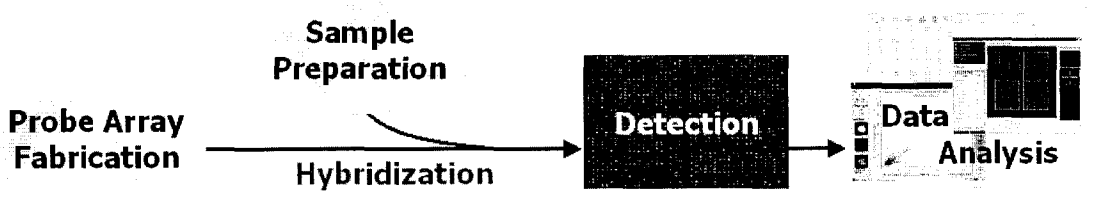

Figure 2.2 Schematic of DNA microarray processing

probe array fabrication in parallel with target analyte sample preparation. The process centers at microarray DNA hybridization, which is followed by data acquisition (detection) and analysis in order to reach end results. Typical probe selection requires probe sequences of low self-complementarity and absence of secondary structure formation. The probe sequences' ability to differentiate a perfect matched target from mismatched target DNAs is essential to the specificity performance of a microarray. Additionally, homogeneity of probe sequences is important to ensure that the probes can bind to target DNAs at the temperature of the experiment. Surface-immobilized DNA probes are expected to demonstrate sufficient spatial freedom to accommodate target approach and binding. For this purpose, end-point covalent attachment of probe DNA is preferred over multi-point attachment and physisorption as a probe tethering method. Target sample pretreatments remain a necessary step in microarray processing at the moment. Current detection limitations require lengthy and expensive sample purification and target amplification as well as target labeling for analyte detection, particularly low abundance gene species. As a result of these pretreatments, e.g., PCR amplification and fluorescent labeling, bias is introduced into the system, making quantitative measurements extremely difficult. The addition of fluorescent or other types of bulky labeling groups also poses potential steric hindrance on DNA duplex formation. Hybridization assay conditions and post hybridization treatments require systematic optimization as they show enormous influence on the results of individual microarray assay experiments. Furthermore, data collected from a DNA microarray experiment, in most cases, is massive. Intelligent statistical analyses are essential to extract useful

information for obtaining meaningful results. Vigilant validation of each assay constituent is crucial to the end performance of the DNA microarray technology.

2.1.3 Current challenges in understanding DNA microarray performance and its potential improvement

Currently, the performance in DNA capture formats (> femtomolar) is woefully below theoretical expectations (<attomolar), particularly in direct assays of complex milieu (e.g., serum, cell lysate). Reasons for such sub-standard performance are unknown. Understandably, methods to improve sensitivity and reliability are largely empirical because very little molecular-level information is reported or known about the chemical, physical or biological fate of full DNA, cDNA or oligo-DNA probes immobilized on any of the diverse set of microarray surfaces. How immobilized DNA surface disposition influences target DNA hybridization efficiency, detection sensitivity, reliability of array data interpretation and assay quantification are correlated empirically. Few systematic studies have been reported.

To date, despite much hyperbole to the contrary, this technology remains primarily a research format, with only one clinical application approved[11], and many unanswered questions regarding specific analytical chemistry issues, including assay repeatability, reproducibility, sensitivity, correlation of signal to sample abundance, and reliability to predict disease conditions.[2,12] The potential of microarray applications and related parallel technologies for gene expression measurements requires more extensive microarray performance validation[12]. Earlier studies have shown poor reproducibility, repeatability and result correlations among different microarray methods, indicating significant challenges for broad application of microarray assays across platforms or

between labs.[13-16] Recent collaborative efforts between microarray laboratories have demonstrated the importance of proper use of microarray technology, stressing the significance of standardizing operating protocols.[17-19] Although not yet optimal, these recent studies have pointed to a much more positive prospect for reliable technology in bioassay and disease diagnosis.

2.2 Fouling consideration for biomedical diagnostic assay devices

2.2.1 Introduction

When it comes to biomedical diagnostic assay devices, performance often relies on deliberate and precise modification of device surface properties attempting to control interfacial behavior with multiple biological components. Typically, two surface properties are sought: (1) selective control of desired surface binding or capture of molecular and cellular species from solution, and (2) elimination of non-specific adsorption or "fouling" of surfaces by any undesired solute. Most often, in complex, "real" biological samples, prevention of non-specific platelet, protein, lipid, cell and bacterial surface attachment (non-specific binding, or NSB) is desired to improve device performance both in vivo and in vitro.[20-23] Surfaces that *eliminate* all non-specific protein adsorption and cell binding are a common desirable endpoint for many diagnostic devices, surgical implants, biological reactors, maritime hardware, and pharmaceutical packaging. Surfaces that *selectively bind* certain desired solutes while resisting other non-specific biological component adsorption are a compelling need for technologies spanning diagnostics, sensors, and tissue-engineered devices. Both performance goals exploit coating chemistries that resist non-specific binding. Additionally, selective surface capture technologies also incorporate biological recognized or synthetically designed

surface-bound ligands with high affinity for desired targets. This is required for many biosensors, diagnostic assays, and for some implant applications where specific interactions are required to improve performance through capture, integration or surface interfacial response. All surface-design approaches require a base surface coating to resist non-specific binding events together with a coupled ability to further tailor specific surface binding interactions with desired solutes. Importantly, surface binding should, in some cases, maintain captured molecule native structure and essential bioactivity (e.g. growth factor immobilization in tissue engineering and enzyme antibody or nucleic acid immobilization in sensing and diagnostics).

Unfortunately, many of these NSB and specific surface performance requirements have not been met to date, providing plenty of opportunity to innovate improved surface performance across many technology bases using surface modification: no surface reliably exhibits either perfect non-fouling or specific capture capabilities to date. Surfaces and coatings comprising only 100% bound ligands at immobilized densities sufficient to cover the entire surface without defects are not yet synthetically realizable. Any uncoated material surface left exposed as well as defects and most ligand chemistries all produce measurable non-specific binding of undesired biological components. Improved performance in sensing and sophisticated diagnostics therefore requires a technological basis in improved surface designs that reliably resist non-specific binding of biological molecules to preclude adverse performance in each context. Diagnostic signal-to-noise frequently depends critically on surface reactivity differences to specific and non-specific surface-milieu interactions. Given that most bioanalytical identification technologies involve exposure of biological or environmental fluids containing trace

analyte with capture surfaces (ELISA, microarrays, beads, chromatography, gels, membrane sorbents), and that these biotechnological assay materials are pervasive with markets exceeding billions of US dollars annually world-wide, examination of the principles driving rational surface design to improve microarray and diagnostic capture surfaces motivates this review section.

2.2.2 Protein adsorption to diagnostic and bioassay surfaces

Most surface-capture bioassays are ideally intended to discriminate target analyte from complex biological milieu (serum, tissue lysate, food, environmental samples). Serum and cell lysates contain thousands of non-target proteins, peptides and interferants; other samples can be equally complex. Hence, a first-priority for assay effectiveness is to implement a surface that effectively avoids non-specific protein adsorption in order to capture analyte. From first principles for designing improved surfaces effective in these technologies, all protein-surface interactions might be considered as two-body problems. Attraction, adsorption and desorption of solutes at surfaces involve complex physical and chemical time- and space-dependent properties of both the solute and the interfacial chemical binding partners. Adsorption of water, ions and small molecule solutes remains a challenging scenario to model and understand.[24,25] Protein adsorption, subject to intensive study[14,26,27], remains a more complex and largely uncontrolled phenomena addressed by largely empirical approaches in most technologies. As protein fouling remains a primary obstacle to performance across many diagnostic applications, improved surfaces that control protein adsorption remain a major research focus. Imposed upon equilibrium protein-surface thermodynamic considerations are more complex non-equilibrium thermodynamics and kinetic factors for competitive surface

affinity, occupancy, displacement, and protein conformational changes. Hence, rational design features for capture surfaces – both chemical and physical interfacial properties that reliably control protein interfacial behavior are not obvious or intuitive, and in fact have proven literally impossible to realize or perfect in most biological applications to date.

(a). The case for diagnostic surface selectivity. In serum, 90% of the proteome mass content comprises albumin, transferrin, haptoglobin and immunoglobulins (totaling ~50 mg/ml), few of which are ever interesting analytes. Typical target protein analytes for clinical diagnostics, proteomics, microarraying and surface capture purposes are low abundance, usually pg/ml or less, embedded within the 80 mg/ml proteome background. Critically, diagnostic or clinical assay signal generation for these analytes must be readily and reliably perceived through high abundance serum or cell protein noise, particularly for small, highly hydrophobic or highly basic protein analytes, or other trace targets with difficult assay parameters.

Reduced assay noise (NSB) remains a critical challenge to capture surface contributions to improving both signal and noise performance in bioassays. In molecular isolations, purifications, manipulations, and assays, the technological benchmarks for proteins contacting surfaces are similar, specifically described in Table 2.1.

None of the thousands of polymer films and organic modifications proposed to date fulfill these important requirements for optimal surface capture from complex milieu. To understand these limitations critical to assay performance, some appreciation of the complexity of the generic protein adsorbate, as both signal and noise on surfaces, is required. Adsorption of globular serum proteins in particular to bioassay surfaces is most

Table 2.1 Performance benchmarks for assay capture surfaces in complex biological milieu.

- Reliable and consistent surface performance without surface defects or interfacial variability.
- Substantial reductions in non-specific protein surface interactions (NSB) to below 1% of a monolayer (< 3 ng/cm^2) in solutions of cell or tissue lysates, serum, homogenized food, or blood.
- Elimination of "blocking" steps using sacrificially adsorbed globular, surface-active proteins such as albumin, lactoglobulin, or casein, or adsorption of amphiphilic surface-active synthetic polymers (e.g., Pluronics™) to proactively mask surfaces against NSB from other sources.
- Effective, direct surface immobilization of capture ligands to substrates to facilitate analyte capture, stringency washing, multiple-step processing under high-shear and extreme pH or solvent conditions.
- Stabilization of immobilized affinity ligands in surface-capture environments to effectively preserve assay bioactivity under long residence times and lyophilized storage conditions.
- Surface immobilization treatments and protocols compatible with substrates comprising metals, plastics, metal oxides, and silicates with disposable economy.
- High-density affinity capture ligand immobilization on surfaces with minimal lateral interaction, competitive interference in assay or steric hindrance issues.
- Lot-lot and areal uniformity of affinity ligand immobilization and assay performance (signal:noise).
- Direct assay from complex milieu (serum, cell lysate, food, environmental samples) without sample pre-purification or analyte amplification or enrichment steps that cost time and money.
- Quantitative, direct correlation of assay analyte signal with sample analyte abundance.
- Reduction in capture feature sizes, surface patterning fidelity, lateral feature spacing for miniaturized formats and integrated approaches to achieve sufficiently discriminating signal:noise performance.

relevant to biomedical and biotechnological applications. As copolymers of some 22 amino acids of varying hydrophobicity, polarity, acidity, positive or negative charged side groups, proteins frequently and spontaneously fold into compact, often globular, domain-containing native (organized) structures upon exposure to aqueous milieu post-

translation in the cell. These globular folded native states represent local structural free energy minima and meta-stability, often only a few kcal/mole deep, permitting reversible unfolding to non-native structures given sufficient energetic drivers (e.g., thermal, mechanical, chemical). Their meta-stable, amphiphilic structural nature makes most proteins intrinsically highly surface active, promoting their spontaneous, non-specific surface adsorption and unfolding. In aqueous solution, compact globular protein native conformations tend to bury non-polar amino acid groups into their interior core region through hydrogen bonding, weak acid-base and hydrophobic interactions. Packing of these non-polar groups away from external bulk water results in a dramatic decrease in protein conformational entropy, which is energetically unfavorable, but compensated by collective hydrophobic associations, increased hydration forces on the resulting, more-polar protein hydration surface, and other enthalpic contributions to structural folding and hydration. Protein globular conformational entropy loss is outweighed by the presence of favorable hydrophobic interactions: dehydration of apolar amino acids by placement in the globular core away from the aqueous environment increases the aqueous entropic part of the system, lowering the overall Gibbs free energy for a folded state. Besides conformational entropy and hydrophobic interactions, collective electrostatic (Coloumbic) and van der Waals interactions, polar hydrogen and acid-base residue bonding and effects of protein folding on bond lengths and angles are also important factors that affect protein folding to least-energy conformations, though to a much lesser extent. Therefore, with protein folding-based hydrophobic effects outweighing protein conformational entropy by small amounts, proteins tend to fold into meta-stable globular conformations often stabilized by multiple hydrogen bonds (each worth a few kcal/mol). Relatively low

energy barriers between various protein domain conformational states make the overall native conformation highly susceptible to local structural changes with any environmental disturbance, including introduction of an interface (e.g., solid surface or air), and a protein's intrinsic surface free-energy driver for adsorption due to intrinsic amphiphilicity. Protein-surface adsorption is often spontaneous - an energetically favored event with both enthalpic and entropic driving forces. Hence, protein non-specific adsorption on assay capture surfaces is generally thermodynamically favored, and difficult to prevent using "simplistic" surface modification approaches.

Within the unstirred fluid boundary layer adjacent to any liquid-solid interface, protein interfacial adsorption is often transport- or diffusion-limited. Recognizing this kinetic constraint to rates of adsorption, proteins diffusing close to a hydrophobic interface adsorb spontaneously regardless of the protein's own hydrophobicity. The same hydrophobic dehydration forces promoting native protein folding in solution work in reverse at the solid-liquid interface to denature the protein over time at the interface (surface residence time), releasing surface-bound water molecules, increasing aqueous entropy of the system.[23,28-31] Surface adsorption energetics are generally sufficient to disrupt metastable protein globular structure, increasing both its conformational and surface hydration entropy. This collective entropy gain may be sufficiently favorable to produce spontaneous adsorption of the protein under otherwise adverse conditions, i.e., even at a hydrophilic, electrostatically repelling surface or unfavorable adsorption enthalpy. Hydration energy at hydrophobic surfaces is unfavorable. Replacement of surface-water molecule contacts with protein-surface contacts can often be energetically favorable if accompanied by sufficient protein conformational loss upon adsorption.

These requirements are usually met for most globular proteins beyond a few kDa in size. The end result in all protein-surface systems, regardless of either protein or surface chemistry, is the adsorption of finite amounts of protein via these non-specific, collective and universal thermodynamic effects. Generally, hydrophobic surfaces adsorb much higher amounts of globular proteins than highly hydrated, polar hydrophilic surfaces.[26] A second important consequence is that the adsorption event is accompanied by sufficient free energy change to produce surface-, time-, and protein-dependent unfolding transitions on the surface. Significantly, this leads to several technologically important endpoints ubiquitously observed in "real systems" that involve surfaces and biological milieu:

- Spontaneous adsorption of proteins to all surfaces, but with increasing affinity (reduced off-rate) for increasingly hydrophobic surfaces;
- Time-dependent denaturation of proteins on surfaces regardless of either protein or surface chemistry;
- Highly irreversible protein adsorbed states, even if physically adsorbed (no covalent bonds);
- Loss of protein structure and bioactivity accompanying surface residence time;

From the standpoint of designing diagnostic surfaces, this means that two general but important first-principle consequences hinder current surface-capture assay performance:

- Non-analyte proteins present as spectators in the assay milieu will adsorb to the bioassay surface, producing assay background noise and blocking desired analyte-surface interactions;

- Capture agents deliberately immobilized on a surface (nucleic acid probes, affinity reagents or antibodies) lose desired native structure and function on surfaces simply due to the heterogeneous interphase energetics and surface residency effects on proximal proteins.

This translates to challenges to limit non-specific binding and capture agent inactivation using new surface features that will improve surface capture performance. Given more than 200 known proteins in serum and thousands more in cell and tissue lysates, the intention to directly assay trace analytes at femtomolar or less abundances from these impure, relevant samples is severely limited by generic interfacial non-specific adsorption dynamics that generate excess noise. Current approaches either pre-purify samples to remove non-specific fouling species and enrich the sample in analyte, or exploit surface designs that select analyte over background fouling species. Surface modification strategies must address the source of the adsorption phenomena with appropriate chemical and physical methods to limit non-specific protein adsorption problems and enhance surface capture bioassay capabilities.

(b). Surface modification strategies to limit protein fouling. Improved surface performance in biological environments often reduces non-specific binding of biologicals to surfaces by exploiting "interfacial energy matching" that typically increases surface hydration stability using polar chemistry applied to diagnostic surfaces by organic coatings.[32] A review of current commercial approaches for microarraying surface chemistries and coatings appears in section 2.3 of this chapter. Surface chemistry polar enough to hydrate heavily reduces surface free energy gradients to adsorption of generally highly hydrated protein "surfaces". Surface hydrophilicity is a critical

parameter used to produce interfacial energy matching in aqueous milieu. "Hydrophilic" in the context of a surface functionally refers to surfaces that readily adsorb, hydrate, swell, or imbibe water, using polar or charged groups that interact strongly with water. Stable surface hydration minimizes interaction energies with other hydrated biological chemistries since most biological molecule surfaces are also highly hydrated due to surface structures with polar groups. At the molecular level, native protein structures exhibit highly hydrated surfaces contributing to their folded stability. Empirically, material surface resistance to protein adsorption by most criteria appears to correlate directly (although not completely) with the surface's degree of hydrophilicity and stable, structured water. Bulk water exhibits a strong self-association through multiple clathrate hydrogen bonds. Any disturbance of this self-associated network increases its entropy, decreases enthalpy, and increases water free energy.[25,33,34] Importantly, some polar, uncharged hydrophilic surfaces such as poly(ethylene glycol) (PEG) and polysaccharides[35,36] exhibit Lewis acid/base strength comparable to that of water, facilitating energetically favorable donation/accepting of electron density between water and these hydrophilic surface moieties (hydration). Anionic and cationic groups on surfaces also cluster water around each charged group based on ion-dipole forces. These cases of surface hydration are spontaneously stable. Hydrophobic surfaces, on the other hand, provide little chemical or energetic grounds for hydrogen bond formation or other dipole interactions with contacting water molecules, forcing water self-network breakdown and re-structuring at hydrophobic surfaces with unfavorable thermodynamic consequences.

By interacting with water through multiple interactions, hydrophilic surfaces reduce their surface energy over hydrophobic surfaces that interact with water only through pair-wise dispersion forces.[37] More specifically, a hydrophilic, hydrated interface creates a low interfacial tension between the material and the aqueous solution in which it resides. This leads to a low Gibbs free energy change for solute adsorption to the surface from biological fluids. In this case, highly hydrated solutes perceive little energetic difference between the solution in which they reside fully solvated and the surface to which they might potentially adsorb. Hence, reduced biological adsorption is often observed on highly hydrated surfaces over more apolar or hydrophobic surfaces where energies of hydration are less stable. Hydrophobic surfaces exhibit unfavorable hydration enthalpy and entropy, where contacting water is more liable to be displaced by other more favorable surface contacts through adsorption. Energetics, therefore, favor interfacial adsorption, particularly with proteins that dynamically restructure to expose core hydrophobic residues to contact hydrophobic surfaces, displacing surface-structured water through protein adsorption and denaturation. This mechanism has been reviewed extensively.[26-27, 29, 37-50]

2.2.3 Functional non-fouling assessments of surface chemistries in biological systems

The term "non-fouling" has been empirically defined to represent those surfaces that resist the adsorption of proteins and/or adhesion of cells under biological conditions. No standard technical definition for "protein adsorption resistance", for "non-specific binding", or conditions under which these properties are measured has been developed for functional assays. While protein adsorption assays are widely used as a "direct" raw

measure of a surface's non-fouling capability, each different research and application focus arbitrarily selects proteins of different size, charge and concentrations, sometimes as complex mixtures (e.g., dilute serum) and sometimes alone in buffer. "Protein resistance" is typically reported as a percent reduction in protein adsorption at a specific time as compared to an untreated control, over time-scales of minutes to days. Very few studies actually examine adsorption levels at equilibrium under relevant assay conditions, despite theoretical predictions that PEG brush mechanisms inhibiting fouling are kinetic.[51] To be functionally relevant, assay protocols for new applications generally require experimental verification that the surface remains sufficiently inert to adsorption under specific conditions in which it will be used.[52] Additionally, equilibrium surface-protein interactions in multi-component systems are recognized for decades to be a function of competitive conditions distinct from single protein isotherms. The "Vroman effect" [53,54] and other kinetic phenomena [55,56] occurring in multi-component competitive protein-surface milieu clearly limit the utility of single protein adsorption assays in predicting more complex performance. Effects of post-assay rinsing, removal of loosely adsorbed proteins and effects of air-drying must also be considered in the context of actual use to define protein resistance.[57] Single protein adsorption assay from buffer is widely known to produce distinct, and often falsely encouraging "non-specific binding" results completely different than either this same protein's surface uptake from binary or more complex solutions, or total protein uptake from relevant biological fluids (cell lysate, serum, or bacterial broths). Inequity of these "non-fouling" claims under widely varying conditions has led to confounding, often misleading conceptions of true performance in "real conditions." In fact, all claims to "complete protein resistance" or

"non-specific binding" performance *in vitro* in simple assay systems have rarely proven valid in more complex biological milieu, either *in vitro* or *in vivo*. Lack of surface performance "connectivity" between *in vitro* and *in vivo* protein fouling assays is problematic, as little predictive relevance from *in vitro* simplified assays can be extended to *in vivo* performance in complex host fluids, *in vitro* in full serum or cell lysate assays. This has profound implications for "ab initio" design of functional surface coatings where interactions of proteins with surfaces might be better understood and thereby controlled for any desired technology.

The current lack of surface adsorption performance correlations and fabrication methods that create surface chemistry reliably and defect-free at sufficient molecular resolution to block protein-surface interactions stymie most efforts to move this field forward rationally and scientifically. It is also critical to note that reported protein resistance performance is also dependent on the surface techniques utilized to measure it. With the development of high sensitivity surface analytical techniques (e.g., OWLS, ToF-SIMS), lower levels of protein surface deposition are detectable with greater certainty.[58,59] Finally, it should be noted that protein adsorption (or non-adsorption) may not correlate to a desired performance endpoint in specific applications. For example, PEO-like plasma polymerized tetraglyme surfaces that reduce fibrinogen adsorption to less than 10ng/cm^2 in vitro failed to reduce leukocyte or macrophage adhesion in the presence of plasma, whole blood, or when implanted in mice.[57] Several *in vivo* studies on PEO-containing surfaces even showed increased neutrophil or macrophage adhesion over control surfaces.[60,61] Additionally, bacteria tend to adhere and colonize almost any type of surface.[62,63] These microorganisms deposit their own binding proteoglycan adhesives,

called adhesins, independent of surface composition or charge. Surface resistance to bacterial adhesion remains an unsolved problem with the same challenges as all other non-fouling surfaces. Therefore, a "low-fouling" designation for these surfaces seems more appropriate since none truly show complete resistance despite reduced protein interfacial activity. Hence, a truly completely "non-fouling" surface is not yet achievable, especially in complex milieu relevant to most biological samples.[20,62]

2.2.4 Summary: surface chemistry design principles in diagnostic applications

The limitations of surface chemistry in improving the performance of diagnostic capture assays, particularly those operating in complex biological multi-component systems, are widely acknowledged, and many precedents can be traced back to fundamental mechanisms described for biointerfacial adsorption for 50 years. Microarray miniaturization does not eliminate any of these mechanisms and, in fact, makes their analysis more difficult. Assay performance is most frequently limited by sub-standard surface properties that are unable to eliminate non-specific adsorption of proteins and other components (noise) that compromise capture and detection of analytes (signal). Microarray assay devices compound signal:noise performance issues by reducing platform dimensionality (capture area) without commensurate reduction in confounding noise. Interfacial physical chemical requirements for ideal surfaces for these applications are well-developed from a first-principles perspective: interfacial energy gradients at interfaces that produce adsorption through several types of intermolecular forces can be explained and surfaces that minimize these forces have been described and experimentally attempted. Hydrophilic coatings incorporating high

densities of polar, Lewis base chemistry design features that stabilize interfacial hydration are currently a major focus. Immobilized polymer brush coatings fabricated with various surface-grafting methods are also a focus for several technologies, involving mixed immobilized coatings of hydrophilic and reactive functionalized polymer chains. Polyethylene glycol is a prominent chemistry because of its demonstrated success and versatility in reducing non-specific binding in interfacial applications, commercial availability in many different terminal chemistries and highly purified forms. Many architectures and theoretical studies aim to explain its performance in context. Microarray, spatially patterned fluidics and diagnostic technologies will all benefit from improved surface capture chemistries where affinity reagents can be immobilized to operate with high capacity and high selectivity within a non-fouling, low adsorption background surface matrix. Unfortunately, few successful solutions with sufficient performance in "real" biological samples are available for commercial application to immobilize proteins and nucleic acids.

2.3 Materials chemistry and analytical chemistry issues involved with DNA microarrays

Section 2.2 has focused on the non-fouling property consideration of biological assay surfaces. In this section, practical assay surface formats, both those under development in academic research and those commercially available on market, are discussed.

2.3.1 Microarray surface chemistry overview

Substantial attention has been paid to producing new information on aspects of DNA surface immobilization, array fabrication variables, target surface capture dynamics, hybridization efficiencies and assay signal-to-noise variables on both commercial microarray slides[15, 64-66] and model surface formats, including gold[67-72], silicon[73,74] and newly developed polymer coatings[75].

Given progress in the field over the last several years, individual researchers are now less likely to build microarrays entirely from scratch, instead relying on commercially manufactured microarray slides for self-spotting applications or even moving to manufactured, complete array platforms entirely. This is particularly true for DNA arrays where, from a surface chemistry perspective, most of the activity has consolidated to a relatively narrow, well-defined set of surface technologies.

Surface chemistry directly affects several important mechanistic aspects of microarraying, including probe loading, spot morphology, backgrounds, and hybridization yields. Figure 2.3 illustrates several of the processing parameters and non-idealities of microarraying that are directly impacted by surface chemistry.

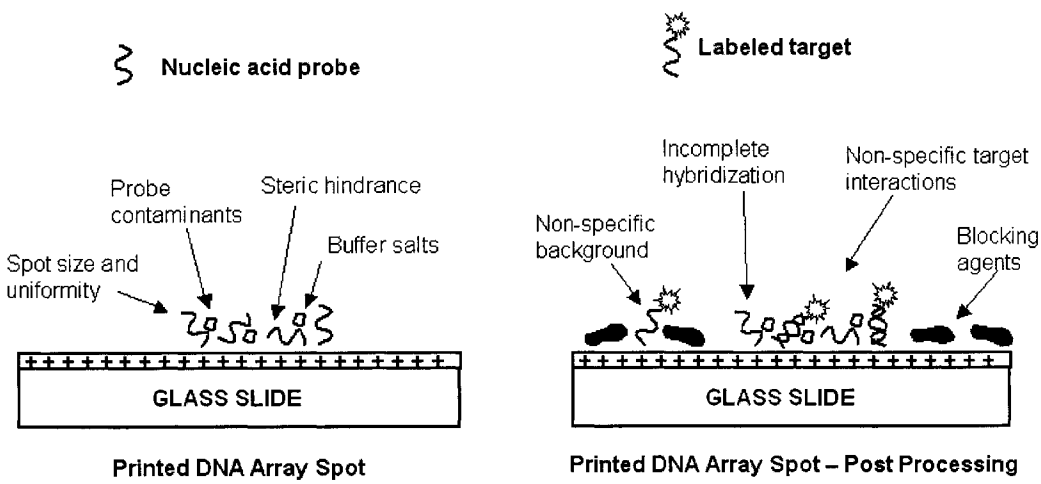

Figure 2.3 Non-idealities of microarray impact from surface chemistry

Probe loading refers the amount of probe immobilized in an array spot. Optimal loading can increase assay dynamic range and improve the capability to detect low copy number gene products. *Significantly, optimal loading is not necessarily the same as maximum loading.* Experimental and theoretical studies have shown that excess immobilized DNA can produce electrostatic repulsion between surface-immobilized probe and target during hybridization, lowering hybridization efficiency[72,76,77]. Reducing probe density on surfaces eventually compromises assay sensitivity. Hence, an optimum probe immobilization process is sought that eliminates both of these problems. The goal of an engineered surface chemistry therefore is to provide high signal, large dynamic range, and high hybridization efficiency.

Probe spot morphology in all printed microarray formats is critically dependent on surface chemistry. Whether contact or non-contact printing is used, spot morphology and the efficiency of any surface-probe coupling reactions both depend on an intimate balance between the probe drop delivery system, spotting solution properties (surface tension, viscosity, ionic strength) and the surface energy of the slide chemistry. For this reason, every commonly used slide surface chemistry has an optimized spotting protocol that matches print buffer and conditions to the specific surface chemistry characteristics. Diverging from the optimized printing can dramatically lower the quality of printed arrays. Many core labs have invested substantial effort to establish well-developed protocols (usually empirically based) for a given slide type or vendor, which makes these users less likely to try alternative surface chemistries. Many commercial slide vendors sell optimized reagent buffers as part of a microarraying slide kit.

A general comment on probe spot morphology is that surface chemistries that are relatively hydrophobic (apolar) yield uniform, small, reliably sized spot morphologies, a highly desired property for assay. Surface hydrophobicity reduces printed spot size, allowing higher density arrays, reduced drying artifacts, and more uniform spots. Slide surface chemistry vendors will often advertise "high water contact angle" (equated to low surface polarity, wettability or interfacial tension in this context) as a performance feature of their particular array surface chemistry.

Background is typically defined in terms of off-feature (off-spot) fluorescence signal that interferes with on-spot signal contrast, assay signal:noise ratios and dynamic range and sensitivity. Two sources of off-feature background in a microarray experiment are commonly recognized and directly associated with surface properties: intrinsic fluorescence of the coated slide itself, and non-specific binding of assay components. Until recently, intrinsic surface fluorescence was an important contributor to array assay backgrounds. Now nearly all slide vendors have consolidated onto high quality, low fluorescence glass substrate selections, and have developed low-fluorescence surface chemistry coating formulations.

Non-specific binding (NSB), however, remains an important contributor to background in many array experiments. Non-specific surface binding of biological components is most commonly dealt with using surface blocking strategies as part of the microarray slide processing protocol. Blocking is typically a post-print, pre-hybridization step in which the regions between arrayed spots are masked with a surface-active blocking agent that adsorbs irreversibly to the off-spot array features so that nothing else will. Common blocking agents include bovine serum albumin (BSA), sodium dodecyl

sulfate (SDS) and salmon sperm DNA. Proprietary blocking formulations have also been developed specifically for microarrays (e.g., Corning-Promega Pronto!™, Surmodics StabilGuard™). A general disadvantage of surface-specific adsorptive strategies is that they can be difficult to perform consistently. Despite relatively well-developed products and protocols for masking, background signal variations remain a source of both intrinsic variability and frustration to the microarraying community.

Surface chemistries engineered to have low intrinsic non-specific background without masking or blocking offer a potential solution to this blocking problem. For example, Schott Nexterion Slide H™ is a polyethylene glycol (PEG)-based polymer coating designed to have extremely low non-specific binding backgrounds without any adsorptive blocking requirement.

Finally, surface chemistry plays a critical role in defining the interfacial physico-chemical environment of the immobilized biomolecule (e.g., probe). Since the ultimate goal of the microarray experiment is to represent a biologically relevant interaction with reliability, sensitivity and fidelity, the microarray should ideally mimic a biological environment as closely as possible in order to preserve the native physical chemistry responsible for the capture interaction.

Current DNA microarray technology can be divided into two major categories: commercially produced arrays from industrial vendors and custom-made arrays produced by genomic core facilities and individual research labs. For commercially produced DNA arrays, nucleic acid probes are either synthesized directly on the solid support or are synthesized by traditional methods and then printed onto the substrates. Custom-made arrays are produced within individual labs or institutional core labs in which the

arraying facility selects the print technology, array substrates, and detection technologies. Nucleic acid content is typically purchased in library form from oligo-DNA vendors. A large number of core labs have evolved into relatively sophisticated operations with well-established array manufacturing and quality control procedures. Many offer nucleic acid arrays for sale within the research community, functioning as quasi-commercial entities.

2.3.2 Commercial DNA Arrays

A large fraction of microarray-based gene expression research reported in the literature is based on commercially produced arrays from vendors such as Affymetrix, Agilent, and GE Healthcare. All commercial array vendors have array products based on propriety surface chemistries. Commercial DNA arrays can be divided into two general categories based on a specific production method: (1) on-chip oligonucleotide synthesis and (2) printed, pre-synthesized oligo-DNAs.

Affymetrix, Agilent, and Nimblegen all utilize on-chip oligonucleotide synthesis to build the array. The Affymetrix GeneChip® microarrays comprise 25-mer probes synthesized directly on the solid support using a sequential, light-directed photolithography process[78,79]. The surface chemistry exploited for this strategy is a proprietary hydroxy-terminated organosilane layer on fused silica[78,79]. Nimblegen uses a light-directed, non-photolithographic approach based on an array of micromirrors[80]. The substrate is a silanized glass[80]. Agilent performs an in-situ synthesis of 60-mer probes on a silanized glass slide surface using a high-fidelity inkjet process. All three major on-chip synthesis vendors use proprietary surface chemistries optimized for their particular synthesis approach. From the perspective of the end-user, the surface chemistry used by the on-chip synthesis vendors is a two-dimensional organic-based linker layer that

covalently attaches the *in situ* synthesized oligonucleotide probes to the solid substrate. Significantly, this surface is also then present during the biological assay, and therefore must serve a second important function to facilitate sufficient target capture while avoiding NSB.

The second major category of commercial microarray vendors prints pre-synthesized oligonucleotides onto solid substrates coated with specific organic capture chemistry. Examples of this approach include GE Healthcare (formerly Amersham) and Mergen, both of which use the traditional glass slide substrate format with proprietary linker coatings. The GE Healthcare CodeLink™ platform is a three-dimensional, cross-linked polyacrylamide matrix on the glass slide, onto which amine-terminated oligonucleotide 30-mers are printed in a non-contact mode[64,81]. Mergen's arrays are also based on amine-modified 30mers printed onto a three-dimensional polymer coated glass slide [82].

2.3.3 Custom-made DNA microarrays

DNA microarray researchers who do not select a commercial array platform typically build custom arrays within their own lab or utilize the expertise of a local core facility to manufacture arrays. Two types of nucleic acid content are commonly used in the fabrication of these arrays: cDNA and oligonucleotide probes. The latter category can be further broken down into short (< 40 bases) and long (>40 bases) oligonucleotides. The intent of this section is to highlight the major classes of surface chemistries currently used on glass supports by the custom-made DNA microarray community. Table 2.2 provides a 2005 survey of vendors that supply coated glass slides for custom array printing applications.

Table 2.2 Example commercial microarray slide vendors

Vendor (listed alphabetically)	Example Products
Asper Biotech www.asperbio.com	GenoramaTM (aminosilane)
BioCat www.biocat.de	EasySpotTM (epoxide)
Bioslide www.bioslide.com	Precision CT (aminosilane, epoxide, aldehyde, PLL)
Corning www.corning.com	GAPS II (aminosilane); UltraGAPS (aminosilane); Epoxide
Erie Scientific www.eriemicroarray.com	SuperChipTM (aminosilane, epoxide, aldehyde, PLL)
Full Moon Bio www.fullmoonbio.com	cDNA Slides; PowerMatrix (3D, oligo); Protein Slides
GE Healthcare (formerly Amersham) www1.amershambiosciences.com	CodeLinkTM (amine-reactive, 3D polymer thin film)
Genetix www.genetix.com	ArrayXL cDNA; ArrayXL 3D; Epoxy, amine, aldehyde slides
GenTel Biosurfaces www.gentel.com	PATHTM slides (ultrathin nitrocellulose)
Matrix Technolgies www.matrixtechcorp.com	ez-rays (3D polymer, activatable)
Matsunami Glass www.matsunami-glass.co.jp	various
Nunc www.nalgenunc.com	ArrayCoteTM; MaxiSorpTM; NucleoLinkTM
Pall, Inc. www.pall.com	VividTM Gene Array (nylon membrane)
Perkin Elmer www.perkinelmer.com	MICROMAXTM (various) HydrogelTM
Sigma-Aldrich www.sigmaaldrich.com	SigmaScreen® slides
Schott Nexterion www.schott.com/nexterion	Slide A, A+ (aminosilane); Slide E (epoxide); Slide AL (aldehyde); Slide H (amine-reactive, 3D polymer thin film)
Takara www.takara-bio.co.jp	Takara-HubbleTM slide
TeleChem, Inc. www.arrayit.com	SuperAmine 2; SuperEpoxide 2; SuperAldehyde 2; SuperProtein; SuperAvidin, Streptavidn
Whatman Schleicher & Schuell www.schleicher-schuell.com	FASTslides (nitrocellulose membrane)
Xenopore www.xenopore.com	Various

(a). Aminosilane Surfaces. The first function of glass slide surface chemistry is to provide robust immobilization of nucleic acid probes. Given that nucleic acids are poly-anions of high polyphosphate charge density, electrostatic interactions with a

positively charged surface chemistry have been the most commonly used mechanism for DNA surface immobilization. Amine-terminated organosilane-coated slides are the dominant cationic surface in practice for both cDNA and oligo arraying.

Silanization of glass is a well-established and extensively reviewed technique[83] wherein the native, negatively charged, silanol-terminated surface of inorganic silicate glass is derivatized with organosilanes. Exact mechanisms and precise control of this chemistry remain elusive, despite its popularity. In the aminosilane treatment, clean glass surfaces are converted to a primary amine-containing organo overlayer surface through either solution-phase or vapor-phase deposition. Because of the terminal amine functional group, the aminosilane surface carries a net positive charge when exposed to aqueous solutions below approximately pH 9. During microarray printing, anionic oligonucleotides or cDNA in the aqueous print buffer are electrostatically immobilized to this basic, cationic surface. A post-print UV or thermal cross-linking step is often used to covalently attach the printed molecules to the surface.

Organosilane adlayer films on glass are typically on the order of ~ 1-2 nm thick, and can thus be considered ultra-thin organic surface-modifying films. Figure 2.4 depicts the relative sizes of a silane film and commonly printed biomolecules.

Despite the long history of silanization of glass surfaces, generating silane films with the uniformity and consistency required for microarray applications is generally not practical for most individual labs. DNA microarray researchers therefore most often utilize commercially produced aminosilane slides that have undergone product development and are subjected to manufacturing quality assurance and quality control.

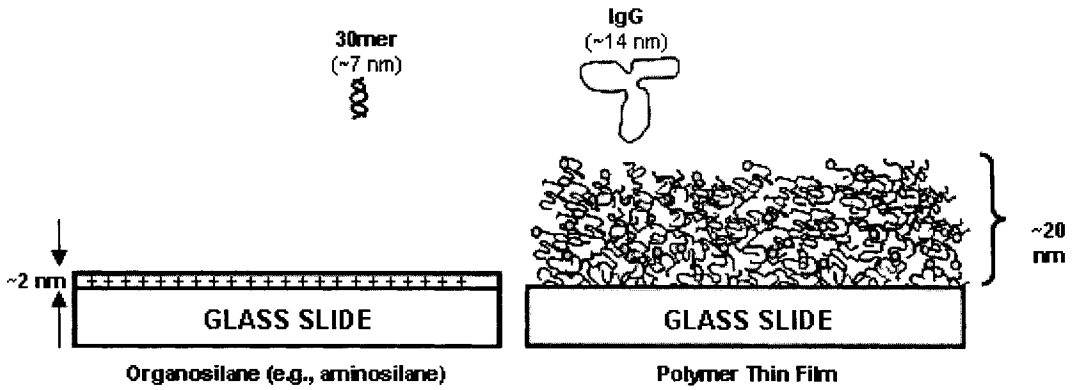

Figure 2.4 Comparison of biomolecular and organic surface-modifying film dimensions

Commercially produced aminosilane slides are available from a large number of vendors, including Corning, TeleChem, Schott Nexterion, and Erie Scientific (see Table 2.2).

Aminosilane array slides are relatively inexpensive and a growing legacy dataset has been built on this substrate. Well-developed protocols and reagent kits can deliver high quality arrays. A downside of the aminosilane format is that it lacks proper capabilities to reduce NSB during assay: careful blocking strategies are required to reduce off-feature backgrounds during hybridization. Blocking strategies vary from lab to lab, and several microarray slide vendors now offer packaged array processing kits that include blocking reagents. An additional concern for aminosilane slides is that electrostatic and subsequent photo- or thermal-immobilization reactions between DNA and the surface are condition- and probe sequence-specific, and could lead to steric hindrance of the immobilized probe during hybridization, particularly for short oligo probes highly reacted to the surface, and for low copy-number targets.

Poly-L-Lysine (PLL) Surfaces. Like the aminosilane surface, poly-L-lysine (PLL)-modified slides also provide cationic immobilization of nucleic acid probes. PLL

is a basic, synthetic, positively charged, poly(aminoacid) polyelectrolyte that adsorbs from aqueous solution to the negatively charged surface of glass. PLL surfaces have historically been used to facilitate cell adhesion for histology and cell culture applications. Consequently, poly-L-lysine solutions formulated specifically for glass slide treatments are available commercially (e.g., through Sigma-Aldrich). These commercial formulations are typically 0.01% aqueous solutions of 75,000 to 150,000 molecular weight poly-L-lysine (e.g. Sigma P-4707). Protocols for PLL slide preparation for DNA microarraying are readily available, and all are closely related to the protocol originally described by Pat Brown's lab at Stanford[84].

The primary advantage of PLL slides is that they are inexpensive and simple to produce within individual labs. The main disadvantage of PLL-coated slides is that intra-slide uniformity and batch-to-batch performance can be inferior to other slide formats. The preparation is particularly sensitive to the quality of the glass cleaning process, and because the PLL surface ages with time, most protocols recommend a two-week aging period between preparation and use. Because the PLL adheres to the underlying glass through electrostatic interactions, these surfaces are also subject to delamination under high salt conditions.

Epoxide and Aldehyde Surfaces. Silanized slides that provide active binding chemistries are becoming increasingly popular within the custom-made arraying community. This is particularly true for labs migrating from cDNA or PCR probe product platforms to those based on oligonucleotide probes. The most popular active silane chemistry is epoxide, which provides covalent immobilization of both amine-modified and unmodified oligos. The epoxide surfaces are typically based on a

glycidoxy-functionalized organosilane or related epoxide molecule derivative. The main advantages of epoxide chemistry are its relative stability and generally lower background than aminosilane[85]. Several commercial vendors of epoxide slides are listed in Table 2.2.

Aldehyde-terminated silanes are another class of active chemistries used for DNA immobilization. Aldehyde-functionalized surfaces selectively react with amine-terminated oligos through a well-known Schiff base reaction, which is often driven to completion through the addition of a reducing agent to the reaction solution.

Polymer Thin Films. Glass slides treated with polymer coating formulations are designed to provide a degree of three-dimensionality and theoretically higher probe loading capacities. Polymer-coated slides are also designed to provide additional performance features such as tethered probe immobilization with a more benign, "solution-like" environment, and low non-specific binding backgrounds. We use the term "polymer film" here to generally describe polymer thin films residing on glass slides, ranging in thickness from about 20 to 2000 nm. We treat these supported films separately from thicker polymer monolithic membrane materials such as nitrocellulose and nylon, which are discussed in more detail below.

Commercial polymer film formulations generally comprise hydrophilic polymer formulations activated with reactive chemistries that provide chemical capabilities for covalent immobilization of appropriately modified oligonucleotides. Polyacrylamides and polyethylene glycol (PEG) derivatives are common polymer components in this category. Because of their hydrophilic nature, coated slides in this category are often referred to as "hydrogels" or "hydrogel-like" materials with porous, three-dimensional

character and some water imbibition. Hydrogel™ is also the trade name of the Perkin Elmer protein array slide product.

Here we first consider thin polymer films, typically transparent coated layers less than a few hundred nanometers thick immobilized on a glass slide. Figure 2.4 provides an illustration of a 20 nm-thick polymer film in size-scale relation to a silane film and some molecular dimensions. This thickness disparity distinguishing the silane from the polymer films is readily apparent. A well-known formulation in this category underlies the CodeLink™ microarray platform (GE Healthcare), exploiting a proprietary crosslinked, and chemically activated polyacrylamide formulation to enable covalent immobilization of amine-modified oligonucleotides in a three-dimensional, solution-like environment[64]. Another example is Schott Nexterion Slide H™, a crosslinked, multi-component polyethylene glycol (PEG)-coated glass slide activated with succinimidyl esters (NHS) to provide covalent immobilization of amine groups. Both CodeLink™ and Slide H™ exhibit extremely specific reactivity for the amine groups on amine-modified probes. Other commercial polymer thin film formulations include the PowerMatrix™ slides from FullMoonBio and ez-rays™ Universal™ slides from Matrix Technologies.

Thicker (> 1000 nm) polymer films have also been demonstrated, the most celebrated of which is the gel-pad technology described by Mirzabekov and co-workers[86,87]. Commercial applications of thick hydrogel technologies have been marketed primarily for protein applications, as discussed in more detail below.

Membranes. DNA microarray analysis has been described as a natural progression from dot blot analysis in which the DNA probe is adsorbed in a thick membrane for analysis[88]. In moving from traditional dot blot analysis to microarray

formats, new products have been introduced that provide dot blot-like membrane layers immobilized onto glass slides, giving the functionality of membranes but in the standard glass slide microarray format. These are particularly useful for DNA array analysis that uses radioactive labeling and chemiluminescence, where high probe loading is needed for good signal to noise generation. For example, Pall Vivid™ gene array slides feature a nylon membrane immobilized on a glass slide. Whatman Schleicher and Schuell offer nitrocellulose membrane slides (FASTslides), but these are marketed primarily for protein arrays and are discussed below.

In conclusion, both commercially produced and custom-made arrays have seen significant development over the last several years. In the context of surface chemistry, much of the glass slide DNA array work has consolidated onto a relatively well-defined set of surface chemistries, dominated by organosilane coatings (aminosilane and epoxide) and a subset of three-dimensional, active polymers. The driving forces of data quality (signal to noise, reproducibility, etc.) and biological accuracy will lead to continued improvements in DNA microarray surface chemistries.

2.4 Surface Analyses to improve understanding of DNA microarray

2.4.1 Analytical methods that have been directed at understanding DNA microarray

Quantitative, high-resolution, highly surface sensitive techniques, including Fourier transform infrared spectroscopy (FTIR)[74, 89], X-ray photoelectron spectroscopy (XPS)[69, 74, 89-91], secondary ion mass spectrometry (SIMS)[90, 92-94 95], near edge X-ray absorption fine structure (NEXAFS)[96] and radiometric assays[68,69,97-100], have provided

data on both the properties of model sensing surfaces as well as immobilized biomolecular affinity capture components (antibodies, nucleotides) on surfaces, usually averaging surface spatial information across macroscopic features. However, these efforts for studying both individual and oligomeric nucleotides on various surfaces frequently do not directly address microarray technology in an assay-relevant context, especially with commercially available microarray surfaces and assay conditions. Additionally, many studies immobilize DNA to assay surfaces using bulk solution reactions that provide nucleotide immobilization dynamics, densities and assay results distinct from commercial methods using microspotting in air where nanoliter DNA solution droplets evaporate on the assay surface in seconds. Different immobilization densities resulting from these two immobilization conditions have profound implications for subsequent assay performance differences. Nonetheless, previous studies were able to show that XPS and SIMS are well suited for sensitive characterization of surface-bound DNA. In particular, previous reports have identified unique nucleotide signals (nitrogen and phosphorus DNA-specific spectra) and demonstrated method utility in characterizing both composition and structure of DNA immobilized on to surfaces[69,70,101,102]. Applying highly surface-sensitive techniques directly to microscopic microarray features remains a challenge. Improved resolution may be obtained at the expense of higher sensitivity, and vice versa. Microarray feature sizes typically range from several tens to several hundreds of microns in diameter, making it difficult to achieve reasonable sensitivity along with suitable resolution for surface analysis.

2.4.2 Aim of research and proposed analytical schematics for further understanding of DNA microarray

Specifically, this dissertation research is motivated by the following observations that are critical to the utility of these array devices for reliable, quantitative prediction of disease: Observation #1: Quantitative interpretation of DNA microarray signal intensity is currently unreliable. Molecular factors influencing DNA probe-target interactions at microarray surfaces have not been analyzed with high-resolution surface analytical methods often applied to other biomedical surface problems, limiting progress in quantitative analysis. Observation #2: Improving reliability, sensitivity, and quantitation of DNA microarray signal intensity must rely upon a technical understanding of limiting surface reactions and probe DNA immobilized microenvironments on microarray platforms. Observation #3: Utility of microarray data to interpret disease states or assist in reliable diagnosis of pathogenesis markers will remain limited until quantitation variables and variable signal generation parameters in arrays are first discovered, then analyzed and finally resolved. Observation #4: High resolution surface analytical methods have seldom been applied to analysis of microarray surface chemistry, probe DNA adsorbed states and their relationships to DNA target capture intensities or signal variability, but would provide useful, timely data to understand the issues and then direct requisite performance improvements.

It is proposed that the now-routine methods involved in microarray fabrication and data interpretation for disease profiling are dangerously presumptuous simply because most are anecdotal and developed without much surface analytical support, nor published analytical protocols. Assay performance across a wide variety of spotting,

hybridization and detection conditions is disappointing and limited: signal is lower than expected, noise remains a problem, and reproducibility permitting quantitation is not possible. Given the enormous growth and focus on microarray technology for disease diagnosis and detection, it is believed that a thorough surface analytical study of DNA immobilized density, orientation and interfacial hybridization properties is important and justified. Therefore, a set of logical, complementary bioanalytical studies crossing several sets of expertise are proposed: DNA surface and analyte capture analysis will be performed on two type of surfaces: (1) model surfaces with mixed thiol-DNA/mercaptoundecanol (MCU) adlayers on gold, and (2) DNA microarrays on commercial amine-reactive microarraying polymer slides (CodeLink™ and OptArray™). Assay surface reliability, DNA density, hybridization efficiency and influence of complex milieu (serum dilutions, cell lysate) on hybridization will be assessed using surface analytical techniques (XPS, NEXAFS, SPR) and more traditional biological and microarray analysis techniques (radiometric assay and fluorescence intensity measurements). These studies are directed at providing new, reliable data regarding DNA microarray surface chemistry and its correlation to target DNA hybridization efficiency in bioassays.

The intent of this work is to provide an accurate assessment of molecular variables involved in DNA microarray methods from a surface immobilization perspective. These data, currently not available in the public domain, are direly needed to understand limitations of current DNA assay methods in biomedical applications. The outcome of these studies should prove of general utility to a broad set of scientific

communities that increasingly exploit this nucleic acid microarray technology without true knowledge of the constraints of the methods.

2.5 References

(1) Gong, P.; Grainger, D. W. In *Microarrays: Methods and Protocols (Methods in Molecular Biology),* 2nd ed.; Rampal, J. B., Ed.; Humana: Totowa, New Jersey, 2006.

(2) Grainger, D. W.; Greef, C. H.; Gong, P.; Lochhead, M. J. In *Microarrays: Methods and Protocols (Methods in Molecular Biology),* 2nd ed.; Rampal, J. B., Ed.; Humana Press: Totowa, New Jersey, 2006.

(3) Ramsay, G. *Nat. Biotechnol.* **1998**, *16*, 40-44.

(4) Schena, M.; Heller, R. A.; Theriault, T. P.; Konrad, K.; Lachenmeier, E.; Davis, R. W. *Trends Biotechnol.* **1998**, *16*, 301-306.

(5) Sanchez-Carbayo, M.; Bornmann, W.; Cordon-Cardo, C. *Curr. Org. Chem.* **2000**, *4*, 945-971.

(6) Freeman, W. M.; Robertson, D. J.; Vrana, K. E. *BioTechniques* **2000**, *29*, 1042-1044, 1046, 1048-1055.

(7) van Hal, N. L. W.; Vorst, O.; van Houwelingen, A. M. M. L.; Kok, E. J.; Peijnenburg, A.; Aharoni, A.; van Tunen, A. J.; Keijer, J. *J. Biotechnol.* **2000**, *78*, 271-280.

(8) Beaucage, S. L. *Curr. Med. Chem.* **2001**, *8*, 1213-1244.

(9) Ekins, R. P.; Chu, F. W. *Clin. Chem. (Washington, DC, U. S.)* **1991**, *37*, 1955-1967.

(10) Ekins, R. P.; Chu, F. W. *ACS Sym. Ser.* **1995**, *586*, 153-174.

(11) http://www.roche-diagnostics.com/products_services/amplichip_cyp450.html.

(12) Sherlock, G. *Nat. Methods* **2005**, *2*, 329-330.

(13) Kuo, W. P.; Jenssen, T.-K.; Butte, A. J.; Ohno-Machado, L.; Kohane, I. S. *Bioinformatics* **2002**, *18*, 405-412.

(14) Ross, D. T.; Scherf, U.; Eisen, M. B.; Perou, C. M.; Rees, C.; Spellman, P.; Iyer, V.; Jeffrey, S. S.; Van de Rijn, M.; Waltham, M.; Pergamenschikov, A.; Lee, J. C.; Lashkari, D.; Shalon, D.; Myers, T. G.; Weinstein, J. N.; Botstein, D.; Brown, P. O. *Nat. Genet.* **2000**, *24*, 227-235.

(15) Tan, P. K.; Downey, T. J.; Spitznagel, E. L., Jr.; Xu, P.; Fu, D.; Dimitrov, D. S.; Lempicki, R. A.; Raaka, B. M.; Cam, M. C. *Nucleic Acids Res.* **2003**, *31*, 5676-5684.

(16) Yauk Carole, L.; Berndt, M. L.; Williams, A.; Douglas George, R. *Nucleic acids res.* **2004**, *32*, e124.

(17) Larkin, J. E.; Frank, B. C.; Gavras, H.; Sultana, R.; Quackenbush, J. *Nat. Methods* **2005**, *2*, 337-344.

(18) Irizarry, R. A.; Warren, D.; Spencer, F.; Kim, I. F.; Biswal, S.; Frank, B. C.; Gabrielson, E.; Garcia, J. G.; Geoghegan, J.; Germino, G.; Griffin, C.; Hilmer, S. C.; Hoffman, E.; Jedlicka, A. E.; Kawasaki, E.; Martinez-Murillo, F.; Morsberger, L.; Lee, H.; Petersen, D.; Quackenbush, J.; Scott, A.; Wilson, M.; Yang, Y.; Ye, S. Q.; Yu, W. *Nat. Methods* **2005**, *2*, 345-350.

(19) Bammler, T.; Beyer, R. P.; Bhattacharya, S.; Boorman, G. A.; Boyles, A.; Bradford, B. U.; Bumgarner, R. E.; Bushel, P. R.; Chaturvedi, K.; Choi, D.; Cunningham, M. L.; Deng, S.; Dressman, H. K.; Fannin, R. D.; Farin, F. M.; Freedman, J. H.; Fry, R. C.; Harper, A.; Humble, M. C.; Hurban, P.; Kavanagh, T. J.; Kaufmann, W. K.; Kerr, K. F.; Jing, L.; Lapidus, J. A.; Lasarev, M. R.; Li, J.; Li, Y. J.; Lobenhofer, E. K.; Lu, X.; Malek, R. L.; Milton, S.; Nagalla, S. R.; O'Malley J, P.; Palmer, V. S.; Pattee, P.; Paules, R. S.; Perou, C. M.; Phillips, K.; Qin, L. X.; Qiu, Y.; Quigley, S. D.; Rodland, M.; Rusyn, I.; Samson, L. D.; Schwartz, D. A.; Shi, Y.; Shin, J. L.; Sieber, S. O.; Slifer, S.; Speer, M. C.; Spencer, P. S.; Sproles, D. I.; Swenberg, J. A.; Suk, W. A.; Sullivan, R. C.; Tian, R.; Tennant, R. W.; Todd, S. A.; Tucker, C. J.; Van Houten, B.; Weis, B. K.; Xuan, S.; Zarbl, H. *Nat. Methods* **2005**, *2*, 351-356.

(20) Hoffman, A. S. *J Biomater. Sci. Polym. Ed.* **1999**, *10*, 1011-1014.

(21) Andrade, J. D.; Nagaoka, S.; Cooper, S.; Okano, T.; Kim, S. W. *ASAIO Transactions* **1987**, *33*, 75-84.

(22) Merrill, E. W. *Ann. N. Y. Acad. Sci.* **1987**, *516*, 196-203.

(23) Malmsten, M. Ed. *Biopolymers at Interfaces*, 2nd ed.; CRC Press, 2003.

(24) Garcia, C. A.; Hummer, G.; Soumpasis, D. M. In *Water in Biomaterials Surface Science*; Morra, M., Ed.; John Wiley & Sons Ltd.: West Sussex, England, 2001, pp 25-52.

(25) Vogler, E. A. In *Water in Biomaterials Surface Science*; Morra, M., Ed.; John Wiley & Sons Ltd.: West Sussex, England, 2001, pp 149-181.

(26) Norde, W. In *Biopolymers at Interfaces, Surfactant Science Series*, Malmsten, M. Ed.; 2003; Vol. 110, pp 21-43.

(27) Ramsden, J. J. In *Biopolymers at Interfaces, Surfactant Science Series*, Malmsten, M. Ed.; 2003; Vol. 110, pp 199-220.

(28) Britt, D. W.; Jogikalmath, G.; Hlady, V. In *Biopolymers at Interfaces, Surfactant Science Series*, Malmsten, M. Ed.; 2003; Vol. 110, pp 415-434.

(29) Brash, J. L.; Horbett, T. A. *ACS Symp. Ser.* **1995**, *602*, 1-23.

(30) Horbett, T. A.; Brash, J. L. *ACS Symp. Ser.* **1987**, *343*, 1-33.

(31) Andrade, J. D. Ed. *Surface and Interfacial Aspects of Biomedical Polymers*; Plenum Press: New York, 1985.

(32) Coleman, D. L.; King, R. N.; Andrade, J. D. *J Biomed. Mater. Res.* **1974**, *8*, 65-76.

(33) Andrade, J. D.; Hlady, V. *Adv. Polym. Sci.* **1986**, *79*, 1-63.

(34) Vogler, E. A. *J. Biomater. Sci., Polym. Ed.* **1999**, *10*, 1015-1045.

(35) Alcantar, N. A.; Aydil, E. S.; Israelachvili, J. N. *J Biomed. Mater. Res.* **2000**, *51*, 343-351.

(36) Israelachvili, J.; Wennerstrom, H. *Nature* **1996**, *379*, 219-225.

(37) Vogler, E. A. *Adv Colloid Interface Sci.* **1998**, *74*, 69-117.

(38) Andrade, J. D.; Hlady, V.; Feng, L.; Tingey, K. *Bioprocess Technol.* **1996**, *23*, 19-55.

(39) Bhaduri, A.; Das, K. P. *J. Dispersion Sci. Technol.* **1999**, *20*, 1097-1123.

(40) Elwing, H.; Askenda, A.; Ivarsson, B.; Nilsson, U.; Welin, S.; Lundstroem, I. *ACS Symp. Ser.* **1987**, *343*, 468-489.

(41) Greig, R. G.; Brooks, D. E. *J. Colloid Interface Sci.* **1981**, *83*, 661-662.

(42) Hlady, V. V.; Buijs, J. *Curr. Opin. Biotechnol.* **1996**, *7*, 72-77.

(43) Kleijn, M.; Norde, W. *Heterogeneous Chem. Rev.* **1995**, *2*, 157-172.

(44) Malmsten, M. *Protein Architecture* **2000**, 1-23.

(45) Nakanishi, K.; Sakiyama, T.; Imamura, K. *J. Biosci. Bioeng.* **2001**, *91*, 233-244.

(46) Norde, W. Ed., *Polymer Science and Technology*, Plenum Press, 1980; Vol. 12B, pp 801-825.

(47) Norde, W. Ed., *Physical Chemistry of Biological Interface,* Marcel Dekker, 2000, pp 115-135.

(48) Ramsden, J. J. *Conference on Colloid Chemistry: In Memoriam Aladar Buzagh, Proceedings, 7th, Eger, Hung., Sept. 23-26* **1996**, 148-151.

(49) Roth, C. M.; Lenhoff, A. M. In *Biopolymers at Interfaces, Surfactant Science Series*, Malmsten, M. Ed.; 2003; Vol. 110, pp 71-94.

(50) Wahlgren, M.; Arnebrant, T. *Trends Biotechnol.* **1991**, *9*, 201-208.

(51) Szleifer, I. *Biophys. J.* **1997**, *72*, 595-612.

(52) Griffith, L. G. *Acta Mate.* **2000**, *48*, 263-277.

(53) Ball, V.; Schaaf, P.; Voegel, J.-C. In *Biopolymers at Interfaces, Surfactant Science Series*, Malmsten, M. Ed.; 2003; Vol. 110, pp 295-320.

(54) Slack, S. M.; Horbett, T. A. *ACS Symp. Ser.* **1995**, *602*, 112-128.

(55) Krishnan, A.; Siedlecki, C. A.; Vogler, E. A. *Langmuir* **2004**, *20*, 5071-5078.

(56) Krishnan, A.; Sturgeon, J.; Siedlecki, C. A.; Vogler, E. A. *J. Biomed. Mater. Res. A* **2004**, *68*, 544-557.

(57) Shen, M.; Martinson, L.; Wagner, M. S.; Castner, D. G.; Ratner, B. D.; Horbett, T. A. *J. Biomater. Sci. Polym. Ed.* **2002**, *13*, 367-390.

(58) Wagner, M. S.; McArthur, S. L.; Shen, M.; Horbett, T. A.; Castner, D. G. *J. Biomater. Sci. Polym. Ed.* **2002**, *13*, 407-428.

(59) Pasche, S.; Textor, M.; Meagher, L.; Spencer, N. D.; Griesser, H. J. *Langmuir* **2005**, *21*, 6508-6520.

(60) Ronneberger, B.; Kao, W. J.; Anderson, J. M.; Kissel, T. *J. Biomed. Mater. Res.* **1996**, *30*, 31-40.

(61) Suggs, L. J.; Krishnan, R. S.; Garcia, C. A.; Peter, S. J.; Anderson, J. M.; Mikos, A. G. *J. Biomed. Mater. Res.* **1998**, *42*, 312-320.

(62) Kingshott, P.; Wei, J.; Bagge-Ravn, D.; Gadegaard, N.; Gram, L. *Langmuir* **2003**, *19*, 6912-6921.

(63) Johnston, E. E.; Bryers, J. D.; Ratner, B. D. *Langmuir* **2005**, *21*, 870-881.

(64) Ramakrishnanm, R.; Dorris, D.; Lublinsky, A.; Nguyen, A.; Domanus, M.; Prokhorova, A.; Gieser, L.; Touma, E.; Lockner, R.; Tata, M.; Zhu, X.; Patterson, M.; Shippy, R.; Sendera, T. J.; Mazumder, A. *Nucleic Acids Res.* **2002**, *30*, e30/31-e30/12.

(65) Gong, P.; Grainger, D. W. *Surf. Sci.* **2004**, *570*, 67-77.

(66) Gong, P.; Harbers, G. M.; Grainger, D. W. *Anal. Chem.* **2006**, *in press*.

(67) Steel, A. B.; Levicky, R.; Herne, T. M.; Tarlov, M. J. *Proc. - Electrochem. Soc.* **1999**, *99-5*, 132-143.

(68) Steel, A. B.; Levicky, R. L.; Herne, T. M.; Tarlov, M. J. *Biophys. J.* **2000**, *79*, 975-981.

(69) Herne, T. M.; Tarlov, M. J. *J. Am. Chem. Soc.* **1997**, *119*, 8916-8920.

(70) Petrovykh, D. Y.; Kimura-Suda, H.; Tarlov, M. J.; Whitman, L. J. *Langmuir* **2004**, *20*, 429-440.

(71) Wolf, L. K.; Gao, Y.; Georgiadis, R. M. *Langmuir* **2004**, *20*, 3357-3361.

(72) Peterson, A. W.; Heaton, R. J.; Georgiadis, R. M. *Nucleic Acids Res.* **2001**, *29*, 5163-5168.

(73) Jin, L.; Horgan, A.; Levicky, R. *Langmuir* **2003**, *19*, 6968-6975.

(74) Shen, G.; Anand, M. F. G.; Levicky, R. *Nucleic Acids Res.* **2004**, *32*, 5973-5980.

(75) Pirri, G.; Damin, F.; Chiari, M.; Bontempi, E.; Depero, L. E. *Anal. Chem.* **2004**, *76*, 1352-1358.

(76) Vainrub, A.; Pettitt, B. M. *Phys. Rev. E: Stat., Nonlinear, and Soft Matter Phys.* **2002**, *66*, 041905/041901-041905/041904.

(77) Vainrub, A.; Pettitt, B. M. *J. Am. Chem. Soc.* **2003**, *125*, 7798-7799.

(78) McGall, G.; Labadie, J.; Brock, P.; Wallraff, G.; Nguyen, T.; Hinsberg, W. *Proc. Natl. Acad. Sci. USA* **1996**, *93*, 13555-13560.

(79) McGall, G. H.; Christians, F. C. *Adv. Biochem. Eng. Biotechnol.* **2002**, *77*, 21-42.

(80) Nuwaysir, E. F.; Huang, W.; Albert, T. J.; Singh, J.; Nuwaysir, K.; Pitas, A.; Richmond, T.; Gorski, T.; Berg, J. P.; Ballin, J.; McCormick, M.; Norton, J.; Pollock, T.; Sumwalt, T.; Butcher, L.; Porter, D.; Molla, M.; Hall, C.; Blattner, F.; Sussman, M. R.; Wallace, R. L.; Cerrina, F.; Green, R. D. *Genome Res.* **2002**, *12*, 1749-1755.

(81) Shippy, R.; Sendera, T. J.; Lockner, R.; Palaniappan, C.; Kaysser-Kranich, T.; Watts, G.; Alsobrook, J. *BMC Genomics* **2004**, *5*, 61.

(82) www.mergen.com.

(83) Mittal, K. L. Ed., *Silanes and Other Coupling Agents*; VSP International Science Publishers: Utrecht, The Netherlands, 1992.

(84) http://cmgm.stanford.edu/pbrown/protocols/1_slides.html.

(85) Morgan, H.; Taylor, D. M. *Biosen. Bioelectron.* **1992**, *7*, 405-410.

(86) Vasiliskov, A. V.; Timofeev, E. N.; Surzhikov, S. A.; Drobyshev, A. L.; Shick, V. V.; Mirzabekov, A. D. *Biotechniques* **1999**, *27*, 592-594, 596-598, 600 passim.

(87) Zlatanova, J.; Mirzabekov, A. D. In *DNA Arrays: Methods and Protocols*; Rampal, J. B., Ed.; Humana Press: Totowa, New Jersey, 2001; Vol. 170, pp 17-38.

(88) Southern, E. M. In *DNA Microarrays: Methods and Protocols*; Rampal, J. B., Ed.; Humana Press: Totowa, New Jersey., 2001; Vol. 170, pp 1-15.

(89) Petrovykh, D. Y.; Kimura-Suda, H.; Whitman, L. J.; Tarlov, M. J. *J. Am. Chem. Soc.* **2003**, *125*, 5219-5226.

(90) Boland, T.; Ratner, B. D. *Proc. Natl. Acad. Sci. U S A* **1995**, *92*, 5297-5301.

(91) Rabke, C. E.; Wenzler, L. A.; Beebe, T. P., Jr. *Scanning Microsc.* **1994**, *8*, 471-478; discussion 478-480.

(92) Patrick, J. S.; Cooks, R. G.; Pachuta, S. J. *Biol. Mass. Spectrom.* **1994**, *23*, 653-659.

(93) Boland, T.; Ratner, B. D. *Langmuir* **1994**, *10*, 3845-3852.

(94) Benninghoven, A. *J. Vac. Sci. Technol. A* **1985**, *3*, 451-460.

(95) Arlinghaus, H. F.; Kwoka, M. N.; Jacobson, K. B. *Anal. Chem.* **1997**, *69*, 3747-3753.

(96) Crain, J. N.; Kirakosian, A.; Lin, J. L.; Gu, Y. D.; Shah, R. R.; Abbott, N. L.; Himpsel, F. J. *J. Appl. Phys.* **2001**, *90*, 3291-3295.

(97) Cavic, B. A.; McGovern, M. E.; Nisman, R.; Thompson, M. *Analyst (Cambridge, U. K.)* **2001**, *126*, 485-490.

(98) Zammatteo, N.; Jeanmart, L.; Hamels, S.; Courtois, S.; Louette, P.; Hevesi, L.; Remacle, J. *Anal. Biochem.* **2000**, *280*, 143-150.

(99) Balladur, V. V.; Theretz, A.; Mandrand, B. *J. Colloid Interface Sci.* **1997**, *194*, 408-418.

(100) Halliwell, C. M.; Cass, A. E. *Anal. Chem.* **2001**, *73*, 2476-2483.

(101) May, C. J.; Canavan, H. E.; Castner, D. G. *Anal. Chem.* **2004**, *76*, 1114-1122.

(102) Samuel, N. T.; Lee, C.-Y. L.; Gamble, L. J.; Fisher, D. A.; Castner, D. G. *J. Electron Spectrosc. Relat. Phenom.*, *submitted.*

Chapter 3 Hybridization Behavior of Mixed DNA/Alkylthiol Monolayers on Gold: Characterization by SPR and ^{32}P-Radiometric Assay

Reprinted with permission from: P. Gong, C.-Y. Lee, L.J. Gamble, D.G. Caster and D.W. Grainger, Analytical Chemistry **2006**, *in press*

This dissertation chapter contains the manuscript of a full paper published in *Analytical Chemistry*. The manuscript was written by Ping Gong and Chi-Ying Lee, and edited by Lara J. Gamble, David G. Castner and David W. Grainger. This chapter describes DNA density quantification of DNA/mercaptoundecanol mixed adlayers formed on gold by ^{32}P-radiometric assay and the hybridization performance of these mixed adlayers in buffer and serum dilutions monitored with SPR. The DNA adlayers on gold have been thoroughly characterized previously and reported in a companion paper shown as Appendix A. The SPR experiments were planned and initiated by Ping Gong and Chi-Ying Lee and finished by Chi-Ying Lee at the University of Washington.

Hybridization Behavior of Mixed DNA/Alkylthiol Monolayers on Gold: Characterization by SPR and ^{32}P-radiometric Assay

Ping Gong, Chi-Ying Lee, Lara J. Gamble, David G. Castner and David W. Grainger

3.1 Abstract

Nucleic acid assay from complex biological milieu is attractive but currently difficult and far from routine. In this study, DNA hybridization from serum dilutions into mixed DNA/mercaptoundecanol (MCU) adlayers on gold was monitored by surface plasmon resonance (SPR). Immobilized DNA probe and hybridized target densities on these surfaces were quantified using ^{32}P-radiometric assays as a function of MCU diluent exposure. SPR surface capture results correlated with radiometric analysis for hybridization performance, demonstrating a maximum DNA hybridization on DNA/MCU mixed adlayers. The maximum target surface capture produced by MCU addition to the DNA probe layer correlates with structural and conformational data on identical mixed DNA/MCU adlayers on gold derived from XPS, NEXAFS and fluorescence intensity measurements reported in a related study (Appendix A: *Lee et al., Anal. Chem., 2006, in press*). MCU addition into the DNA adlayer on gold also improved surface resistance to both non-specific DNA and serum protein adsorption. Target DNA hybridization from serum dilutions was monitored with SPR on the optimally mixed DNA/MCU adlayers. Both hybridization kinetics and efficiency were strongly affected by non-specific protein adsorption from complex milieu even at a

minimal serum concentration (e.g., 1%). No target hybridization was detected in SPR assays from serum concentrations above 30%, indicating non-specific protein adsorption interference of DNA capture and hybridization from complex milieu. Removal of non-signal proteins from nucleic acid targets prior to assay represents a significant issue for direct sample-to-assay nucleic acid diagnostics from food, blood, tissue, PCR mixtures and many other biologically complex sample formats.

3.2 Introduction

Nucleic acid and related microarray assay technology has promised a revolution in bioassay performance and bioanalytical capabilities.[1] Despite much hyperbole about potential applications, this technology remains primarily a research format, with only one clinical application approved to date[2], and many unanswered questions regarding specific analytical chemistry issues, including assay repeatability, reproducibility, sensitivity, correlation of signal to sample abundance, and reliability to predict disease conditions.[1,3] Substantial effort has produced new information on aspects of DNA surface immobilization, array fabrication variables, target surface capture dynamics, hybridization efficiencies and assay signal:noise variables on both commercial microarray slides[1,4-7] and model surface formats, including gold[8-14], silicon[15,16] and newly developed polymer coatings[17].

In a companion article (Appendix A)[18] we evaluated the effects of a short alkylthiol [11-mercapto-1-undecanol, (MCU)] surface diluent on the surface chemistry, density, and orientation of thiolated-ssDNA oligomer probes adlayers on gold. X-ray photoelectron spectroscopy (XPS), fluorescence intensity measurements and near-edge X-ray absorption fine structure spectroscopy (NEXAFS) were used to determine the

composition, density, and orientational changes of these adsorbed DNA monolayers as a function of MCU diluent thiol exposure, co-adsorption and DNA surface displacement. As MCU molecules first incorporate into pre-adsorbed DNA monolayers, DNA oligomers adopt a more upright orientation, possibly due to MCU displacement of DNA nucleotide base amine groups from the gold interface.[18] At longer MCU backfill times thiolated-ssDNA surface concentration steadily decreases, suggesting competitive displacement by MCU diluent.

In this contribution, the molecular densities of these DNA/MCU mixed thiol adlayers on gold are further investigated and correlated with their DNA hybridization efficiencies using radiometric ^{32}P-labeling, surface target capture and SPR real-time assays. Hybridization results from both assay methods demonstrate maximum target hybridization after short-term exposure of pre-adsorbed ssDNA surfaces to MCU diluent short chain thiols to create mixed co-adsorbed films on gold. This suggests that the thiol diluent changes the molecular conformation of pre-adsorbed oligo-DNA probes on gold, providing increased accessibility to incoming target DNA. Among several possible explanations for this effect, two more likely mechanisms include either that (1) adsorbing small molecule MCU diluent alters the adsorbed ssDNA probe conformation *in situ* to enhance hybridization capabilities, or (2) MCU diluent adsorption displaces a fraction of pre-adsorbed ssDNA in a time-dependent manner, resulting in reduced amounts of surface-bound probe DNA, reduced steric issues and reduced charge density, enhancing dsDNA duplex formation on the surface. In general, maximum target hybridization results from an optimum DNA probe density that provides high target capture efficiency with minimum electrostatic blockade[19,20] and steric hindrance of DNA target binding.

This optimum DNA adlayer composition on gold is further explored by monitoring DNA hybridization from complex milieu (serum dilutions) with SPR. Addition of MCU diluent thiol into the DNA monolayer improves surface resistance toward non-specific adsorption of ssDNA, thereby increasing the probe hybridization efficiency. Results of DNA hybridization in various serum dilutions show that both hybridization kinetics and efficiency are adversely affected by non-specific protein adsorption, even at minimum serum concentration of 1 vol%, compared to target capture from pure buffer.

3.3 Experimental section

Materials. Sodium hydroxide, sodium chloride, and mercaptoundecanol (MCU, 97% purity) were purchased from Sigma-Aldrich (St. Louis, MO) and used as received. The buffer, denoted as 1 M NaCl-TE, used for both solution DNA probe assembly and DNA target hybridization, contained 1.0 M NaCl (Fisher, Fair Lawn, NJ), 10 mM Tris-HCl (Sigma, St. Louis, MO), and 1 mM ethylenediaminetetraacetic acid (EDTA, Fisher) adjusted to pH 7.0 by adding 1.0 M NaOH. Fetal bovine serum (FBS, Premium, US Origin, Hybridoma Screened, 14-901F, Lot 01103197, total protein 3.5-6 g/dl) was purchased from Cambrex (Baltimore, MD), carefully aliquoted and diluted with Millipore H_2O by volume% and frozen at –20°C for storage, and further diluted with 1M NaCl-TE just prior to hybridization experiments. DNA oligonucleotides were purchased from TriLink Biotechnologies (San Diego, CA); all oligonucleotides were HPLC-purified for highest purity.[21] The oligonucleotide sequence 5'-CTGAACGGTAGCATCTTGAC-3' was selected because it forms a stable duplex with its complement at room temperature,

with minimum interference due to self-complementarity or secondary structure.[22,23] Table 3.1 lists all oligonucleotide sequences and modifications involved in this work.

Table 3.1 Oligonucleotide Sequences

Description	5' modification	Oligonucleotide Sequence	3' modification
probe sequence for DNA SAMs preparation	$HS-(CH_2)_6-$	CTGAACGGTAGC-ATCTTGAC	
target sequence for hybridization		GTCAAGATGCTA-CCGTTCAG	
non-complementary sequence used as controls		CTGAACGGTAGC-ATCTTGAC	
probe sequence for density quantification	$HS-(CH_2)_6-$	CTGAACGGTAGC-ATCTTGAC	$-^{32}P$-dATP
target sequence for density quantification	$^{32}P-$	GTCAAGATGCTA-CCGTTCAG	
non-complementary sequence used as controls in density quantification	$^{32}P-$	CTGAACGGTAGC-ATCTTGAC	

Radiometric assay of probe and target DNA interactions on gold surfaces. Probe immobilization and target hybridization densities on gold as a function of MCU surface exposure were measured using radiometric methods. Thiolated DNA probes were radiolabeled on the 3' ends with α-^{32}P-ddATP (Amersham Biosciences, Piscataway, NJ) using terminal transferase according to kit instructions (Roche Diagnostics, Indianapolis, IN).[8] DNA targets were labeled on the 5' ends with γ-^{32}P-ATP (Amersham Biosciences, Piscataway, NJ) using T4 polynucleotide kinase according to kit instructions (Promega, Madison, WI).[10] Both probe and target DNAs were purified with oligo mini-spin columns (Roche) after ^{32}P-radiolabeling. ^{32}P-radiolabeled DNA were quantified using a calibrated Tri-Carb 1500 liquid scintillation analyzer (Packard, Meriden, CT) and

subsequently diluted with non-radiolabeled DNA analogs in solution for surface probe immobilization and target hybridization.

Gold substrates were prepared by thermal evaporation of 100 nm of Au onto a 10 nm Cr adhesion layer using an Auto306 Coating System (Edwards, Wilmington, MA) on commercial semiconductor-grade silicon oxide wafer supports. Gold substrates were then cleaned with O_2 plasma (5 min, 100 W, 0.1 torr) just prior to immersion into DNA probe solutions. Pure DNA monolayers were prepared by immersing freshly gold-coated substrates in 1 μM HS-ssDNA solutions in 1 M NaCl-TE buffer (1 M NaCl, 10 mM Tris-HCl, 1 mM EDTA, pH 7.4, Fisher, Fair Lawn, NJ) for 5 hours. After HS-ssDNA assembly, samples were rinsed with Millipore-grade water for 15 seconds to remove loosely bound HS-ssDNA. These DNA-adsorbed samples were then immersed in 10 μM MCU (97% purity, Sigma-Aldrich) diluent thiol solution (in water) for backfill times ranging from 30 minutes to 18 hours. After the specified MCU backfill-time, samples were removed from the solutions and rinsed thoroughly in Millipore-grade water for 15 seconds then blown dry with N_2. The resulting probe-immobilized gold samples were immersed into hybridization buffer (1 M TE-NaCl, pH 7.0) for 90 min to simulate possible probe surface desorption losses during actual hybridization in TE-NaCl. Probe samples were then rinsed with Millipore-grade water for 15 seconds and dried with N_2. Hybridization of target DNA was performed at room temperature with 1 μM total target DNA concentration in 1 M TE-NaCl hybridization buffer for 90 min under static conditions. Hybridized samples were then further rinsed with hybridization buffer for 15 seconds and dried with N_2. Samples were exposed to a storage phosphor imager (Amersham Biosciences, Piscataway, NJ) for surface radioactivity quantitation. Gray-

scale pixelated radiographic images were obtained using STORM™ and analyzed by ImageQuant software (Amersham Biosciences). Quantitation of sample DNA surface density using gray-scale image analysis was performed by constructing ^{32}P-calibration curves for each labeling reaction as described by Steel et al.[8] DNA surface density values were averaged from three individual experiments. Radiolabeled non-thiolated probe DNA was diluted with non-radiolabeled thiolated probe DNA and assembled onto gold as a probe control. Radiolabeled non-thiolated probe DNA without terminal thiol was also diluted with non-radiolabeled probe and used as a target control (non-complementary to itself) in hybridization experiments.

Surface plasmon resonance (SPR). SPR studies were conducted on low fluorescence SF14 glass slides (Schott Glass Technology, Durea, PA) coated with 2 nm Cr and 50 nm gold (99.99%), then modified with DNA probe and MCU diluent molecules using methods and conditions described in a companion article (Appendix A)[18]. Briefly, probe immobilization was performed with 1 μM thiolated DNA probe in 1 M TE-NaCl at pH 7.4 for 5 hours followed by various timed exposures (0.5 to 18 h) to 10 μM MCU solutions in Millipore H_2O. After the specified MCU exposure-time, samples were removed from the solutions and rinsed thoroughly in Millipore H_2O for 1 minute. Samples were blown dry with N_2 and stored under N_2 until analysis.

The home-built SPR liquid sensing system used in this study has been described and characterized in more detail elsewhere.[24] Briefly, this SPR system is set up with a planar prism (Kretschmann) configuration. The glass side of the gold-coated substrate is index-matched to the prism while the functionalized surface is mechanically pressed against a milled Teflon flow cell. A polychromatic light beam is passed through the

prism and the backside of a gold-coated substrate to excite surface plasmon waves at the metal-dielectric interface. The reflected light is analyzed with a spectrograph. During SPR measurements, buffer (1 M TE-NaCl) and target ssDNA solutions (1 μM complementary and non-complementary ssDNA in 1 M TE-NaCl buffer) were sequentially delivered to the SPR probe-immobilized surface at a flow rate of 50 μl/min. Interactions at the gold surface were observed by monitoring the wavelength shift of the SPR reflected minimum. Data quantification was performed by first converting the measured wavelength shift into effective adlayer thicknesses (defined as the thickness that the same amount of adsorbate per unit area would have if packed at its bulk density without any trapped solvent in the adlayer), then by subsequent conversion into absolute adsorbate coverages (e.g., molecues/cm^2 of hybridized target DNA) using the method published by Jung et. al.[24] This method requires a simple calibration of the instrumental sensitivity based on SPR response to changes in bulk solution refractive index, the known index of refraction for the adsorbate and buffer, and an exponential optical sampling depth estimated from Fresnel equations. The effective adlayer thickness, d, was calculated using the equation:

$$d = \left(\frac{l_d}{2}\right)\left[\frac{\Delta R}{S(\eta_a - \eta_s)}\right]$$

where l_d is the decay length of the evanescent field near the gold surface (362 nm), ΔR is the measured reflected wavelength shift, S is the SPR system sensitivity factor (3500 reflected wavelength shift/RIU obtained by monitoring the SPR wavelength shift as a series of ethanol/water calibration solutions with varying refractive index of 1.333 to 1.3425 were injected over the Au surface following the procedure described in reference

24), η_a is the index of refraction for the DNA adsorbate (1.7[25,26]), and η_s is the buffer index of refraction (1.343). Note that the refractive indices of the calibration solutions and buffer were measured on an Abbe-3L refractometer (Bausch & Lomb, Depew, NY). Once the effective thickness of the adsorbed layer is calculated, the SPR surface coverage of adsorbed molecules can be estimated by multiplying *d* by the density of the pure adsorbate[24] using a density value of 1.7 g/cm^3 for hybridized dsDNA[27]:

Adsorbed DNA density (molecules/cm^2) = [effective thickness (*d*) (cm)] • [bulk density (*N*) (molecules/cm^3)]

3.4 Results and Discussion

Determination of DNA Probe Surface Densities by ^{32}P Radiometric Assays. Surface densities of pre-adsorbed thiolated oligoDNA single-strand probes as a function of MCU diluent 'backfill' time were quantified using the ^{32}P radiometric method described in the experimental section. Results are shown in Table 3.2. Maximum probe

Table 3.2 Surface densities of thiolated ssDNA probes and hybridized ssDNA targets as a function of MCU diluent backfill time as determined by ^{32}P radiometric and SPR methods.

10μM MCU Backfilling Time (hours)	Probe Density (10^{13} molecules/cm^2)	Target Density from ^{32}P-labeling (10^{12} molecules/cm^2)	Target Density from SPR (10^{12} molecules/cm^2)
0	4.4 (± 0.4)	4.7 (± 0.3)	3.7 (± 0.5)
0.5	3.8 (± 0.4)	7.7 (± 0.1)	5.4 (± 0.8)
1	3.6 (± 0.5)	8.9 (± 0.1)	7.0 (± 0.4)
2	3.1 (± 0.2)	7.6 (± 0.1)	6.4 (± 0.5)
5	2.3 (± 0.4)	4.4 (± 0.5)	4.5 (± 0.4)
18	1.7 (± 0.4)	2.0 (± 0.7)	2.2 (± 0.8)

coverage was observed to be 4.4 (+/-0.4) x10^{13} probes/cm^2 for pure thiol-ssDNA adlayers without MCU backfill. Previous modeling work has calculated density for a close-

packed ssDNA strand with estimated cross-sectional radius of 0.6-0.7 nm/strand oriented normal to the surface to be $8x10^{13}$ probes/cm^2, excluding effects of counterions and hydration.[8] Experimental values of approximately $4x10^{13}$ probes/cm^2 have been reported for probes shorter than 24 nucleotides[8], with standard deviation of approximately 10%. Probe ssDNA density of $4.4x10^{13}$ probe/cm^2 detected here agrees well with these previous values, presenting the same level of standard deviation from three independent determinations. MCU backfill was shown to reduce pre-adsorbed DNA surface probe density by surface site competition and probe dilution in a time-dependent manner.[10,18] As shown in Table 3.2, adlayer backfilling from a 10 μM MCU solution gradually replaced ssDNA probe molecules with increasing backfill time, eventually reaching a DNA probe density of ~$1.7x10^{13}$ probes/cm^2 after 18 hours. This MCU mixing-DNA displacement trend on gold over time has been fully characterized in a companion work (Appendix A).[18] All ssDNA probe density values examined in this context were collected after 90 min incubation in hybridization buffer without any target DNA present to simulate possible probe loss encountered during hybridization.[28]

Trends observed from the ^{32}P radiolabel surface density studies and previously reported XPS data on identically prepared surfaces[18] (i.e., XPS N1s and P2p DNA photoelectron signals) for immobilized DNA probe and mixed DNA/MCU adlayers on gold are in close agreement (see Figure 3.1). DNA probe immobilization exhibits a maximum density with no MCU backfill that steadily decreases as MCU diluent molecules incorporate into the pre-adsorbed DNA adlayer with increasing incubation time. This ^{32}P-XPS DNA signal correlation for surface density allows a new, convenient route to XPS-based surface density determinations of DNA adsorbed on gold[18] using

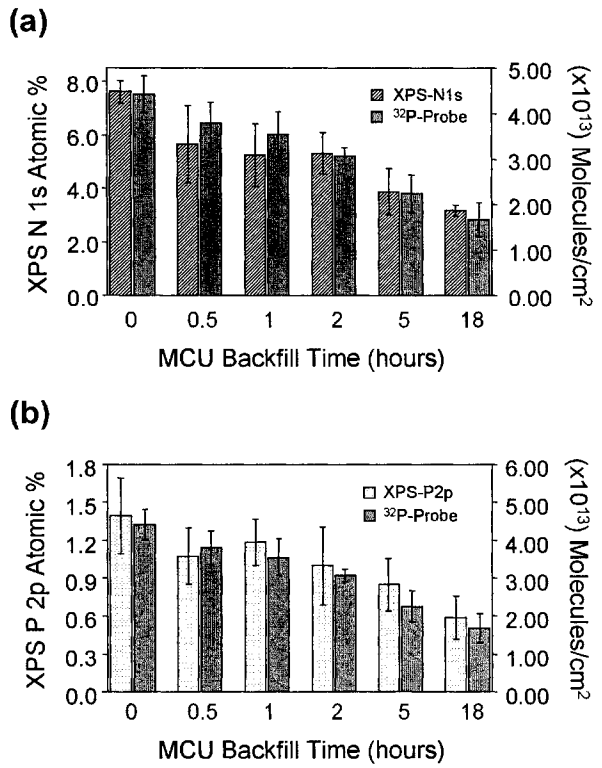

Figure 3.1 Correlation of ^{32}P-radiolabeled DNA surface density determinations with previously reported XPS data on gold surfaces from a companion paper (Appendix A)[18] (i.e., XPS N1s signal correlations shown in Fig. 1A and XPS P2p signal correlations from identical adlayers shown in Fig. 1B) for DNA probe immobilization on pure DNA and mixed DNA/MCU monolayers. The two measurements display close agreement. Probe immobilization density is maximum in pure DNA adlayers (4.4×10^{13} probes/cm^2), steadily decreasing as MCU diluent molecules initially incorporate into the DNA adlayer and then begin to displace probe DNA from the gold surface with increasing backfill time.

standard curves based on more-sensitive radiometric measurements. Such an approach for DNA surface density determinations has also been successful for oligoDNA printed probe immobilization comparisons on commercial microarraying surfaces.[7]

SPR and ^{32}P Measurements of DNA Target Hybridization from Buffer on Pure DNA and Mixed DNA/MCU adlayers. SPR has been frequently used to detect the binding of biological molecules such as DNA[13,14,29-33] and proteins[34-39] onto chemically and biologically modified surfaces without the need for target labeling and complex

sample preparation. Here, SPR was used to report target DNA hybridization efficiencies to pure and mixed DNA monolayers, comparing parallel experiments in pure buffer and serum dilutions (see next section), as well as effects of MCU backfill on DNA hybridization. To test target hybridization specificity to surface-bound ssDNA probes, SPR responses to both complementary and non-complementary DNA target were measured. As shown in Figures 3.2a and b, striking differences are observed in target hybridization efficiencies when different DNA/MCU mixed adlayers were hybridized. MCU backfill not only affects hybridization efficiency but also target capture kinetics. Various DNA surface coverages calculated from these SPR response curves in Figure 3.2 are listed in the farthest right (SPR) column of Table 3.2.

For the pure DNA probe surfaces (Figure 3.2a, step1), SPR response to the non-complementary ssDNA target indicates a small amount of non-specific ssDNA binding ($\sim 0.7 \times 10^{12}$ molecules/cm^2) to the ssDNA probe adlayer surface. This is evidenced by the observed increase in the reflected SPR wavelength above the baseline after the probe surface was rinsed by replacing the non-complementary ssDNA with pure running buffer (Figure 3.2a, step 2). Subsequent injection of complementary DNA target (Figure 3.2a, step 3) followed by buffer rinse (Figure 3.2a, step 4) produced a much higher SPR wavelength shift ($\sim 3.7 \pm 0.45 \times 10^{12}$ molecues/cm^2), indicating hybridization of surface-bound ssDNA probes with complementary ssDNA target. While the magnitude of SPR wavelength shift is indicative of hybridization efficiency, the slope of the mass loading SPR curve is indicative of the rate of hybridization to the probe surface. As shown in Figure 2a, target hybridization occurs slowly on the pure DNA probe surface, as the SPR

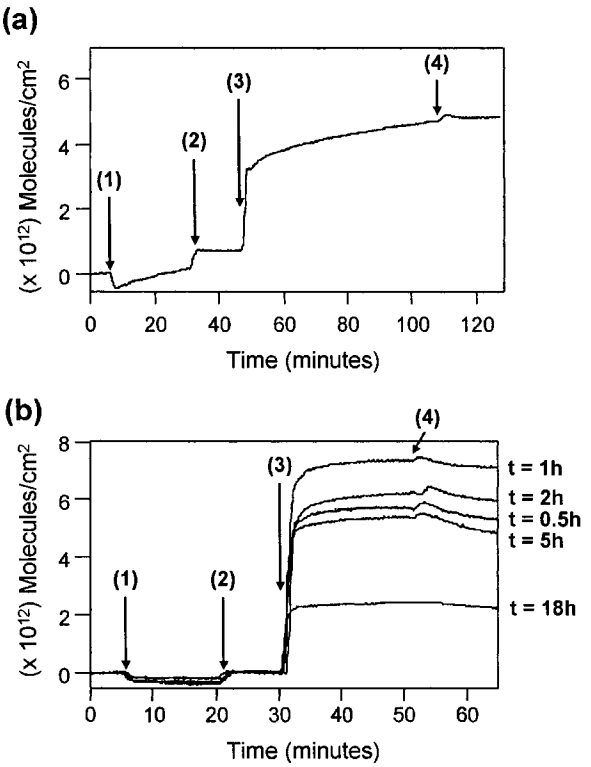

Figure 3.2 Real-time SPR measurement of target DNA hybridization on (a) pure DNA and (b) mixed DNA/MCU adlayers from buffer (1 M TE-NaCl, pH 7.0) demonstrating the effects of MCU diluent backfill on DNA target hybridization. Kinetic sensorgram traces were characterized by the following common step-wise features: a measurement baseline was established by introducing running buffer to the probe surface (1). Then non-complementary DNA (1 μM) in running buffer was injected to test non-specific target binding onto the probe surface (2). As the non-complementary DNA adsorption approached saturation, the non-complementary DNA solution was replaced with pure running buffer to re-establish the baseline (3). Complementary DNA target (1 μM) was then injected to determine amounts of hybridization (4). As DNA hybridization approached saturation, the complementary DNA solution was replaced with pure running buffer to rinse away loosely bound DNA molecules from the probe surface. Data indicate that target hybridization reaches a maximum at 1h MCU backfill (surface density of 3.55×10^{13} molecules/cm^2).

curve for complementary ssDNA does not reach saturation even after 60 min of target incubation.[40]

In contrast, when MCU was incorporated into the DNA adlayer before hybridization, non-specific binding of non-complementary ssDNA (Figure 3.2b) to any of

the DNA/MCU probe surfaces was not detected. This suggests that the MCU backfill effectively blocks unoccupied surface sites to prevent non-specific ssDNA surface binding, thereby increasing hybridization selectivity to target. Furthermore, target hybridization to the mixed DNA/MCU probe surfaces also reached saturation much more rapidly than to the pure DNA probe surface (~ 10 minutes, Figure 3.2).

The observed increase in hybridization kinetics as well as hybridization efficiency on surfaces with 30 minutes of MCU backfill (for which ^{32}P-labeling results indicate DNA surface probe densities are comparable to the non-backfilled pure DNA adlayer, see Table 3.2) indicates that more than simply ssDNA surface density may be controlling hybridization efficiency of surface-bound ssDNA. Orientation studies of probe DNA chains in identical adlayers using NEXAFS and fluorescence intensity measurements, as discussed in the companion article (Appendix A)[18], demonstrate that initial MCU addition into the pure DNA adlayer removes non-specifically adsorbed DNA nucleobase amines from gold surface sites and reorients the probe DNA chains to a more upright configuration. With nucleobase amines detached from the gold surface, probe DNA molecules are more likely single point end-tethered, therefore more configurationally mobile than those in a pure DNA monolayer. This produces DNA/MCU mixed adlayers that are more accommodating for target DNA molecules to approach and to hybridize. Amounts of target DNA hybridized onto these mixed DNA/MCU probe surfaces, as calculated from SPR measurements, range from 2.2 to 7.0 x 10^{12} molecues/cm^2 depending on the ssDNA probe densities (Table 3.2). SPR results indicate that target hybridization signal reaches a maximum on surfaces with 1 h MCU diluent backfill (a surface ssDNA probe density of 3.6 x 10^{13} molecules/cm^2), after which target

hybridization signal decreases due to significant MCU displacement of DNA probes off the adlayer surface, as measured by the ^{32}P assays.

To accurately determine the absolute amounts of hybridized DNA targets on the different adlayer surfaces, surface densities of hybridized DNA target as a function of MCU backfill time were also measured using ^{32}P radiometric methods. Valid comparisons of probe and target densities were ensured using non-radiolabeled and radiolabeled DNA probe surfaces made with identical DNA preparations. Radiolabeled probe surface densities were measured and identical non-radiolabeled probe surfaces were subsequently hybridized with ^{32}P-labeled target. Results are shown in Table 3.2. At the highest adlayer probe density (pure ssDNA, 4.4 $x10^{13}$ probes/cm^2), hybridization of $4.7x10^{12}$ targets/cm^2 is observed, a hybridization efficiency of 11%. As DNA probe surface density decreases with increasing MCU backfilling time, target hybridization reaches a maximum value at intermediate ssDNA probe density, then decreases as probe density decreases further. Maximum amounts of hybridization are achieved on the 1 h MCU-backfilled surface (DNA probe density = $3.6x10^{13}$ molecules/cm^2), yielding $8.9x10^{12}$ targets/cm^2. Figure 3.3 shows close agreement of trends observed from radiometric ^{32}P assay and SPR hybridization data for target hybridization. Lower absolute target densities estimated from SPR compared to ^{32}P quantitation measurements can be explained by the use of dsDNA bulk density for estimating surface coverage, while the actual SPR DNA adlayer is primarily ssDNA, known to have higher density than dsDNA.[41] In addition, this trend concurs with results previously reported by Herne and Tarlov,[10] where a maximum value of $5.7x10^{12}$ targets/cm^2 was observed on similarly prepared surfaces (dual probe-target ^{32}P-labeling studies were not reported). Because

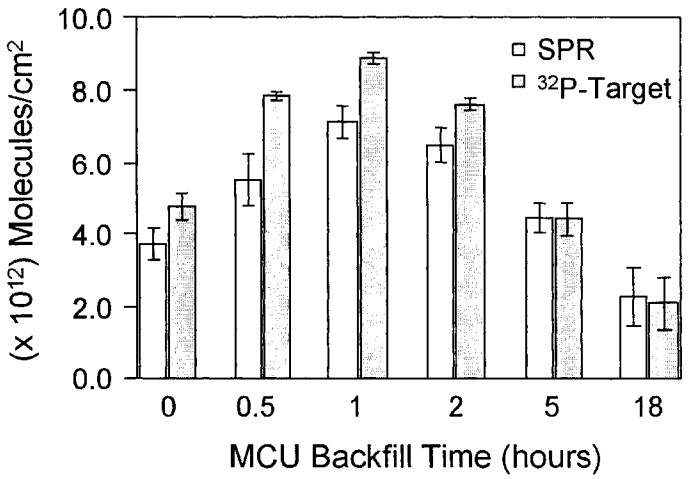

Figure 3.3 Correlation of ^{32}P-DNA radiolabeling and SPR data on gold surfaces for target hybridization on pure DNA and mixed DNA/MCU adlayers. The two methods display close agreement. Target hybridization is not maximized at maximal DNA probe density in the pure DNA adlayer. Rather, hybridization reaches maximum at 1h MCU diluent backfill of the probe surface (8.9×10^{12} targets/cm^2). With further MCU backfilling exposure, the amount of target hybridization decreases due to decreased DNA probe density (i.e., significant DNA probe displacement from the surface).

both DNA adlayer and target were ^{32}P-labeled in matched experiments, target capture densities can be converted to hybridization efficiencies as a function of MCU diluent exposure. Pure thiolated-DNA probe surfaces show 11% efficiency, increasing to a maximum of 25% at intermediate probe density then decreasing at lower probe density. Lower target hybridization efficiency at higher probe density is explained by target repulsion from steric effects (e.g., molecular crowding) as DNA probe density reaches a maximum, and corresponding Coulombic surface blockade produced by excess polyanion charge density residing in the dense probe layers.[14,19,20] As these two effects are inter-related, it is difficult to distinguish individual contributions to DNA-DNA surface repulsion. As the hybridization buffer is 1 M NaCl, double layer electrostatic repulsion should be minimized by charge screening (i.e., Debye length shorter than the tethered DNA probe length).

Hybridization efficiency is also affected significantly by immobilized DNA probe orientation and resulting accessibility to target.[42] Using 0.34 nm as the axial base rise and 2 nm as double helix diameter[43], a 13.60 nm^2 low-density footprint was calculated for a dense-packed DNA 20mer lying *flat* on the surface, corresponding to an ideal double-strand density of $7.4x10^{12}$ duplexes/cm^2; a 3.14 nm^2 high-density footprint for dense-packed double-stranded DNA oriented *perpendicular* to the surface corresponds to $3.2x10^{13}$ duplexes/cm^2. Hence, ssDNA probe densities experimentally realized in the highest-density regime ($4.4 x10^{13}$ probes/cm^2) slightly exceed ideal densities calculated to yield maximum possible hybridization. It is therefore reasonable to presume that the pure thiolated DNA adlayers are densely packed, and that steric, electrostatic and orientational influences likely contribute to the low hybridization yields observed. Hybridization efficiencies on similarly prepared gold-DNA probe surfaces and on silicon substrates have been previously reported. Hybridization efficiencies close to 100% have been reported for DNA-modified gold and silicon substrates when immobilized probe density was below $5x10^{12}$ probes/cm^2 and probe-substrate interactions were not strong.[13,16,43,44]

Direct comparisons of probe and target densities have been conducted using fluorescent-labeling[15,44], chronocoulometry[43] and XPS[16]. In general, these other studies have shown higher hybridization efficiencies as a function of probe surface density. However, few studies actually directly determined or compared absolute probe densities at high precision with direct hybridization efficiencies from target capture to the same or identically matched surfaces. Previous studies frequently report calculated hybridization efficiencies from assumptions based on indirect or separate measurements of probes and

targets. For example, measurements of DNA surface coverage using fluorescence methods were indirect, either by quantification of fluorescently labeled DNA removed from surface[44] or by determination from observed decrease in bulk DNA concentration[15]. In both of these cases, non-matched or mis-matched physisorption was not clearly excluded from the interpretation. Measurement of surface coverage using XPS was more direct than fluorescence, but involved subtraction of significant background control numbers from sample densities of similar signal magnitudes.[16] Specifically, radiometric comparisons have been previously employed only separately and indirectly in surface DNA probe or target density determinations[8,10,45], but not directly for both using identically prepared substrates and samples in parallel. To our knowledge, this is the first direct comparison of matched, identical surface probe and target assays using the sensitive radiometric method. Lower hybridization efficiencies detected here (not approaching 100%) are based on determining both probe and target on identical surfaces at high sensitivity. We note that the hybridization efficiency depends on the specific DNA sequences and lengths used in complementary pairs.

Previously, ssDNA probe densities on similarly prepared mixed adlayer surfaces on gold have been quantified by Steel using ^{32}P-radiolabeling.[8] Pure DNA probe surface densities agree well between the two studies, but rather significant differences in hybridization performance are observed. Maximum target hybridization has been observed on DNA probe surfaces densities ranging from $1.5 \times 10^{12} - 2.1 \times 10^{13}$ probe/cm^2 by SPR[10,13], chronocoulometry[43], XPS[16] and fluorescence[15,44] methods, with hybridization efficiencies ranging from 70%-100% as DNA probe densities drop below 4×10^{12} probes/cm^2. Vainrub and Pettitt modeled the effect of possible surface

electrostatic blockade of target capture, assuming oligonucleotides 25 bases long: in this model, suppression of hybridization begins as low as 10^{12} probes/cm^2 surface density.[19,20] This is well below experimental densities for pure thiolated probe DNA adlayers on gold. No theoretical studies of probe adsorption density maxima are known, and are likely difficult to accurately model since most experimentally created high density ssDNA probe surfaces (i.e., ~$4x10^{13}$ probes/cm^2 as reported here and by others[8,11]) are made under high ionic strength (~1M salt) conditions. Theoretical studies cannot yet adequately consider high ionic strength, counterions or local surface configurational effects that play a significant role in DNA duplex formation and stability. In fact to date, theoretical models for DNA on surfaces often treat DNA as a blob, sphere or infinite chain with limited abilities to interact with charges, either in solution (i.e., target), on the surface (i.e., other probes), or from dissolved small ions.[19,20,46-50] It is clear that a full understanding of molecular requirements for hybridization on dense ssDNA surfaces requires further work.

Practically, it is difficult to understand why limited hybridization efficiency is observed experimentally in these adlayers. Since two DNA molecules in a duplex (dsDNA) occupy slightly less surface area than two non-associated, but densely packed, separate ssDNA molecules, a probe density of $2x10^{13}$ probes/cm^2 (e.g., achieved experimentally by MCU replacement of 50% of the pure DNA adlayer of ~$4x10^{13}$ probes/cm^2) in theory, should be able to experimentally produce an ultimate duplex density of $2x10^{13}$ duplexes/cm^2 (i.e., 100% hybridization efficiency). That is, the product of the hybridization, resulting in $4x10^{13}$ oligos/cm^2 (as $2x10^{13}$ duplexes/cm^2), has the identical charge-mass ratio as the original stable thiol-assembled DNA adlayer on gold

($4x10^{13}$ probes/cm^2), suggesting that the electrostatic blockade or steric arguments limiting surface density would guide both situations.

SPR Measurement of Target Hybridization from Serum. To provide a more realistic evaluation of the probe surface performance for microarray applications that might eventually seek to measure target directly from sample (i.e., from food, cell culture, PCR mix, or blood), SPR was used to investigate DNA hybridization on mixed DNA/MCU adlayer surfaces directly from serum-containing solutions. Using experimental controls, DNA hybridization from serum versus both non-specific DNA and serum protein adsorption onto DNA probe surfaces was determined. Mixed DNA/MCU surfaces with maximal target hybridization from pure buffer (i.e., the 1h MCU backfilled DNA adlayer, probe surface density of 3.55 x 10^{13} molecules/cm^2) were used for SPR serum assays. Sequential SPR experimental steps are described in Figure 3.4. To ensure that all DNA probe surfaces exhibit the same hybridization specificity, SPR response to both complementary and non-complementary DNA targets is measured using the same procedure described in the previous SPR section (*vida infra*, Figure 3.2, steps 1-4). After hybridization with complementary targets, DNA/MCU probe surfaces are regenerated by injecting 0.5 M NaOH into the flow cell (Figure 3.4, step 5). SPR response to the NaOH rinse is out of the range of the plotted SPR wavelength values, but after the NaOH solution is replaced with pure running buffer (Figure 3.4, step 6), the SPR signal wavelength for the probe surface returns to a value close to the original baseline measured prior to injection of the non-complementary DNA. This suggests that the NaOH rinse removes only complementary target DNA molecules from the hybridized dsDNA sequences on the sensing surface, not the ssDNA adlayer probe molecules. The

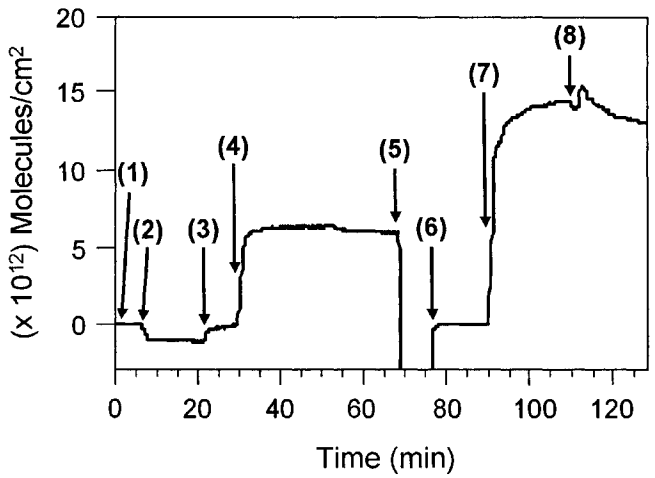

Figure 3.4 SPR kinetic traces showing the process of sensor surface regeneration and exposure to serum-based DNA hybridization assay. After hybridization with the complementary targets (following experimental steps 1-4 as described in Figure 3.2), DNA/MCU probe surfaces are regenerated with 0.5 M NaOH (labeled step 5). SPR response to the NaOH is out of range of the plotted wavelength values. After the NaOH solution was replaced with the original running buffer (6), the detected wavelength returns to a value close to the original baseline value measured prior to injection of the non-complementary DNA. The SPR probe surface is subsequently exposed to either the complementary or non-complementary ssDNA in serum dilutions (7) and rinsed with pure buffer when adsorption saturation was reached (8).

regenerated DNA probe surface is subsequently exposed to either the complementary or non-complementary ssDNA in serum (Figure 3.4, step 7) and rinsed with pure buffer once signal saturation was attained.

SPR results for DNA hybridization performed in assay solutions containing 0, 1, 30, and 100% serum are presented in Figure 3.5a-d. Note that the SPR response to the more concentrated serum solutions (i.e., > 30%) is out of range of the plotted wavelength values due to significant increase in the bulk refractive index. Although previous reports demonstrated that DNA probe surfaces treated with a co-adsorbing diluent thiol showed no non-specific adsorption when exposed to highly purified complementary ssDNA solutions[12, 13], this is not the case in serum. Comparison of Figure 3.5a with 3.5b

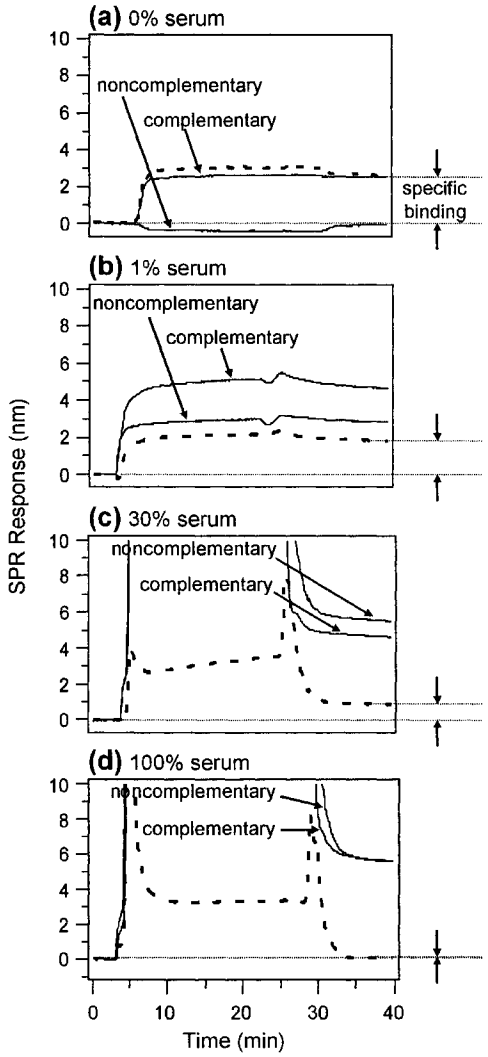

Figure 3.5 SPR DNA hybridization results for target capture assays performed from solutions containing (a) 0%, (b) 1%, (c) 30%, and (d) 100% serum. The curves show responses from the SPR when probe surfaces were exposed to complementary and non-complementary DNA in n% serum at approximately 5 min and rinsed with buffer when adsorption saturation was reached at approximately 30 min. DNA hybridization is obtained by subtracting the SPR response for the non-complementary DNA in *n*% serum from the SPR response for the complementary DNA in *n*% serum solution (dashed line). Note that the SPR response to the more concentrated serum solutions (i.e., > 30%) is out of range of the plotted wavelength values due to significant increase in the bulk refractive index.

suggests that hybridization kinetics and efficiency of probe surfaces are both strongly affected by non-specific protein adsorption, even at a minimal serum concentration of 1%,

although the surfaces are resistant to non-specific DNA adsorption from pure ssDNA buffer solution (Figure 3.2b). To determine wavelength shifts due to DNA target hybridization under serum conditions (i.e., SPR signal distinct from protein adsorption), SPR response of the non-complementary DNA in *n*% serum is subtracted from that of the complementary DNA in *n*% serum solution. The hybridization wavelength shifts are shown as dashed lines in Figures 3.5. As seen in Figures 3.5a-d, the amount of target hybridization decreases with increasing serum concentrations, likely due to increasing amounts of non-specific protein adsorption to the probe surface at higher serum concentrations. In 50% and higher serum concentrations, SPR response from complementary DNA solution overlaps the non-complementary DNA SPR response, indicating no detectable hybridization (Figure 3.5d).

DNA target binding hybridization from various serum concentrations is summarized in Figure 3.6. The molecular densities were estimated using the wavelength shift due to DNA hybridization. As seen in Figure 3.6, hybridization efficiency in mixed DNA/MCU surfaces reduces significantly (by approximately 50%) in 15% serum. In 50% serum and higher concentrations, hybridization is detected on the probe surface, likely due to rapid, overwhelming amounts of non-specific protein adsorption. Since the capability to capture target DNA via hybridization directly from complex milieu (e.g., PCR mix, serum, tissue lysates, food and environmental samples) without extensive amplification or purification is desirable for microarray applications, improvements in developing protein-resistant hybridization platforms are necessary for reliable, specific and quantitative detection that minimizes signal aberration caused by non-specific adsorption.

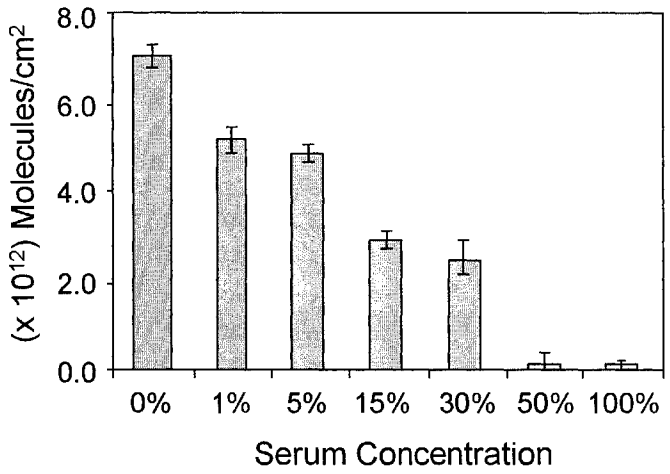

Figure 3.6 Amounts of DNA hybridization from various serum concentrations determined by SPR using the procedure described by Figure 3.5. Hybridization efficiency observed in pure ssDNA buffer solutions is profoundly affected by non-specific protein adsorption, even at a minimal serum concentration of 1%. Hybridization efficiency was significantly reduced (by roughly 50%) from 15% serum, and in 50% serum and higher concentrations, no hybridization was detected on the probe surface due to rapid, overwhelming amounts of non-specific protein adsorption.

3.5 Conclusions

New parallel studies of DNA-surface properties using identically prepared, highly sensitive ^{32}P-labeled immobilized probe and complementary target capture assays were compared with label-free SPR assays. The surface density of immobilized ssDNA probe adlayers strongly influenced hybridization and target capture capabilities. DNA surface densities were controlled using a small molecule diluent (MCU). Radiolabeling methods demonstrated that maximum amounts of DNA target hybridization were achieved on mixed DNA/MCU surfaces where DNA probes were less densely packed than in pure DNA adlayers on gold, and likely oriented more favorably[18]. Tethered probe adlayers exposed to 1h MCU backfilling (3.6×10^{13} probes/cm^2) captured 8.9×10^{12} targets/cm^2, a hybridization efficiency of 25%. Radiolabeled DNA surface densities on gold correlated

well to label-free SPR data on identical systems, providing corroborative support for assay sensitivity and specificity. These results are also consistent with previously reported XPS nitrogen and phosphorus quantification of surface-immobilized DNA probes in identical systems,[18] allowing a convenient basis for XPS-based DNA surface density determinations.[7] Additionally, short-time MCU exposure, while not significantly displacing pre-adsorbed DNA probes from the gold surface, improved DNA target capture efficiencies. This supports other data for orientational influences on adsorbed DNA probe layers by co-adsorbing MCU,[18] perhaps by removing non-specifically adsorbed segments of immobilized DNA from the gold interface and improving their bulk-phase availability for hybridization. SPR hybridization performance on gold-immobilized DNA probe surfaces from buffer supports radiometric data, showing a hybridization optimum after short-term exposure of pure ssDNA adlayer surface to diluent short-chain MCU. In addition, SPR-based DNA hybridization from various serum dilutions demonstrated that MCU addition into the DNA adlayer improved surface resistance to non-specific ssDNA adsorption, increasing specific target hybridization efficiency. Both hybridization kinetics and efficiency of the probe capture surface are strongly affected by non-specific protein adsorption from complex milieu even at a minimal serum concentration of 1%.

While substantial attention has been directed to construction and performance of potential microarraying and biosensing surfaces assaying in simple systems (e.g., single component buffers), less effort has been directed to developing surfaces capable of more practical applications (e.g., direct assay from complex sample milieu). To the best of our knowledge, real-time DNA target surface capture from serum dilutions or relatively

concentrated protein media has not been previously reported, particularly not in a dynamic flow cell format. Results from this study indicate that even at a minimal serum concentration (e.g., 1%), both DNA hybridization kinetics and efficiency of these probe capture surfaces are strongly affected by non-specific protein adsorption from complex assay milieu. Requirements for sample analyte amplification (e.g., PCR) and pre-purification (deliberate sample analyte enrichment and removal of competing, interfering non-analytes) will remain until direct assay is possible with sufficient sensitivity and reliability. Assay performance in complex milieu should become more common to capture assay surface development in order to remove long-standing barriers to improving clinical sensing applications.

3.6 Acknowledgements

Support from NESAC/BIO (NIH P41 EB-2027) and NIH R01 EB-1473 are gratefully acknowledged. Dr. G. Harbers and Dr. C. Campbell are thanked for their technical discussions and assistance with experiments.

3.7 References

(1) Grainger, D. W.; Greef, C. H.; Gong, P.; Lochhead, M. J. In *Microarrays: Methods and Protocols (Method in Molecular Biology),* 2nd ed.; Rampal, J. B., Ed.; Humana Press: Totowa, New Jersey, 2006, in press.

(2) http://www.roche-diagnostics.com/products_services/amplichip_cyp450.html.

(3) Sherlock, G. *Nat. Methods* **2005**, *2*, 329-330.

(4) Ramakrishnanm, R.; Dorris, D.; Lublinsky, A.; Nguyen, A.; Domanus, M.; Prokhorova, A.; Gieser, L.; Touma, E.; Lockner, R.; Tata, M.; Zhu, X.; Patterson, M.; Shippy, R.; Sendera, T. J.; Mazumder, A. *Nucleic Acids Res.* **2002**, *30*, e30/31-e30/12.

(5) Tan, P. K.; Downey, T. J.; Spitznagel, E. L., Jr.; Xu, P.; Fu, D.; Dimitrov, D. S.; Lempicki, R. A.; Raaka, B. M.; Cam, M. C. *Nucleic Acids Res.* **2003**, *31*, 5676-5684.

(6) Gong, P.; Grainger, D. W. *Surf. Sci.* **2004**, *570*, 67-77.

(7) Gong, P.; Harbers, G. M.; Grainger, D. W. *Anal. Chem.* **2006,** *in press.*

(8) Steel, A. B.; Levicky, R. L.; Herne, T. M.; Tarlov, M. J. *Biophys. J.* **2000**, *79*, 975-981.

(9) Steel, A. B.; Levicky, R.; Herne, T. M.; Tarlov, M. J. *Proc. - Electrochem. Soc.* **1999**, *5*, 132-143.

(10) Herne, T. M.; Tarlov, M. J. *J. Am. Chem. Soc.* **1997**, *119*, 8916-8920.

(11) Petrovykh, D. Y.; Kimura-Suda, H.; Tarlov, M. J.; Whitman, L. J. *Langmuir* **2004**, *20*, 429-440.

(12) Wolf, L. K.; Gao, Y.; Georgiadis, R. M. *Langmuir* **2004**, *20*, 3357-3361.

(13) Peterson, A. W.; Wolf, L. K.; Georgiadis, R. M. *J. Am. Chem. Soc.* **2002**, *124*, 14601-14607.

(14) Peterson, A. W.; Heaton, R. J.; Georgiadis, R. M. *Nucleic Acids Res.* **2001**, *29*, 5163-5168.

(15) Jin, L.; Horgan, A.; Levicky, R. *Langmuir* **2003**, *19*, 6968-6975.

(16) Shen, G.; Anand, M. F. G.; Levicky, R. *Nucleic Acids Res.* **2004**, *32*, 5973-5980.

(17) Pirri, G.; Damin, F.; Chiari, M.; Bontempi, E.; Depero, L. E. *Anal. Chem.* **2004**, *76*, 1352-1358.

(18) Lee, C.-Y.; Gong, P.; Harbers, G. M.; Grainger, D. W.; Castner, D. G.; Gamble, L. J. *Anal. Chem.* **2006**, *in press*

(19) Vainrub, A.; Pettitt, B. M. *Phys. Rev. E* **2002**, *66*, 041905/041901-041905/041904.

(20) Vainrub, A.; Pettitt, B. M. *J. Am. Chem. Soc.* **2003**, *125*, 7798-7799.

(21) Lee, C.-Y.; Canavan, H. E.; Gamble, L. J.; Castner, D. G. *Langmuir* **2005**, *21*, 5134-5141.

(22) Mazzola, L. T.; Frank, C. W.; Fodor, S. P. A.; Mosher, C.; Lartius, R.; Henderson, E. *Biophys. J.* **1999**, *76*, 2922-2933.

(23) Forman, J. E.; Walton, I. D.; Stern, D.; Rava, R. P.; Trulson, M. O. *ACS Symp. Ser.* **1998**, *682*, 206-228.

(24) Jung, L. S.; Campbell, C. T.; Chinowsky, T. M.; Mar, M. N.; Yee, S. S. *Langmuir* **1998**, *14*, 5636-5648.

(25) Wu, P. G.; Fujimoto, B. S.; Song, L.; Schurr, J. M. *Biophys. Chem.* **1991**, *41*, 217-236.

(26) Harrington, R. E. *J. Am. Chem. Soc.* **1970**, *92*, 6957-6964.

(27) Darnell, J. E.; Lodish, H. *Molecular Cell Biology*; Scientific American Books: New York, 1990.

(28) Moses, S.; Brewer, S. H.; Lowe, L. B.; Lappi, S. E.; Gilvey, L. B. G.; Sauthier, M.; Tenent, R. C.; Feldheim, D. L.; Franzen, S. *Langmuir* **2004**, *20*, 11134-11140.

(29) Brockman, J. M.; Frutos, A. G.; Corn, R. M. *J. Am. Chem. Soc.* **1999**, *121*, 8044-8051.

(30) Nelson, B. P.; Grimsrud, T. E.; Liles, M. R.; Goodman, R. M.; Corn, R. M. *Anal. Chem.* **2001**, *73*, 1-7.

(31) Smith, E. A.; Wanat, M. J.; Cheng, Y. F.; Barreira, S. V. P.; Frutos, A. G.; Corn, R. M. *Langmuir* **2001**, *17*, 2502-2507.

(32) Shumaker-Parry, J. S.; Zareie, M. H.; Aebersold, R.; Campbell, C. T. *Anal. Chem.* **2004**, *76*, 918-929.

(33) Peterson, A. W.; Heaton, R. J.; Georgiadis, R. *J. Am. Chem. Soc.* **2000**, *122*, 7837-7838.

(34) Xia, N.; Shumaker-Parry, J. S.; Zareie, M. H.; Campbell, C. T.; Castner, D. G. *Langmuir* **2004**, *20*, 3710-3716.

(35) Green, R. J.; Frazier, R. A.; Shakesheff, K. M.; Davies, M. C.; Roberts, C. J.; Tendler, S. J. B. *Biomaterials* **2000**, *21*, 1823-1835.

(36) Pavey, K. D.; Olliff, C. J. *Biomaterials* **1999**, *20*, 885-890.

(37) Green, R. J.; Davies, M. C.; Roberts, C. J.; Tendler, S. J. B. *Biomaterials* **1999**, *20*, 385-391.

(38) Morgan, H.; Taylor, D. M. *Biosens. Bioelectron.* **1992**, *7*, 405-410.

(39) Daniels, P. B.; Deacon, J. K.; Eddowes, M. J.; Pedley, D. G. *Sens. Actuators* **1988**, *15*, 11-18.

(40) For these experiments, "saturation" is defined as the level of hybridization where the rate of hybridization decreases several orders of magnitude below its initial value, e.g., in Figure 2b, the initial rate of hybridization for the 1 h MCU backfill

SPR curve around 30 min is approximately $5.0x10^{12}$ molecules/cm^2·min while the rate of hybridization around 50 min has decreased to approximately $0.03x10^{12}$ molecules/cm^2·min.

(41) Watson, J. D.; Hopkins, N. H.; Robers, J. W.; Steitz, J. A.; Weiner, A. M. *Molecular Biology of the Gene,* 4th ed.; The Benjamin/Cumings Publishing Company, Inc.: Menlo Park, 1987.

(42) Su, X.; Wu, Y.-J.; Robelek, R.; Knoll, W. *Langmuir* **2005,** *21,* 348-353.

(43) Steel, A. B.; Herne, T. M.; Tarlov, M. J. *Anal. Chem.* **1998,** *70,* 4670-4677.

(44) Castelino, K.; Kannan, B.; Majumdar, A. *Langmuir* **2005,** *21,* 1956-1961.

(45) Cavic, B. A.; McGovern, M. E.; Nisman, R.; Thompson, M. *Analyst (Cambridge, U. K.)* **2001,** *126,* 485-490.

(46) Wong, K.-Y.; Pettitt, B. M. *Theor. Chem. Acc.* **2001,** *106,* 233-235.

(47) Wong, K.-Y.; Pettitt, B. M. *Biopolymers* **2004,** *73,* 570-578.

(48) Crozier, P. S.; Stevens, M. J. *J. Chem. Phys.* **2003,** *118,* 3855-3860.

(49) Hagan, M. F.; Chakraborty, A. K. *J. Chem. Phys.* **2004,** *120,* 4958-4968.

(50) Halperin, A.; Buhot, A.; Zhulina, E. B. *Biophys. J.* **2004,** *86,* 718-730.

Chapter 4 Comparison of DNA Immobilization Efficiency on New and Regenerated Commercial Amine-reactive Polymer Microarray Surfaces

Reprinted with permission from: P. Gong, D.W. Grainger, Surface Science **2004**, *570*, 67-77.

This dissertation chapter contains the manuscript of a full paper published in *Surface Science*. The manuscript was written by Ping Gong and edited by David W. Grainger. This chapter describes how reactivity loss on commercial microarraying slides can be restored through a simple straightforward reaction and how the regenerated slides perform in microarray DNA probe immobilization compared with fresh and unregenerated slides.

Comparison of DNA Immobilization Efficiency on New and Regenerated Commercial Amine-reactive Polymer Microarray Surfaces

Ping Gong, David W. Grainger

4.1 Abstract

Reactive polymer-coated microarray substrates based on nucleophile-reactive N-hydroxysuccinimide (NHS) active ester chemistry lose their bio-immobilization reactivity to amine-terminated probe nucleophiles over time, both in print use and "dry" storage, due to their intrinsic hydrolytic instability. Poor or inconsistent DNA and protein probe immobilization efficiency is often observed with routine microarray printing conditions, with accompanying reliability and stability issues for assay. Because of surging popularity of microarraying applications, expectations for consistent assay results and the expense of losing microarray substrate immobilization performance, we report a one-step reaction to regenerate NHS-reactive chemistry *in situ* on these microarray polymer surfaces with simple, straightforward reaction chemistry. Surfaces regenerated with this method perform equal to freshly prepared slides in print-immobilization of oligonucleotide probes functionalized with primary amine reactive groups. DNA probe specific and non-specific surface binding due to physisorption versus nucleotide base amine covalent attachment was analyzed using both fresh and slides regenerated with NHS chemistry. Commercial reactive microarray substrates appear to retain DNA probes

with both substantial covalent immobilization as well as some non-specific adsorption to the commercial arraying surface.

4.2 Introduction

Use of microarray substrates for printing and archiving of biomolecule arrays, including nucleic acids and antibodies for multiplex miniaturized bioassays, now exceeds 10^6 pieces annually. DNA microarrays are becoming a powerful tool for large-scale parallel analysis of genome sequences and gene expression in biological and biomedical research, and represent a substantial, maturing scientific method and accompanying commercial industry.[1-8] Protein microarrays, notably antibody arrays, are rapidly developing as a future, even more extensive application arena for rapid analyte assay.[9, 10] For probe immobilization, both microarray platforms currently rely on derivatized surface chemistry reactive to printed nucleic acid or antibody probes. Surfaces are either designed for probe covalent or electrostatic surface immobilization while retaining an intrinsic low-background non-specific binding of non-analytes. Most surface chemistries reported for amine-containing probes are either reactive alkylsilanes on glass supports (e.g., aldehyde- or epoxy-terminated silanes), or thin polymer coatings bearing pendant side groups reactive to probe amines.[11-14] Several different polymer hydrogel-coated layers are designed to accommodate increased densities of reactive groups for microarray probe immobilizations per surface area than planar silane films while retaining hydrogel non-adsorptive responses towards undesired non-analytes. These hydrogel "three-dimensional" polymer coatings often provide higher probe and analyte signal intensities, but also tend to exhibit relatively higher intrinsic background signals as well.[15]

Because many synthetic printable oligonucleotide probes and native peptides and proteins contain terminally labeled or amino acid-derived nucleophilically reactive primary amine groups, respectively, many microarray substrates are paired to be amine-reactive for probe immobilization. Well-known amine-reactive immobilization chemistries include epoxides, aldehydes (Schiffs base formation) and reactive esters including p-nitrophenyl and N-hydroxysuccinimide (NHS) reactive esters.[16, 17] Epoxide reactivity leaves residual secondary hydroxyl groups; aldehyde coupling with amines requires an additional reduction step for stability; NHS groups exhibit high intrinsic reactivity to nucleophiles and are available in many bioconjugation formats for surfaces. NHS coupling chemistry with amines is both rapid and specific, but also suffers from competitive hydrolysis.[16] In aqueous milieu, NHS groups exhibit pH- and temperature-dependent hydrolysis half-lives, generally on the order of a few hours or less in solution and high humidity environments. Because microarray printing processes can require many hours to complete (e.g., to batch print a complete genome slide containing ~10^4 genes in replicates), ambient print-deck humidity is therefore a problem for shelf-life and reliability reasons. For sensitive bioassays, this surface reactivity and probe immobilization problem is central to microarray function and assay reliability, and cannot be overlooked as a source of microarray variability and inconsistent data quality.[18]

In this contribution, we investigated the probe immobilization performance of commercial amine-reactive microarray supports with simple amine-terminated 20-mer DNA printed probes. Specific versus non-specific probe immobilization efficiencies are observed and quantified by fluorescence intensity analysis. We report a simple one-step reaction to regenerate the amine-reactive NHS active groups *in situ* on commercial

polymer-coated microarray slides. With this regeneration protocol, array surface reactivity to DNA probes performance can be reliably restored and ensured equivalent to amine-reactivity originally present as vendor-supplied. Two types of polymer slides were studied for: (1) NHS surface reactivity loss over time, (2) their active group regeneration *in situ*, and (3) their performance in specific chemical immobilization versus non-specific DNA probe adsorption before and after slide reactive group regeneration. These surface properties have a substantial impact on microarray reliability and reproducibility in analyte capture, and profound implications for interpreting microarray assay performance quantitatively.

4.3 Experimental section

Reagents. Phosphate, borate, and Tris buffer components, dimethylformamide (DMF), dicyclohexylcarbodiimide (DCC), 1-(3-dimethylaminopropyl)-3-ethlcarbodiimide hydrochloride (EDCI), N-hydroxysuccinimide (NHS), Tween 20, sarcosine, sodium citrate (SSC), sodium dodecyl sulfate (SDS) and ethanolamine were purchased from Sigma-Aldrich (St. Louis, MO) and used as received. Commercial polymer-coated microarray slides were purchased from Amersham (Codelink™, Tempe, AZ) and Accelr8 Technology Corp. (OptArray™, Denver, CO). Both microarray surfaces are marketed as amine-reactive three-dimensional (i.e., crosslinked polymer networks of thicknesses greater than monolayer) polymer coatings on low-fluorescence glass substrates. X-ray photoelectron spectroscopy (XPS) of each surface (data not shown) indicates similar surface elemental composition in the top 9nm of the polymer: carbon, nitrogen, and oxygen XPS signals reflect chemical binding environments for these proprietary coatings consistent with known hydrophilic polyacrylamide copolymer

or polyurethane polymer chemistry. Exact matrix chemistries are proprietary and not known.

Oligonucleotide selection. All oligonucleotides were purchased from MWG Biotech (High Point, NC) and are highly purified by RP-HPLC to be high purity salt-free (HPSF, certified 98.5~99.5% purity). The oligonucleotide sequence 5'-CTGAACGGTAGCATCTTGAC (probe) forms a stable duplex with its complementary pair at room temperature, with minimal interference due to self-complementarity or secondary structure.[19, 20] Both terminal hexylamine-functionalized H_2N-3'-probe-Cy3 and non-functionalized probe-Cy3 nucleotides were used to study specific surface chemical immobilization versus probe non-specific binding (NSB) using fluorescence microarray detection.

Microarray surface NHS regeneration. Polymer-coated commercial microarray slides from two different vendors were compared in NHS regeneration experiments. Commercial slides taken directly from vendor-packaged original storage boxes and printed immediately were denoted "fresh" slides. Other slides were deliberately deactivated to amine-reactive coupling by several different chemical treatments. One sub-set was treated with 10mM NaOH for 0.5h to hydrolyze surface NHS groups in a short time and is denoted "deactivated" slides. A second subset of slides was regenerated according to protocol (see below for details) following the same NaOH deactivation process and is denoted "regenerated". A third subset of slides was 'blocked' using 50mM ethanolamine aqueous solution for 0.5h to quench NHS amine-reactive groups after the regeneration and is denoted "blocked". A final subset of microarray slides was

kept on the shelf at room temperature in their sealed vendor-supplied storage bag for two months and aged under these routine conditions, and denoted as "aged" slides.

NHS reactive group surface regeneration was performed on "deactivated" slides, which are then re-named "regenerated" slides post-treatment. Two NHS regeneration approaches based on carbodiimide surface re-esterification were used: (1) using DMF as the solvent ("organic" or DCC regeneration method), (2) under aqueous conditions using Millipore™ purified H_2O ("aqueous" or EDCI regeneration method). Regeneration under organic conditions includes full immersion of deactivated slides in 0.55M N-hydroxysuccinimide (NHS) and 0.5M DCC in dry DMF for 3h at -20°C, then left to stand overnight at +4°C.[21] Slides were rinsed thoroughly with dry DMF then blown dry with nitrogen. Regeneration under aqueous conditions included full immersion of deactivated slides in 0.55M N-hydroxysuccinimide (NHS) and 0.5M EDCI in Millipore™ H_2O for 15min at room temperature, followed by brief H_2O rinse. Slides were promptly blown dry with nitrogen.[16, 22]

DNA probe printing on microarray slides. Commercial polymer-coated amine-reactive slides from Amersham (Codelink™) and Accelr8 Technologies (OptArray™) were stored in vendor-sealed packaging per each vendor's recommendations. HPLC-purified oligonucleotides containing a 3'-terminal hexylamine group were spotted onto microarray slides using a TeleChem SpotBot™ pin spotter. TeleChem SMP3-1 pins were used for all printings because these print with smaller diameter spots on the two types of slides used. Oligonucleotide solution spot volumes of ~0.7 nanoliters (http://www.arrayit.com/Products/Printing/Stealth/stealth.html) were spotted in replicates at concentrations of 20, 10, 5 and 1 μM DNA. These print conditions provide dried spots

approximately 90-150 microns in diameter, depending on the substrate vendor. Print buffer was 150mM PBS (pH 8.5) with 0.001% Tween20 and 0.001% sarcosine. Humidity was set at 40%. For each print run, each slide vendor's printing specifications were closely followed for handling, printing, buffers and rinsing. Stable surface immobilization was attempted by incubating the printed slides overnight at room temperature under 75% relative humidity.

Post-print substrate treatment. Residual NHS reactive groups remaining on slides post-printing were blocked using blocking solution A (50mM ethanolamine in 0.05M borate buffer, pH 9.2) for 1h at room temperature or pre-warmed blocking solution B (50mM ethanolamine in 0.1M Tris, pH 9.0) at 50°C for 30 min or according to slide manufacturer's specifications. Slides were then rinsed briefly with deionized water, then with 4X saline sodium citrate (SSC), 0.1% sodium dodecyl sulfate (SDS, pre-warmed to 50°C) for 30 min., and blown dry with N_2.

Microarray scanning and fluorescence detection. Microarray slides were scanned using a Packard BioChip Imager. Laser power and PMT sensitivity were set at 70% and 80%, respectively, for the probe immobilization fluorescence intensity measurements. Resolution was set to 10 microns. Channel 1, corresponding to 543μm, was selected for Cy3-labeled experiments. The scanner automatically rotates the appropriate emission filter wheel into the proper position for Cy3 fluorescence emission detection.

Image processing for spot fluorescence intensity normalization. The microarray scanned fluorescence images were processed with ScanAlyze™ software written by Dr. Michael Eisen (UC Berkeley, USA, see http://rana.lbl.gov/EisenSoftware.htm). Arrays

were first gridded with circles according to printing parameters, i.e., resolution of scanned images, location of spots and their position in the array. Grid parameters such as spot size and array tilt can be further fine-tuned according to the array image. Position of individual grid elements (circles) can be adjusted to fit each print spot image if necessary. ScanAlyze™ separates the image into pixels either contained within the identified spot or those that are not. Any pixel through which the spot circle passes is defined as being within the spot. Any pixels not within the spot but within a square, centered at the spot center, with side lengths of two-times the print spot radius (default value of 20) are defined as background pixels for this spot, excluding pixels contained within another spot. Pixel data intensities are imported into a spreadsheet program where background intensities are subtracted from corresponding spot intensities. Spots with defects that can be visually identified are excluded from replicate averaging (no more than 1 out of 5 replicates). Pixel intensities from replicates of 5 (or 4 in case of a defective spot) were averaged and standard deviations were calculated.

4.4 Results and Discussion

Comparison of Cy3-labeled probe oligonucleotide surface retention with and without reactive terminal amine groups using the organic carbodiimide regeneration method. Retention of Cy3-labeled probe oligonucleotides with and without reactive terminal amine groups was compared in order to assess relative amounts of covalent versus physisorbed immobilization on commercial array surfaces. Amine-derivatization after DNA oligomer probe synthesis is a convenient synthetic strategy to enable microarray substrate immobilization: nucleophilic amine functional groups readily covalently react with NHS active esters to create covalent amide linkages.[16]

Oligonucleotides lacking amine functional groups can also attach to surfaces via either physisorption (e.g., combinations of hydrogen bonding, acid-base, hydrophobic, electrostatic interactions) or possible (though unlikely due to poor nucleophilicity at printing pH <11) covalent attachment through pyrimidine or purine amine groups pendant on nucleotide bases.[23-26] Strongly physisorbed probes may be more readily removed by stringent wash steps, but may not be completely rinsed away, particularly when absorbed and dried into crosslinked three-dimensional polymer hydrogel arraying surfaces. Therefore, fractions of specifically immobilized versus non-specifically attached probes remaining prior to hybridization steps are of interest to know, quantify and control.

During probe printing, ambient humidity can be controlled to approx. 40%, and water in the printed probe solution (nanoliters) evaporates rapidly (within seconds), leaving the hydrophobic Cy3 probe-labeled amphipathic DNA chains dried onto and into the polymer array surface with printing solution excipients (e.g., salts, surfactants). The hydrophobic heterocyclic Cy3 dye label on the probe oligonucleotide provides one driver of probe physisorption and non-specific probe binding. Physisorption from acid-base, polar or even electrostatic forces between the polymer surface matrix and the oligonucleotide chains cannot be avoided, even without the Cy3 label. DNA probes lacking this hydrophobic Cy3 dye label (i.e., conventional oligoDNA probe prints for microarraying assay use) behave differently upon printing based on hybridization efficiencies from solution (data not shown). Printed DNA (amine-labeled or not) probe irreversible physisorption caused by spot rapid drying onto the polymer arraying matrix is demonstrated by evidence below showing substantial non-specific probe surface

adsorption resilient to rinsing in printed spots. Altering the printing solution components, ionic strength and pH, or increasing the post-print slide wash solution temperature lessens probe non-specific binding, but only to a limited extent. Certain non-specific aspects of the probe print process are irreversible using either microarray slide vendor protocols or modifications.

Figure 4.1 shows scanned fluorescent images and associated plots and tables of probe fluorescence signals from printed "Deactivated", "Regenerated", "Blocked" ,"Fresh" and "Aged" commercial polymer slides (shown side by side in this order) using the organic method with DMF as solvent and DCC as coupling agent (Accelr8 OptArray™ slides, Fig. 4.1AB, Amersham Codelink™ slides, Fig. 4.1CD). The upper regions of the array images outside the grey boxes in both Figs. 4.1A and 4.1C represent identical amine-functionalized oligonucleotides printed and processed as described above for the two amine-reactive polymer substrates. Both of these upper regions in Figures 4.1A and 4.1C share fluorescence intensity features where increasing amine-functionalized DNA probe print concentrations exhibit increasing Cy3 intensities post-rinsing. This is consistent with probe covalent stabilization against rinse removal. Figure 1(A) has visibly smaller printed spots (average spot diameter ~ 90 microns for OptArray™ slides) and Fig. 4.1C larger 150 micron printed spots for Codelink™ slides. Resulting average RFU intensities for all five arraying conditions for OptArray™ slides in Figure 4.1A are plotted in Figures 4.1B. Resulting average RFU intensities for all five array conditions for Codelink™ surfaces in Figure 4.1C are plotted in Figures 4.1D. Grey line-demarked regions in lower halves of Figs. 4.1A and 4.1C indicate NHS-surfaces printed with Cy3-oligonucleotides lacking any 3' hexylamine-derivatized end

(A)

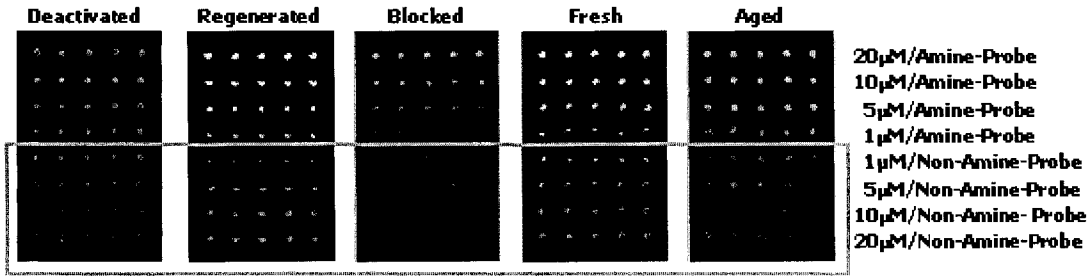

(B)

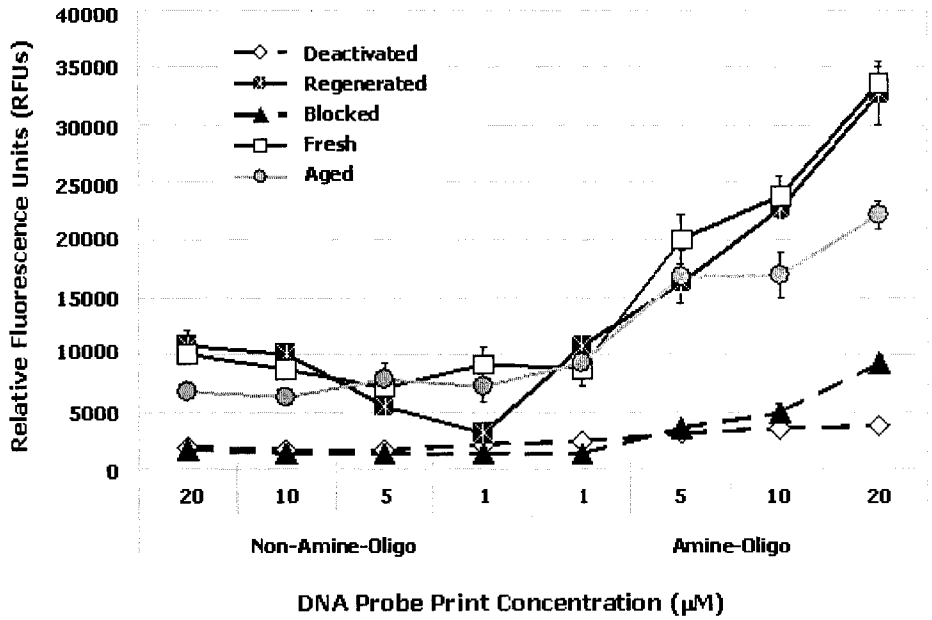

Figure 4.1 Microarray fluorescent scanning images and image pixel quantification for oligo-DNA probe printing and immobilization onto two commercial amine-reactive polymer-coated microarray substrates regenerated with the DCC organic method under various substrate treatments and probe reactivity conditions. (A) Microarray slide images (pixelated RFUs) for amine-terminated (upper) and non-amine terminated (lower gray box enclosed) Cy3-labeled oligoDNA probes printed onto and processed on Accler8 OptArray™ polymer supports per vendor protocols. (B) Plots of these arrayed RFU data obtained from (A) showing changes in spot pixel average intensities as a function of probe print concentration and slide treatment conditions; -◇- Deactivated; -✳-Regenerated; -▲- Blocked; -□- Fresh and -●- Aged slide processing protocols, respectively. Error bars shown as standard deviations; (C) Microarray slide images (pixelated RFUs) for amine-terminated (upper) and non-amine terminated (lower gray box enclosed) Cy3-labeled oligoDNA probes printed onto and processed on Amersham Codelink™ polymer supports per vendor protocols. (D) Plots of these arrayed RFU data obtained from (C) showing changes in spot pixel average intensities as a function of probe print concentration and slide treatment conditions; -◇- Deactivated; -✳-Regenerated; -▲- Blocked; -□- Fresh and -●- Aged slide processing protocols, respectively. Error bars show standard deviations.

(C)

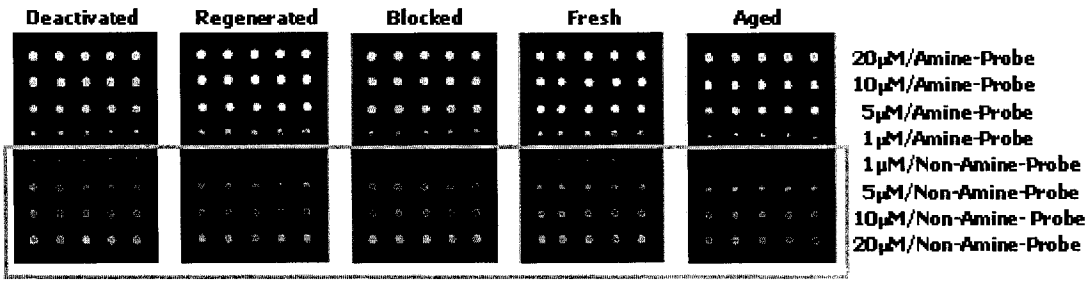

(D).

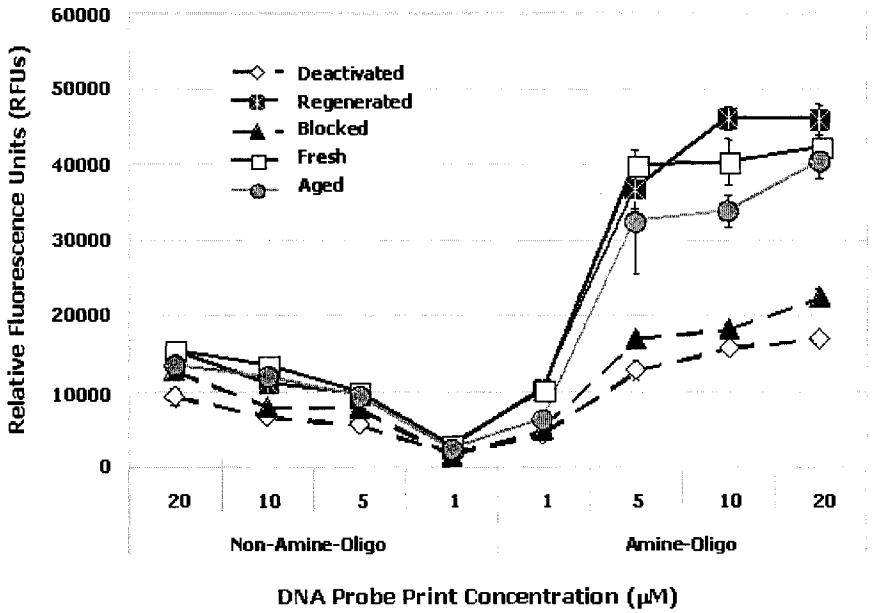

groups (no covalent immobilization capability). Signal in this region therefore results only from non-specific probe-surface attachment since no deliberate attachment chemistry is present, despite the NHS presence on each array surface. Figures 4.1B and 4.1D show corresponding graphs for these RFU spot intensities averaged over the printed spot sets for these conditions as well. Similar results were obtained in each case for DNA probes lacking hexylamine termini printed on both "fresh" and "regenerated" slides, i.e., overlapping lines on these intensity plots, suggesting similar "noise" levels on these slides from non-specific oligonucleotide attachment.

Both "Deactivated" and "Blocked" subsets of slides were also studied for non-specific probe attachment. Treatment with 10mM NaOH (30min) hydrolyzes slide NHS groups, leaving residual carboxylate groups. In the "Blocked" case using regenerated arraying surfaces, active NHS groups were deliberately quenched with 50mM ethanolamine in appropriate buffers according to vendor's protocols. This blocking step replaces NHS with hydroxyl groups. Hence, both treatments eliminate direct surface NHS-probe covalent coupling capability. Spot intensities for oligonucleotides printed on both "Deactivated" and "Blocked" surfaces exhibit similar probe non-specific attachment on both Codelink™ and OptArray™ slides, much less than on the corresponding "Regenerated" and "Fresh" slides, but still significant (20% of these levels or even higher). Less probe is retained (80% below that observed on NHS "Regenerated" and "Fresh" prints) for both the "Blocked" and "Deactivated" slide cases for both amine-terminated and non-specific attachment experiments (compare intensities in Fig. 4.1A compared to 4.1C). These levels are similar in both cases, indicating substantial non-specific DNA attachment in these cases.

Comparison of organic and aqueous regeneration methods with Cy3-labeled probe printing. Surface NHS regeneration with the aqueous EDCI method is significantly faster and simpler compared to the DCC organic method: the EDCI procedure requires only 15 minutes of aqueous incubation with no drying procedures required for reagents and glassware. Long-time immersion of polymer microarray slides under potentially surface-altering organic solvent can also be avoided, limiting damage to the hydrogel matrix layer. Figure 4.2A and 4.2C show slide sets regenerated with the EDCI aqueous method. Improved printed spot homogeneity was obtained over those

(A)

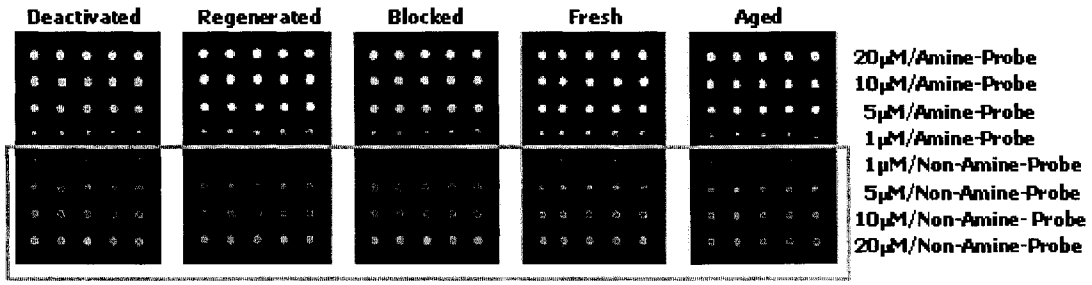

(B)

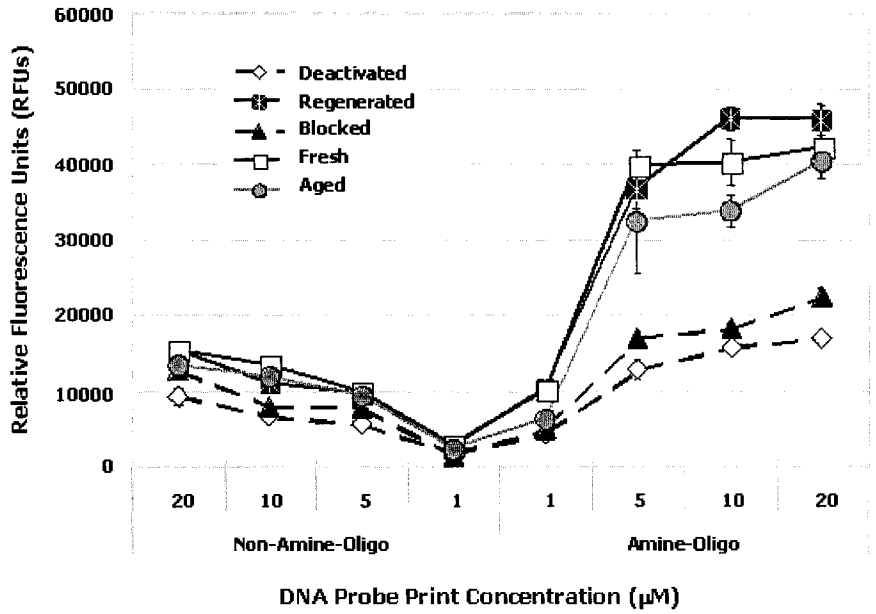

Figure 4.2 Microarray images and image quantification for probe printing and immobilization onto two commercial reactive polymer-coated microarray substrates regenerated with the EDCI aqueous method under various substrate treatments and probe reactivity conditions. (A) Slide images (pixelated RFUs) for amine-terminated (upper) and non-amine terminated (lower gray box enclosed) Cy3-labeled oligoDNA probes printed onto and processed on Accler8 OptArray™ polymer supports per vendor protocols. (B) Plots of these RFU data obtained from (A) showing changes in spot pixel average intensities as a function of probe print concentration and slide treatment conditions; -◇- Deactivated; -✳-Regenerated; -▲- Blocked; -□- Fresh; -●- Aged slide processing protocols, respectively. Error bars shown as standard deviations; (C) Microarray slide images (pixelated RFUs) for amine-terminated (upper) and non-amine terminated (lower gray box enclosed) Cy3-labeled oligoDNA probes printed onto and processed on Amersham Codelink™ polymer supports per vendor protocols. (D) Plots of these RFU data obtained from (C) showing changes in spot pixel average intensities as a function of probe print concentration and slide treatment conditions; -◇- Deactivated; -✳-Regenerated; -▲- Blocked; -□- Fresh; -●- Aged slide processing protocols, respectively. Error bars show standard deviations.

(C)

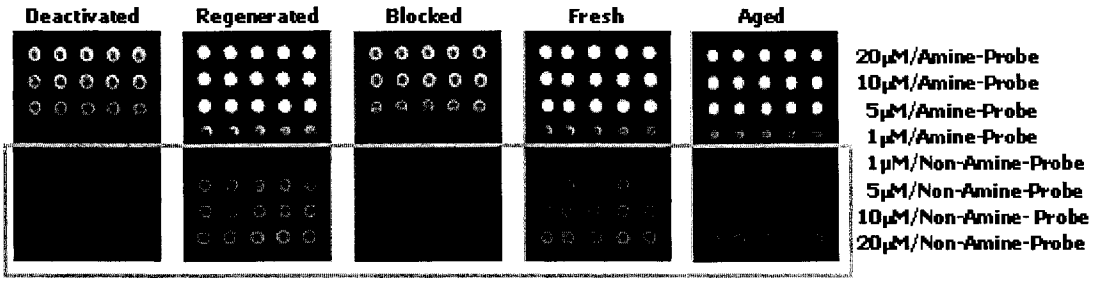

(D)

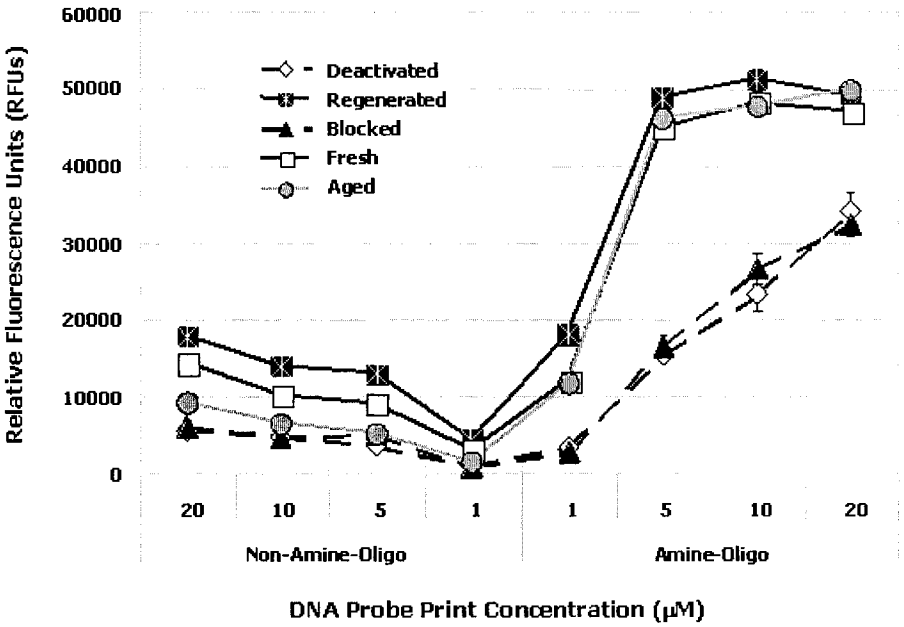

regenerated with the DCC organic method using the same printing probes and conditions. Resulting average spot RFU intensities for five OptArray™ slides treated with the same five conditions from Figure 1 and shown in Figure 4.2A are plotted in Figures 4.2B. The same printed spots on Codelink™ surfaces shown in Figure 4.2C are plotted in Figure 4.2D. Standard deviations from 5 spot replicate averages are noticeably decreased with the aqueous EDCI method over the DCC organic method. Nevertheless, comparison of Cy3-labeled probe oligonucleotide retention with and without reactive terminal amine groups using the aqueous regeneration method shows the same trends as immobilization

results from the organic regeneration method in Figure 4.1. In short, both EDCI and DCC NHS surface regeneration greatly improves amine-surface probe coupling efficiency over deactivated slides. Blocking and deactivation both eliminate specific immobilization while retaining a significant fraction of non-specifically immobilized probe in printing of both amine- and non-amine labeled DNA probes on these surfaces.

Effect of microarray surface aging. Commercial slides aged under the vendor-recommended storage conditions were included in both organic and aqueous regeneration experiments. Figures 4.1AB, and 4.2AB show that deactivated but regenerated OptArray™ slides exhibit similar spot intensity levels to DNA print runs on fresh OptArray™ slides while shelf-aged OptArray™ slides (2 months, ambient conditions in vendor-sealed packaging) show reduced print spot intensities and retention. The same trend was observed for CodeLink™ slides as can be seen in Figure 4.1CD, and 4.2CD. Because production dates for slides from the two vendors are not specified, exact duration of shelf-life aging can only be estimated from dates that slides were received. Hence, while no precise comparison of aging on slide brands can be made at this point, it seems clear to conclude that aging influences DNA probe retention on slides despite commercially recommended storage protocols, and that regeneration protocols can improve this print performance on aged slides to regenerate fresh polymer slides.

Reproducibility of probe immobilization efficiency from run to run. A direct comparison between DCC and EDCI regeneration protocols, including studies on "fresh", "regenerated" and "aged" samples were made for Cy3-labeled DNA probes containing reactive amine groups only. Plots of immobilized DNA spot intensities revealed problems for the reproducibility of the two probe immobilization efficiencies from

individual runs. Intensity plots show that probe immobilization onto OptArray™ slides varied significantly depending on the immobilization method. Figure 4.3A shows intensity differences for the corresponding "fresh", "regenerated" and "aged" slides as large as 50% between NHS/EDCI and NHS/DCC regeneration runs. A possible explanation for such variation stems from the image analysis tool utilized for array

(A)

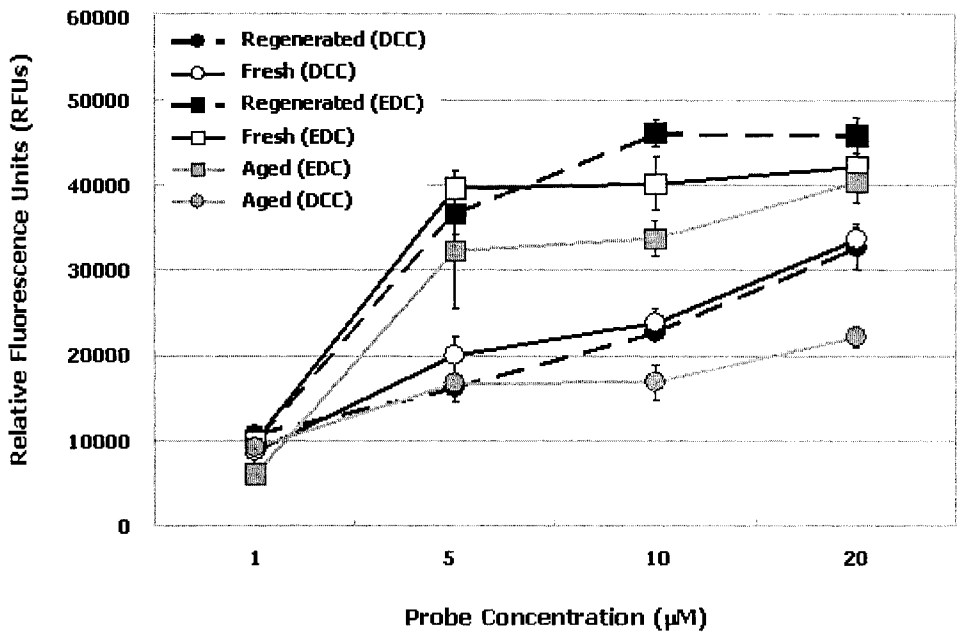

Figure 4.3 Direct comparison of immobilized array intensities between DCC and EDCI regeneration protocols on corresponding "fresh", "regenerated" and "aged" samples for Cy3- labeled DNA probes containing terminal reactive amine groups. These data show differences between regeneration immobilization end-points for NHS/EDCI versus NHS/DCC protocols. (A) Plots of these RFU data obtained from Figures 1(A) and 2(A) on OptArray™ slides, showing changes in spot pixel average intensities as a function of probe print concentration and slide treatment conditions; -■- Regenerated (EDCI); -□- Fresh (EDCI); -▩- Aged (EDCI); -●- Regenerated (EDCI); -○- Fresh (EDCI); -◍- Aged (DCC) slide processing protocols, respectively. Error bars shown as standard deviations. (B) Plots of these RFU data obtained from Figures 1(C) and 2(C) on CodeLink™ slides, showing changes in spot pixel average intensities as a function of probe print concentration and slide treatment conditions; -■- Regenerated (EDCI); -□- Fresh (EDCI); -▩- Aged (EDCI); -●- Regenerated (EDCI); -○- Fresh (EDCI); -◍- Aged (DCC) slide processing protocols, respectively. Error bars show standard deviations.

intensity analysis. When using ScanAnalyze™ software to analyze array intensities, adjustment of grid shape and position proved difficult for some smaller spots (less than 100 micron diameters on Optarray™) and because spot shapes showed certain levels of irregularity. Less variation was observed for analysis of probes immobilized onto CodeLink™ slides, seen in Figure 4.3B. The more hydrophilic CodeLink™ slide

(B)

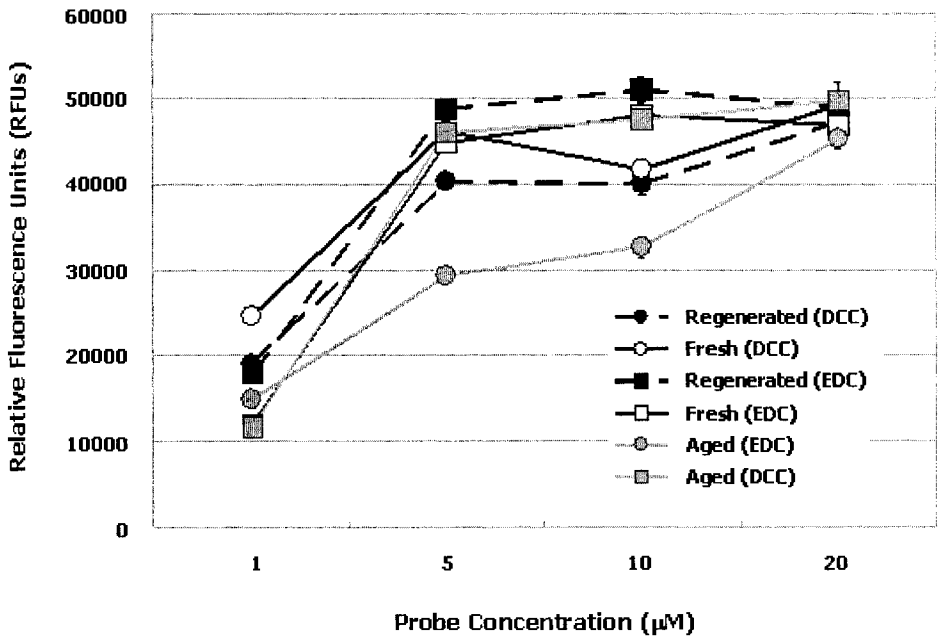

surfaces produced printed spots spread to a larger size (150 microns) with less irregularity, rendering easier, more reliable grid-fitting for integrated spot pixel counting. Even though every attempt was made to achieve identical reaction conditions, certain unavoidable experimental limitations, e.g., slight humidity variation during printing, slides from various batches, different print pins of the same model, DNA probes from different batches,, could easily have produced printed spots with significant differences in their dried morphologies. Due to anticipated effects of water versus DMF solvent immersion on the commercial hydrogel polymer layers, these observed differences might

also result from different polymer film relaxation, extraction, or reorganizational influences during processing, producing different effects on resulting DNA immobilization efficiencies on altered films architectures.

4.5 Conclusions

Reliable microarray performance in bioassays depends critically on several bioassay variables, including the reliability of array substrate probe immobilization, hybridization efficiencies, assay signal and noise determinations and reproducibility of each of these on different arraying surfaces now available. For arraying substrates designed for covalent probe reactions upon printing, probe immobilization reliability can be an important issue affecting assay performance. Inconsistent or unstable amine-reactivity is well-known for NHS chemistry and therefore a concern for probe coupling and reproducible array performance. To restore or standardize probe immobilization, the NHS surface regeneration process is simple and straight forward, allowing microarray substrates adversely affected by NHS hydrolysis and compromised reactivity to be restored to full or even improved amine-coupling functionality. Regenerated polymer arraying slides perform similarly to fresh NHS-derivatized amine-reactive slides from each vendor, providing enhanced reliability, a standardization 'set-point' for immobilization reactions, and high reactivity for standard microarray printing. When NHS chemistry is removed deliberately, non-specific oligonucleotide probe binding is observed as significant background noise on each chemistry resistant to stringency rinsing, occurring both through DNA-surface physisorption mechanisms. These print data establish an initial, general approach to understanding some current assay limitations of widely available commercial microarraying media, and methods to approach

standardization of reactivity and reliability essential for eventual quantitative microarray assay comparisons and accurate biometrics. A follow-on study will compare hybridization efficiencies on these matrices to assess probe print protocols on actual assay performance from buffer.

4.6 Acknowledgements

The authors are grateful for partial research support from both NIH EB001473 and EB00726. Technical assistance for fluorescence scanning from Dr. W. H. Hanneman (CSU) and reproducible spotting protocols and control experiments from Dr. C. Greef are both gratefully acknowledged.

4.7 References

(1) Ramsay, G. *Nat. Biotechnol.* **1998**, *16*, 40-44.

(2) Schena, M.; Heller, R. A.; Theriault, T. P.; Konrad, K.; Lachenmeier, E.; Davis, R. W. *Trends Biotechnol.* **1998**, *16*, 301-306.

(3) Sanchez-Carbayo, M.; Bornmann, W.; Cordon-Cardo, C. *Curr.Org. Chem.* **2000**, *4*, 945-971.

(4) Freeman, W. M.; Robertson, D. J.; Vrana, K. E. *BioTechniques* **2000**, *29*, 1042-1044, 1046, 1048-1055.

(5) van Hal, N. L. W.; Vorst, O.; van Houwelingen, A. M. M. L.; Kok, E. J.; Peijnenburg, A.; Aharoni, A.; van Tunen, A. J.; Keijer, J. *J. Biotechnol.* **2000**, *78*, 271-280.

(6) Helmberg, A. *Exp. Gerontology* **2001**, *36*, 1189-1198.

(7) Beaucage, S. L. *Curr. Med. Chem.* **2001**, *8*, 1213-1244.

(8) Yang, Y. H.; Speed, T. *Nat. Rev. Genet.* **2002**, *3*, 579-588.

(9) Kusnezow, W.; Hoheisel Jorg, D. *Biotechniques* **2002**, *Suppl*, 14-23.

(10) Blawas, A. S.; Reichert, W. M. *Biomaterials* **1998**, *19*, 595-609.

(11) Lenigk, R.; Carles, M.; Ip, N. Y.; Sucher, N. J. *Langmuir* **2001**, *17*, 2497-2501.

(12) Smith, E. A.; Wanat, M. J.; Cheng, Y.; Barreira, S. V. P.; Frutos, A. G.; Corn, R. M. *Langmuir* **2001**, *17*, 2502-2507.

(13) Oh, S. J.; Cho, S. J.; Kim, C. O.; Park, J. W. *Langmuir* **2002**, *18*, 1764-1769.

(14) Strother, T.; Cai, W.; Zhao, X.; Hamers, R. J.; Smith, L. M. *J. Am. Chem. Soc.* **2000**, *122*, 1205-1209.

(15) Lindroos, K.; Liljedahl, U.; Raitio, M.; Syvanen, A.-C. *Nucleic Acids Res.* **2001**, *29*, e69/61-e69/69.

(16) Hermanson, G. T. *Bioconjugate Techniques*; Academic Press: New York, 1995.

(17) Ramakrishnanm, R.; Dorris, D.; Lublinsky, A.; Nguyen, A.; Domanus, M.; Prokhorova, A.; Gieser, L.; Touma, E.; Lockner, R.; Tata, M.; Zhu, X.; Patterson, M.; Shippy, R.; Sendera, T. J.; Mazumder, A. *Nucleic Acids Res.* **2002**, *30*, e30/31-e30/12.

(18) Tilstone, C. *Nature (London, U. K.)* **2003**, *424*, 610-612.

(19) Mazzola, L. T.; Frank, C. W.; Fodor, S. P. A.; Mosher, C.; Lartius, R.; Henderson, E. *Biophys. J.* **1999**, *76*, 2922-2933.

(20) Forman, J. E.; Walton, I. D.; Stern, D.; Rava, R. P.; Trulson, M. O. *ACS Symp. Ser.* **1998**, *682*, 206-228.

(21) Kopecek, J. *Makromolekulare Chemie* **1977**, *178*, 2169-2183.

(22) Steffens, G. C. M.; Nothdurft, L.; Buse, G.; Thissen, H.; Hocker, H.; Klee, D. *Biomaterials* **2002**, *23*, 3523-3531.

(23) Sehgal, D.; Vijay, I. K. *Anal. Biochem.* **1994**, *218*, 87-91.

(24) Huang, E.; Zhou, F.; Deng, L. *Langmuir* **2000**, *16*, 3272-3280.

(25) Millan, K. M.; Mikkelsen, S. R. *Anal. Chem.* **1993**, *65*, 2317-2323.

(26) Millan, K. M.; Saraullo, A.; Mikkelsen, S. R. *Anal. Chem.* **1994**, *66*, 2943-2948.

Chapter 5 Multi-technique Comparison of Immobilized and Hybridized Oligonucleotide Surface Density on Commercial Amine-reactive Microarray Slides

Reprinted with permission from: P. Gong, G. M. Harbers and D.W. Grainger, Analytical Chemistry, **2006**, *in press*

This dissertation chapter contains the manuscript of a full paper published in *Analytical Chemistry*. The manuscript was written by Ping Gong and edited by Greg Harbers and David W. Grainger. This chapter describes how surface-immobilized DNA probe and hybridized DNA target densities were quantified by correlating results from fluorescence intensity measurements, radiometric assays and XPS.

Multi-technique Comparison of Immobilized and Hybridized Oligonucleotide Surface Density on Commercial Amine-reactive Microarray Slides

Ping Gong, Gregory M. Harbers, David W. Grainger

5.1 Abstract

To establish a quantitative, corroborative understanding of observed correlations between immobilized probe DNA density on microarray surfaces and target hybridization efficiency in biological samples, we have characterized amine-terminated, single-stranded DNA probes attached to amine-reactive commercial microarray slides and complementary DNA target hybridization using fluorescence imaging, X-ray photoelectron spectroscopy (XPS) and ^{32}P-radiometric assays. Importantly, we have reproduced DNA probes microarray immobilization densities in macroscopic spotted dimensions using high ionic strength, high concentration DNA probe solutions to permit direct XPS surface analysis of DNA-surface chemistry with good reliability and reproducibility. Target capture hybridization efficiency with complementary DNA exhibited an optimum value at intermediate DNA probe immobilization densities. The macroscopic array model provides a new platform for the study of DNA surface chemistry using highly sensitive, quantitative surface analytical techniques (e.g., XPS, ToF-SIMS). Sensitive ^{32}P-DNA radiometric density measurements were calibrated with more routine XPS DNA signals, facilitating future routine DNA density determinations without the use of hazardous radioactive assay. The objective is to provide new insight

into different surface chemistry influences on immobilized DNA probe environments that affect target capture efficiency from solution in order to improve microarray assay performance.

5.2 Introduction

Microarray technology is evolving rapidly as a powerful tool for large-scale parallel analysis of genome sequences and gene expression in biological and biomedical research, currently representing a substantial, maturing scientific method and accompanying commercial industry.[1-8] The potential of microarray applications and related parallel technologies for gene expression measurements requires more extensive microarray performance validation.[9] Earlier studies have shown poor reproducibility, repeatability and result correlations among different microarray methods, indicating significant challenges for broad application of microarray assays across platforms or between labs.[10-13] Recent collaborative efforts between microarray laboratories have demonstrated the importance of proper use of microarray technology, stressing the significance of standardizing operating protocols.[14-16] Although not yet optimal, these recent studies have pointed to a much more positive prospect for reliable technology in bioassay and disease diagnosis. Nonetheless, several quantitative analytical issues remain in microarray assays, including limited detection sensitivity from complex milieu, absolute abundance, coefficients of variation, and more fundamental insight into assay mechanisms and limitations. With one recent exception[17], lack of FDA approval for all current microarray assays for clinical patient use is one testament to the unsolved reliability and chemometric issues on this assay platform.

Extensive efforts have been directed to developing improved functional microarray surfaces using a broad range of surface chemistries. Surface chemistry serves as the foundation of microarray construction, significantly impacting important performance parameters such as reproducibility, stability and availability of the immobilized biomolecules, and non-specific assay backgrounds that all affect assay signal to noise.[18] Sensing surfaces built on several model substrates, including gold, silicon and glass, have been analyzed extensively. Quantitative, high-resolution, highly surface sensitive techniques, including Fourier transform infrared spectroscopy (FTIR)[19,20], X-ray photoelectron spectroscopy (XPS)[19-23], secondary ion mass spectrometry (SIMS)[22,24-28], near edge X-ray absorption fine structure (NEXAFS)[29] and radiometric assays[21,30-34], have provided data on both the properties of model sensing surfaces as well as immobilized biomolecular affinity capture components (antibodies, nucleotides) on surfaces, usually averaging surface spatial information across macroscopic features. However, these efforts for studying both individual and oligomeric nucleotides on various surfaces frequently do not directly address microarray technology in an assay-relevant context, especially with commercially available microarray surfaces and assay conditions. Additionally, many studies immobilize DNA to assay surfaces using bulk solution reactions that provide nucleotide immobilization dynamics, densities and assay results distinct from commercial methods using microspotting in air where nanoliter DNA solution droplets evaporate on the assay surface in seconds. Different immobilization densities resulting from these two immobilization conditions have profound implications for subsequent assay performance differences. Nonetheless, previous studies were able to show that XPS and SIMS are

well-suited for sensitive characterization of surface-bound DNA. In particular, previous reports have identified unique nucleotide signals (nitrogen and phosphorus DNA-specific spectra) and demonstrated method utility in characterizing both composition and structure of DNA immobilized on to surfaces[21,35-37]. Applying highly surface-sensitive techniques directly to microscopic microarray features remains a challenge. Improved resolution may be obtained at the expense of higher sensitivity, and *vice versa.* Microarray feature sizes typically range from several tens to several hundreds of microns in diameter, making it difficult to achieve reasonable sensitivity along with suitable resolution for surface analysis.

No current single surface analytical method can accurately report absolute densities of microarrayed DNA on surfaces conveniently and consistently at high sensitivity. To facilitate improved microarray surface analysis in this context, we report macroscopic analogs of microarray spotted nucleotide features, allowing surface characterization without sacrificing sensitivity or resolution for widely used analytical techniques. Relevant to real-world microarray applications, immobilized DNA probe properties on commercially available microarraying polymer slides were compared using both microarray and macrospot formats. The primary motivation was to provide the first direct correlation between several surface analytical techniques for an important bioassay format (nucleotide microarrays) to remove the current molecular quantification limitations imposed by relative fluorescence intensity measurements characterizing these assays. First, comparable nucleotide probe immobilization efficiencies for both macro- and micro- spot sizes were demonstrated using fluorescence imaging with fluorescently labeled DNA probes. Immobilized probe and hybridized DNA target densities in

macrospots were quantified using fluorescence, XPS and ^{32}P-labeling and compared to fluorescence results from microarrays. DNA surface densities from these three methods showed very reasonable correlations. Sensitive ^{32}P-DNA radiometric measurements were calibrated with more routine XPS DNA P2p signals, facilitating future microarray immobilized DNA density determinations without the need to use the more hazardous radioactive assay.

5.3 Experimental section

Materials. Phosphate, borate, and Tris buffer components, 1-(3-dimethylaminopropyl)-3-ethlcarbodiimide hydrochloride (EDCI), N-hydroxysuccinimide (NHS), Tween 20, sarcosine, sodium citrate (SSC), sodium dodecyl sulfate (SDS) and ethanolamine were purchased from Sigma-Aldrich (St. Louis, MO) and used as received. Commercial polymer-coated microarray slides were purchased from Amersham (Codelink™, Tempe, AZ). This microarray surface is marketed as an amine-reactive and three-dimensional (i.e., crosslinked polymer networks of thicknesses greater than a monolayer) hydrophilic polymer coating on low-fluorescence glass substrates. All slides were pre-treated prior to probe immobilization to ensure optimum surface amine-reactivity using an aqueous carbodiimide derivatization method previously described.[38]

Oligonucleotide selection. DNA oligonucleotides were purchased from TriLink Biotechnologies (San Diego, CA); all oligonucleotides were HPLC-purified for highest purity[39]. The oligonucleotide sequence 5'-CTGAACGGTAGCATCTTGAC-3' (oligo1) was selected because it forms a stable duplex with its complementary pair at room temperature, with minimal interference due to self-complementarity or secondary structure.[40,41] Table 5.1 lists all oligonucleotide sequences and modifications involved in

Table 5.1 Oligonucleotide sequences and modifications

		5' modification	oligonucleotide sequence	3' modification
A	Cy3-oligo1-NH_2	Cy3-	CTGAACGGTAGCATCTTGAC	-C_6-NH_2
B	Cy3-oligo1	Cy3-	CTGAACGGTAGCATCTTGAC	
C	NH_2-oligo1-^{32}P	NH_2-C_6-	CTGAACGGTAGCATCTTGAC	-^{32}P-dATP
D	oligo1-^{32}P		CTGAACGGTAGCATCTTGAC	-^{32}P-dATP
E	oligo2-^{32}P		GTCAAGATGCTACCGTTCAG	-^{32}P-dATP
F	oligo1-NH_2		CTGAACGGTAGCATCTTGAC	-C_6-NH_2
G	oligo2		GTCAAGATGCTACCGTTCAG	
H	Cy5-oligo2	Cy5-	GTCAAGATGCTACCGTTCAG	

this work. Oligos A and B were used in the fluorescence imaging section relating immobilized DNA microarray and macrospot densities, oligo A for specific end-amine tethering and oligo B as a control for assessing nucleotide amine attachment and physisorption. Oligos C, D (as control of C and E) and E were used in radiometric assays for probe and target DNA density quantification. Oligos F and G were used for macrospot analysis with XPS. Oligo H was used for fluorescence analysis of DNA hybridization. In addition, oligos F and G were used as diluent DNA molecules in all fluorescence and radiometric assays.

Microarray printing. Commercial polymer-coated amine-reactive slides (Amersham Codelink™) were stored in vendor-sealed packaging per vendor recommendations until surface reactivity standardization using a previously described mthod.[38] Oligonucleotides containing a 5'-terminal hexylamine group were spotted onto microarray slides using a TeleChem SpotBot™ pin spotter and TeleChem SMP3-1 pins. Oligonucleotide solutions (Cy3-oligo1-NH2 diluted 100-fold with oligo1-NH2, Cy3-oligo1 diluted 100-fold by oligo1 to exclude dye self-quenching on printed surfaces) at spotting volumes of ~0.7 nanoliters (http://www.arrayit.com/Products/Printing/Stealth/stealth.html) were spotted in replicates

of five at concentrations of 20, 10, 5 and 1 μM DNA in print buffer (150 mM PBS, pH 8.5 with 0.001% Tween20 and 0.001% sarcosine). These print conditions provided dried spots approximately 100-150 microns in diameter. Humidity was set at 50%. Stable surface immobilization was attempted by incubating the printed slides overnight at room temperature under 75% relative humidity.

Macrospot DNA probe immobilization. Probe DNA solutions (Cy3-Oligo1-NH2 diluted 100-fold with Oligo1-NH2 to exclude dye self-quenching on surface) at 50 μM concentrations were prepared in sodium phosphate buffer (pH 8.5) at concentrations ranging from 0.05 M to 1.5 M to study effects of ionic strength on immobilized DNA density. Adhesive silicone isolators (24-well, Grace Bio-Labs, Bend, OR) with 2.5 mm feature well diameters were applied onto substrate glass slides to define spotting areas. DNA solution (5 μl) was placed into each well and incubated at room temperature under 100% humidity for 3 hours (XPS analysis showed little difference between bulk immobilization of DNA at 3 hr and 22 hr; data not shown). Replicates of at least three wells were randomly distributed on slides among the 24 wells.

For density quantification experiments, DNA solutions ranging from 1 μM to 400 μM were prepared in 1.0 M sodium phosphate buffer (pH 8.5) to produce immobilization commensurate with microspot oligoDNA print concentrations of 1-20 μM. The upper limit of 400 μM was restricted by practical limitations on reasonable amounts of DNA available. Adhesive silicone isolators (12-well, Grace Bio-Labs, Bend, OR) with 4.5 mm feature diameters were applied onto substrate glass slides to define spotting areas. DNA solution (10 μl) was added to each 4.5 mm well and incubated at room temperature under

100% humidity for 3 hours. Replicates of at least three wells were randomly distributed on slides across 12 wells.

Post-print array treatment and hybridization with target DNA. Residual amine-reactive groups remaining on slides post-printing were consumed using blocking solution (50mM ethanolamine in 0.1 M Tris, pH 9.0) at 50 °C for 30 min. Slides were then rinsed briefly with deionized water, then incubated in 4X saline sodium citrate (SSC, 1X saline-sodium citrate solution contains 15 mM sodium citrate and 150 mM NaCl) containing 0.1% sodium dodecyl sulfate (SDS) for 30 min, rinsed again with deionized water and finally blown dry with nitrogen. Target hybridization was performed with commercial coverslips (1 ounce micro-cover glasses, VWR, West Chester, PA) at room temperature under 100% humidity for 4 hours in 4X SSC (with 0.1%SDS) solutions containing 1 μM DNA target. Solution ratio of Cy5-labeled DNA to identical non-labeled DNA was 1:100. Slides were rinsed with 4X SSC (0.1%SDS) to remove coverslips, followed by rinsing with 2X SSC/0.1%SDS for 5 min twice, then 0.2X SSC and 0.1X SSC each for 1 min. Slides were finally blown dry with nitrogen.

Fluorescence imaging. Microarray slides were scanned using a ScanArray Express Microarray Imager (Perkin Elmer, Fremont, CA). Laser power and PMT sensitivity were set to 90% and 75%, respectively, for probe immobilization measurements, and 90% and 50%, respectively, for hybridization measurements. When slides were scanned at different power settings as specified above, the collected relative fluorescence units were normalized to values at the specified powers. Scanning resolution was 10 microns for microarrays and 50 microns for macroscopic spot features.

Scanner channels 1 and 2, corresponding to 543-nm and 633-nm irradiations, were selected for the Cy3-labeled and Cy5-labeled experiments, respectively.

Image processing for spot fluorescence intensity normalization. The microarray scanned fluorescence images were processed with ScanAlyze™ software (written by Dr. M. Eisen, Univ. California-Berkeley, USA, see http://rana.lbl.gov/EisenSoftware.htm). Arrays were first gridded with circles according to printing parameters, i.e., resolution of scanned images, location of spots and their position in the array. Grid parameters such as spot size and array tilt can be further fine-tuned according to the array image. Position of individual grid elements (circles) can be manually adjusted to fit each print spot image if necessary. ScanAlyze™ separates the image into pixels either contained within the identified spot or those that are not. Any pixel through which the spot circle passes is defined as being within the spot. Any pixels not within the spot but within a square, centered at the spot center, with side lengths of two-times the print spot radius (default value of 20) are defined as background pixels for this spot, excluding pixels contained within another spot. Pixel data intensities were imported into Microsoft Excel where background intensities were subtracted from corresponding spot intensities. Spots with defects that could be visually identified were excluded from replicate averaging (no more than 1 out of 5 replicates). Pixel intensities from replicates of 5 (or 4 in case of a defective spot) were averaged and standard deviations were calculated.

X-ray Photoelectron Spectroscopy (XPS) of spotted surfaces. XPS surface analyses were performed on a Physical Electronics PE5800 ESCA/AES system equipped with a 7 mm monochromatic Al Kα X-ray source (1486.6 eV) and hemispherical analyzer. All spectra were collected using, an aperture size of 800 μm (diameter) and a

low energy electron flood gun to minimize surface charging. To compensate for residual charging effects, high-resolution spectra were charge referenced by setting the hydrocarbon peak to 285.0 eV. A 35° photoelectron take-off angle, defined as the angle between the surface plane and the axis of the analyzer lens, was used for all spectra. At this angle, sampling depth averages about 4.6nm[42]. Compositional survey scans were initially used to detect all elements present using a pass energy of 187.80 eV and a step size of 0.8 eV. Once elements were determined to be present, all composition data (C1s, O1s, N1s, Si2p, Na1s, Cl2p, Ca2p, and P2p) were collected using a pass energy of 117.40 eV with a step size of 0.25 eV. High-resolution spectra (Si2p, C1s, N1s, and O1s) were collected at a pass energy of 23.5 eV and a step size of 0.05 eV. For P2p analysis on the DNA samples, utility spectra were collected for either 25 minutes or until a S/N ratio of 50 was obtained, whichever came first. Data analysis was conducted with either Multipak™ software (Physical Electronics, Chanhassen, MN) (utility) or Spectral Data Processor (v. 2.3) (XPS International) (high-resolution spectra). For quantitation, high-resolution phosphorus P2p peak areas were integrated using both 100% Gaussian and 90% Gaussian/10% Lorentzian peak fitting constraints (endpoint: minimized chi square residuals). Both methods produced results insignificantly different from each other. Only results from (100% Gaussian) peak fits are shown. All values reported for the analysis of utility P2p spectra are the mean of at least three independent measurements from three experiments. Values reported for composition and high-resolution spectra are the average of three spots from a single Codelink™ microarray slide to allow for easy comparison between modification steps and eliminate the effect of slide-to-slide variability.

^{32}P-Radiometric assay of DNA surface density. Oligonucleotides were labeled with α-^{32}P-ddATP (Amersham Biosciences, Piscataway, NJ) in presence of terminal transferase (Roche Diagnostics Corp., Indianapolis, IN) and purified with an oligo mini-spin column (Roche Diagnostics Corp., Indianapolis, IN). Concentrations of ^{32}P-labeled oligonucleotides were measured with a TriCarb 1500 liquid scintillation analyzer for specific activity determinations. Samples were exposed to a storage phosphor imager (Amersham Biosciences, Piscataway, NJ) for surface radioactivity measurement after DNA immobilization and hybridization. Gray-scale pixelated images of surface ^{32}P density were obtained using a STORM™ (Amersham Biosciences) scanner and analyzed using ImageQuant software (v. 5.1, Amersham Biosciences). Quantitation of sample DNA surface density using gray-scale image analysis was performed by constructing calibration curves for each labeling reaction as described by Steel et al.[31] DNA surface density values were averaged from three individual experiments (3 spots/experiment). Control experiments comprised combinations of non-aminated probe (Oligo D) macrospots and non-complementary targets hybridized to probe surfaces were performed. Non-specific probe and target binding control signals were subtracted from the total assay singals to yield both probe and target signal shown.

5.4 Results and Discussion

Buffer ionic strength and its effect on DNA immobilization efficiency. DNA microarray fabrication on a commercial microarraying substrate involves dispensing of nanoliter drops of liquid onto solid surfaces using a robotic spotter at a typical microarray printing humidity of lower than 50%. The nanoliter drops of liquid evaporate within two or three seconds of residence at the surface, without reaching equilibrium in terms of

DNA-surface interactions, mass transfer, covalent reactions on surfaces or constant ionic strength. This evaporation results in significantly increased ionic strength of the spotting buffer as well as increased DNA concentration, leading to superior DNA probe surface immobilization efficiency to the advantage of microarray printing. This evaporative processing produces distinct differences in immobilized DNA physical chemistry on these surfaces versus bulk solution coupling reactions between DNA and surfaces. Few studies have appreciated these differences; few techniques are amenable to discerning such differences. Therefore, in order to achieve comparable levels of immobilized DNA probe at the macroscopic level, substantially elevated buffer ionic strength and increased DNA concentration are necessary to create macrospots on commercial microarraying substrates.

Polyelectrolyte immobilization efficiency is generally known to change with varying ionic strength of the print buffer.[43] Specific salt identity and ionic strength have also been reported to play a role in thiolated DNA assembly on gold[44,45] Similar ionic strength effects were observed for amine-oligoDNAs immobilized on commercial polymer slides, shown specifically on macro-scale DNA features using fluorescence labeling in Figure 5.1. Relative amounts of immobilized probe molecules are expressed as relative fluorescence units (RFUs). A strong dependence of immobilization efficiency on solution ionic strength was observed. By increasing immobilization buffer concentration from 0.15 M to 1 M, relative amounts of immobilized DNA probe, as indicated by RFUs, increased approximately three-fold, while increasing from 1 M to 1.5 M amplified the signal almost six-fold.

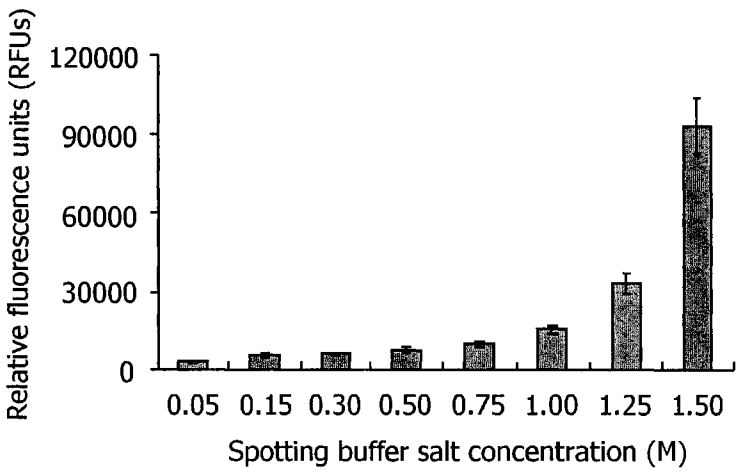

Figure 5.1 DNA probe immobilization dependence on buffer ionic strength studied using Cy3-labeled fluorescent DNA probes. Relative amounts of immobilized DNA probe molecules have been expressed as relative fluorescence units (RFUs). A strong dependence of immobilization efficiency on media salt content was observed. By increasing buffer concentration from 0.15 M to 1 M, the RFU signal from immobilized DNA probe increased approximately three-fold; from 1 M to 1.5 M, the signal amplification was six-fold.

Macrospot analog of microspots analyzed by fluorescence imaging (~4.5 mm spot diameter). Intensities of printed microarray spots (100-150 micron diameter) and bulk-immobilized macrospots (~4.5 mm diameter) were correlated using fluorescence imaging. In these fluorescent-labeled probe immobilization assays, Cy3-oligo1-NH_2 was diluted by oligo1-NH_2 (1:100) and Cy3-oligo1 was diluted by oligo1 (1:100) to exclude dye self-quenching since without dilution (i.e., using 100% labeled probe) fluorescence signal plateaued at higher densities, presumably from fluorophore self-quenching. These probes were printed into microarrays and spotted as macrospot formats to compare amounts of total specific surface binding (Cy3-oligo1-NH_2) with non-specific binding (Cy3-oligo1) resulting from either nucleotide base amine attachment[46] or physisorption. As rapid evaporation eliminates equilibrium reactivity in microarray surface-immobilization reactions, this produces an immobilization endpoint and efficiency

substantially greater than solution-phase immobilization reactions from bulk media, or "evaporation free" equilibrium immobilization conditions. Hence, slowly drying macro-droplets in silicon gasket wells produce different immobilization DNA densities than rapidly evaporating microdrops under identical print conditions. Importantly, relative amounts of DNA probe immobilized onto slides under both microarray and macrospot formats can be directly correlated using fluorescently labeled DNA probes (Figure 5.2). Macro-scale DNA immobilization using oligoDNA solution concentrations ranging from 1 to 400 μM (Fig. 5.2A) produced immobilization yields commensurate with microspot oligoDNA print concentrations of 1-20 μM. Throughout this concentration range, DNA probe immobilization efficiency exhibited a linear dependence on the concentrations of bulk probe solutions applied in both methods. As seen in Figure 5.2, the resulting DNA probe density in a typical 20 μM microarray printing is equivalent to density achieved at ~125 μM macro-scale solution immobilization (Fig 5.2BC). Also worth noting is the amount of non-specific oligoDNA binding produced from either nucleotide base amine attachment or surface physisorption. In both microarray prints and macrospots, non-specific DNA surface binding was negligible, in most cases less than 5% that of the specific end-amine tethering based on fluorescence analysis of total and non-specific fractional DNA immobilization (data not shown). This indicates that lower nucleophilicity of nucleotide base primary amines is insufficient for reaction under these conditions, counter to a previous report[46].

XPS analysis of surface- immobilized and hybridized DNA. DNA macrospots (4.5 mm diameter) on Codelink™ substrate chemistry were analyzed by XPS to compare each additional surface reaction (slide regeneration[38], DNA immobilization, and NHS

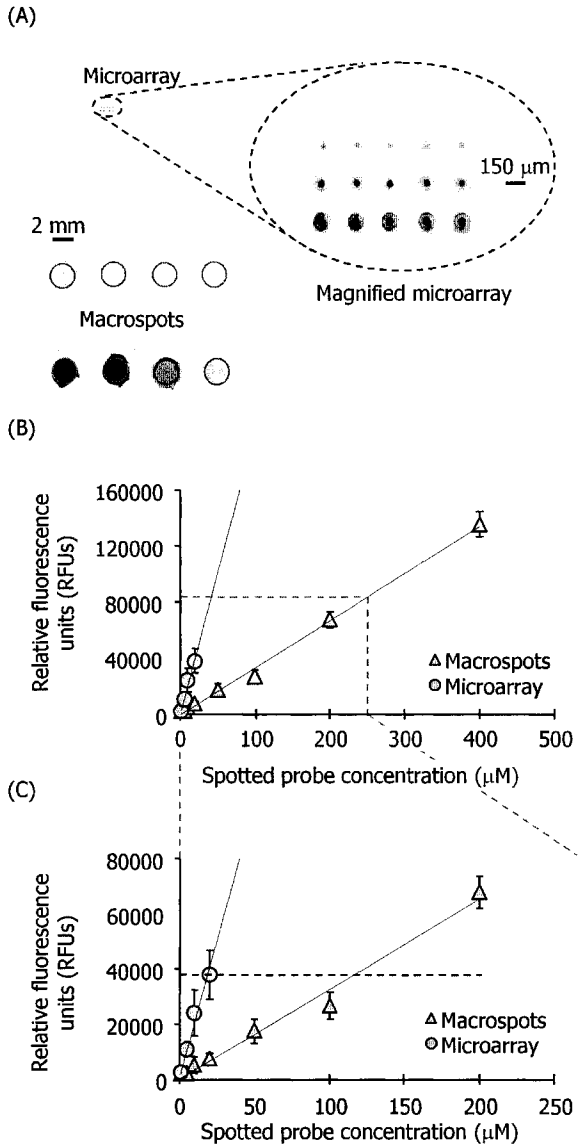

Figure 5.2 Relative amounts of DNA probe immobilized onto CodeLink™ slides are compared on microarray and macrospot formats using fluorescence-labeled DNA probes. (A) Macrospot array and microarray images are shown side by side. Microarrays are printed at four DNA concentrations (top to bottom rows: 1, 5, 10 and 20 μM, 150 mM sodium phosphate buffer, pH 8.5) in replicates of 5. Spotted macrospot (1.0 M sodium phosphate buffer, pH 8.5) concentrations are 1, 5, 10, 20 (upper row from right to left), 50, 100, 200 and 400 μM (lower row from right to left). (B) Macro-scale DNA immobilization was studied using DNA solution concentrations ranging from 1 μM up to 400 μM. A linear dependence of immobilized DNA density on applied solution DNA concentration was observed for both the micro- ($y= 2013.2x$, $R^2=0.9693$) and macro- ($y=336.71x$, $R^2=0.9963$) spotting formats. (C) Resulting DNA probe density in a typical 20 μM microarray printing is equivalent to density from approximately 125 μM macro-scale immobilization.

blocking) to the fresh, as received, microarray slides (Tables 5.2 and 5.3, and Figure 5.3). The slide polymer substrate chemistry has been reported elsewhere[47] and confirmed here by XPS to be consistent with polyacrylamide with activated ester groups providing attachment sites for aminated DNA. Compositional XPS data showed the presence of silicon, carbon, oxygen, nitrogen, and trace ions (calcium, sodium, and chlorine) within the polymer layer (Table 5.2). Compared to slides taken directly from vendor packaging,

Table 5.2 XPS elemental composition analysis of modified Codelink™ microarray slides used in DNA macrospot assays. To facilitate sequential step-wise surface modification comparisons, data were collected from a single slide (n=3 spots; standard deviations shown in parentheses below each mean).

	Atomic %							
Slide Surface	**C1s**	**O1s**	**N1s**	**Si2p**	**Na1s**	**Cl2p**	**Ca2p**	**P2p**
Fresh, unmodified	53.1	25.7	10.3	7.5	2.9	0.3	0.2	nd
	(0.7)	*(0.2)*	*(0.3)*	*(0.3)*	*(0.2)*	*(0.1)*	*(0.0)*	
Regenerated[38]	56.1	24.5	11.6	7.2	0.3	0.2	0.2	nd
	(1.8)	*(0.9)*	*(0.3)*	*(0.6)*	*(0.0)*	*(0.1)*	*(0.1)*	
Blocked (ethanolamine)	53.2	26.5	11.2	8.2	0.8	nd	0.2	nd
	(1.8)	*(0.7)*	*(0.3)*	*(0.7)*	*(0.1)*		*(0.0)*	
DNA (200 μM) + Blocking	52.5	26.6	12.3	7.2	0.8	nd	0.3	0.3
	(0.9)	*(0.3)*	*(0.2)*	*(0.3)*	*(0.1)*		*(0.1)*	*(0.1)*

regenerated slides[38] showed increases in carbon and nitrogen signals and a decrease in oxygen and sodium. Carbon and nitrogen increased signal can be attributed to the re-activation of hydrolyzed carboxylic acid moieties to NHS active ester functional groups by regeneration[38] and the modest decrease in oxygen is due to slight attenuation of the base glass substrate. With the addition of DNA, the most notable changes are the slight increase in nitrogen and the appearance of P2p signal. A pure polyacrylamide layer has a theoretical C/N compositional ratio of ~3.3 and analogous O/N of 1.0. The calculated C/N and O/N ratios of 5.1 and 2.5 from XPS results confirm the presence of additional chemical moieties (i.e., side chain DNA-reactive attachment sites on modified polymer)

as well as the substrate signals and probable organosilane coupling layer and cross-linking agents. Substrate (glass) detection contributes to the increased oxygen signal, and a likely organosilane coupling layer facilitating attachment of reactive modified polyacrylamide to the base glass substrate, polymer active ester moieties, and cross-linking molecules all contribute to the increased C1s content consistent with the detected XPS atomic ratios. Based on the detection of the base silicon Si2p signal, and given the XPS sampling depth of ~ 4.6 nm under these conditions, the overall average dry layer thickness of the Codelink™ polymer layer is apparently < 5 nm to observe these signals.

In addition to the surface elemental composition data, high-resolution XPS data was collected for each of the adlayers (Figure 5.3 and Table 5.3). High-resolution XPS

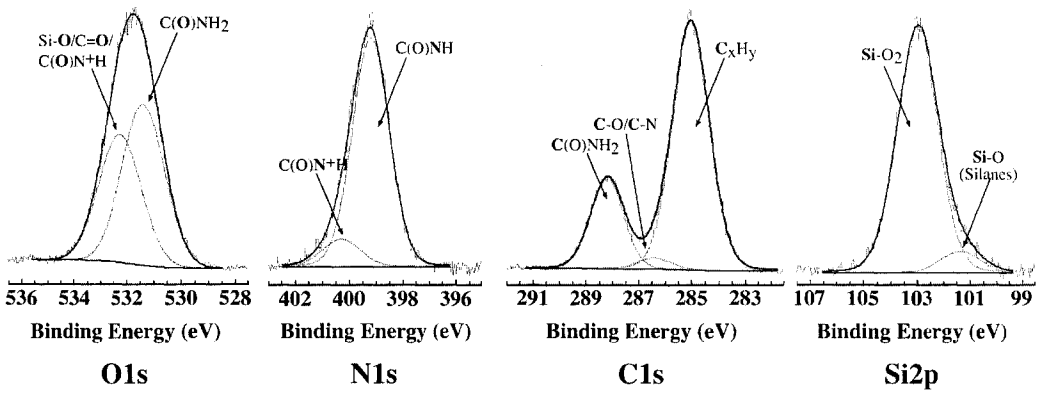

Figure 5.3 XPS high-resolution spectra for Si2p, C1s, N1s, and O1s signals for as-supplied Codelink™ microarray slides collected at a take-off angle of 35° (sampling depth ~ 4.6 nm).

peak fits agree well with published data for polyacrylamide layers but deviate slightly due to the detection of the base substrate signal[48]. With the addition of the different surface reactions, the most notable changes in the high-resolution data are observed in the C1s data. Upon grafting of DNA, XPS hydrocarbon signal (285.0 eV) decreased (probable attenuation of the base substrate organosilane layer), and C-O/C-N content

increased due to presence of the overlayer of DNA bases. Changes within the Si2p, N1s, and O1s high-resolution peaks were only modest due to the overwhelming signal from the Codelink™ slide chemistry.

Substantial amounts of nitrogen (10-11 at.%) in the CodeLink™ polymer layer precluded efficient use of nitrogen for XPS study of DNA immobilization, leaving DNA phosphorus as the only unique characteristic element. Therefore, XPS quantification of relative amounts of surface-immobilized and hybridized DNA oligomers exploited this P2p signal. The intrinsically weak sensitivity of the phosphorus P2p signal combined

Table 5.3 High resolution XPS chemical species analysis of modified Codelink™ microarray slides. To facilitate sequential step-wise surface modification comparisons, data were collected from a single slide (n=3 spots; standard deviations shown in parentheses below each mean).

			Slide Surface			
	(eV)		**Fresh**	**Regenerated**[38]	**Blocked**	**DNA***
Si2p	101.45	Si Silanes	8.4%	7.7%	7.4%	6.8%
	(0.01)		*(0.4%)*	*(1.8%)*	*(1.2%)*	*(1.2%)*
	103.07	Si in **Si**O_2	91.6%	92.3%	92.6%	93.2%
	(0.08)		*(0.4%)*	*(1.8%)*	*(1.2%)*	*(1.2%)*
C1s	285.00	**C**$_x$H$_y$	72.6%	72.0%	71.9%	66.7%
	(0.00)		*(1.1%)*	*(0.4%)*	*(0.9%)*	*(1.2%)*
	286.40	**C**-O/**C**-N	4.3%	6.6%	6.9%	10.5%
	(0.00)		*(1.2%)*	*(1.0%)*	*(1.0%)*	*(0.4%)*
	288.20	**C**(O)NH_2	23.1%	21.4%	21.2%	22.8%
	(0.02)		*(1.0%)*	*(1.0%)*	*(0.6%)*	*(0.8%)*
N1s	399.76	C(O)**N**H	90.9%	96.8%	97.0%	95.2%
	(0.03)		*(0.4%)*	*(1.3%)*	*(2.0%)*	*(1.7%)*
	400.96	C(O)**N**$^+$H	9.1%	3.2%	3.0%	4.8%
	(0.01)		*(0.4%)*	*(1.3%)*	*(2.0%)*	*(1.7%)*
O1s	531.45	C(**O**)-NH_2	59.2%	52.9%	55.6%	55.7%
	(0.02)		*(2.2%)*	*(0.3%)*	*(3.3%)*	*(1.7%)*
	532.43	Si-**O**/C=**O**/ C(**O**)N$^+$H	40.8%	43.7%	43.9%	43.4%
	(0.09)		*(2.2%)*	*(1.2%)*	*(3.1%)*	*(0.6%)*
	533.78	C-**O**	nd	3.4%	0.5%	0.9%
	(0.06)			*(1.4%)*	*(0.4%)*	*(1.2%)*

*For adlayer comparisons, DNA was coupled at 200 μM using the macrospot protocol; reported values are from DNA modified regenerated slides after blocking.

with the resolution of this technique (spot size 800 μm) requires that a DNA feature be analyzed at the millimeter scale for meaningful signal analysis. Microarray-specific on-spot analysis is therefore difficult without new, high-resolution imaging XPS capabilities.[49,50] Even with such imaging capabilities, reliable capture of meaningful nucleotide P2p XPS signals from micron-size DNA features currently requires hours of data collection, significant XPS instrument time and hence substantial resources. Hence, given current surface analytical instrumental limitations, an alternative to high-resolution imaging XPS of microarray DNA spots is the use of macro-scale analogs of microarray spots compatible with conventional XPS resolution for microarray DNA density quantification. The same concept also applies to analyses of microarray DNA by other spatial resolution-limited techniques.

Therefore, XPS P2p spectra were collected for 4.5 mm-diameter macrospots immobilized at 0 μM, 10 μM, 50 μM, 100 μM and 200 μM DNA probe concentrations, and then hybridized with 1 μM DNA target. For elemental comparisons of slides modified with different concentrations of DNA, utility scans were collected for the main elements (Si2p, C1s, N1s, O1s, and P2p). The 0 μM DNA print control samples represent unmodified polymer slides exposed to identical buffer printing, incubation, post-immobilization wash and hybridization steps as the probe DNA-modified samples, but in the absence of DNA. Figure 5.4 shows the relative amount of surface-immobilized probe and hybridized DNA oligomers analyzed using XPS P2p peak integration. DNA surface amounts are proportional to the integrated area underneath the characteristic phosphorus peaks. The first high-resolution XPS P2p spectrum of surface-immobilized oligonucleotides on gold, collected and published by Tarlov et al.[44] showed a single P2p

peak observed at 133.6 eV in good agreement with the location of the P2p peak in single nucleotide species[37]. Integrated P2p peak areas have also been previously reported as a quantification method for immobilized DNA surface abundance on silane-modified silicon substrates when N1s cannot be used as a characteristic indicator of DNA.[20] With these precedents on model systems, we focused on creating an accurate surface quantification method that can be routinely applied to surface-bound DNA on commercial arraying substrates. To allow practical deployment for quality control, an XPS utility mode spectral acquisition with intermediate pass energy and step size was chosen instead of the more commonly used high-resolution mode in order to significantly shorten the sampling time while still maintaining satisfactory analytical spectral features.

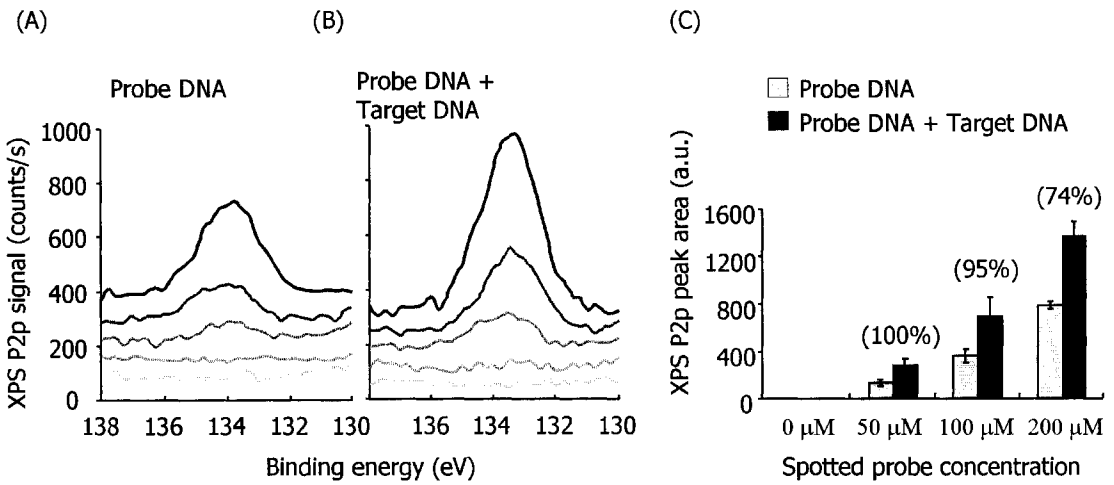

Figure 5.4 Relative amounts of surface-immobilized and hybridized DNA oligomers analyzed using XPS P2p signals. Amounts of DNA on CodeLink™ surfaces are proportional to integrated area underneath the characteristic phosphorus peaks. Integrated P2p peak area of the probe-immobilized (A) and target-hybridized (1 μM) (B) surfaces increased with increasing DNA probe solution concentration (200 μM, 100 μM, 50 μM, 10 μM and 0 μM from top to bottom in figures). (C) XPS P2p peak areas were quantified, yielding hybridization efficiencies shown above each concentration (parentheses) derived as a percentage of probe molecules hybridized [((peak area of hybridized spot/peak area of probe spot) – 1) x 100%]. Hybridization efficiency slightly above 100% was rounded to 100%. Error bars represent results from at least three independent replicates.

Integrated P2p peak areas for probe-immobilized (Figure 5.4A) and target-hybridized (Figure 5.4B) surfaces both increase with DNA probe solution concentration. Quantified peak integrated areas are shown in Figure 5.4C. Consistent with increasing P2p signal, XPS N1s signal also increased slightly and Si2p (glass) signal decreased (data not shown), all consistent with DNA overlayer formation. Hybridization efficiencies were derived as percentage of probe molecules hybridized [((peak area of hybridized spot/peak area of probe spot) – 1) x 100%]. Error bars represent results from three independent replicate experiments. A hybridization efficiency of 100% was obtained for the lower probe concentration samples (^{32}P density of the lower 10^{12} molecules/cm^2); at 200 μM probe print concentration, 70% hybridization efficiency was obtained. This lower hybridization efficiency at higher probe coverage can be explained by steric effects (molecular crowding): tethered polyanionic DNA probes closely packed by immobilization electrostatically repel and sterically hinder DNA targets from forming duplexes on the surface.[51-53]

^{32}P radiometric analysis of DNA surface density. Although XPS analysis provides element-specific, quantitative elemental information on relative amounts of DNA on the surface, it does not readily quantify absolute densities (e.g., molecules/cm^2). Absolute densities of immobilized DNA probes and hybridized DNA targets were quantified using ^{32}P end-labeled DNA. Density values shown in Figure 5.5 are the average of at least three independent experiments with three replicate spots per experiment. Consistent with fluorescence results, for all oligoDNA concentrations studied, a linear ^{32}P signal dependence was observed between immobilized probe density and spotted probe solution concentration the macrospot methods. Corroborating XPS

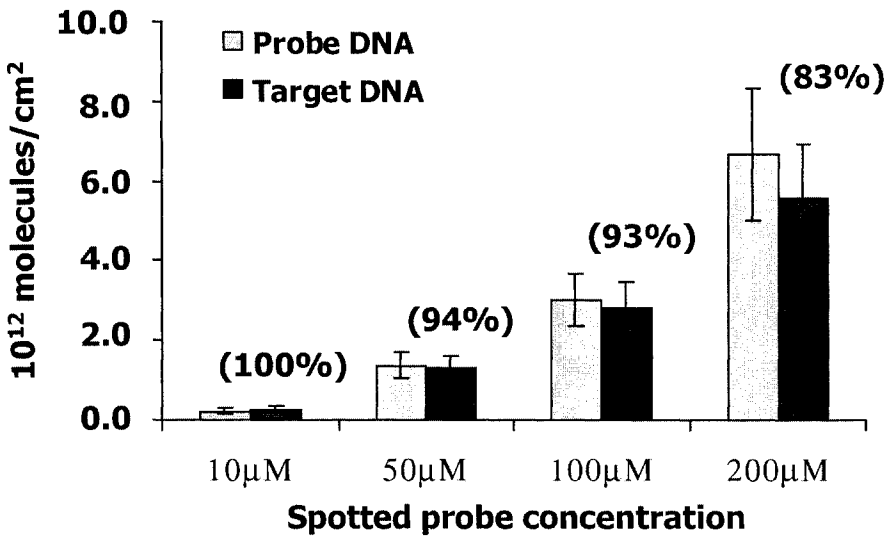

Figure 5.5 Absolute surface densities (molecules/cm^2) for DNA probe and target were quantified using radiometric methods. Hybridization efficiencies shown above each concentration (parentheses) were derived as percentage of probe molecules hybridized (target density/probe density x 100%). Hybridization efficiency slightly above 100% was rounded to 100%. Error bars represent results from at least three independent replicated experiments.

results, ^{32}P-labeling results show that DNA surface probe density increased with increasing probe DNA concentration. Highest densities achieved using the 200 μM DNA probe solution in macrospot (non-drying) protocols were 6.7 x 10^{12} probes/cm^2. This density is limited by the amount of DNA practically available for immobilization (i.e., solution concentration and volume), not surface-activated amine-reactive groups, as the dependence of immobilized probe density on spotting probe concentration did not reach surface saturation (e.g., no plateau was observed). Printed microarray oligoDNA probe density (desiccated nano-drops) at 20 μM DNA concentration, equaling RFUs from that of macro-spotting at 125 μM DNA concentration (Figure 5.2), was extrapolated from ^{32}P data to be 4.1x10^{12} probes/cm^2. Hybridized DNA target density also increased with increasing printed probe DNA solution concentration, but hybridization efficiencies were

higher at lower probe densities (e.g., 100% at $2.1x10^{11}$ probes/cm^2), decreasing slightly at densities of $1.4x10^{12}$ and $3.0x10^{12}$ probes/cm^2, and finally diminishing to 83% at the highest oligoDNA probe density ($6.7x10^{12}$ probes/cm^2). Calculated hybridization efficiencies slightly above 100% were rounded to 100%. Non-specific protein binding, via base amine reaction[46] or by physisorption, may contribute to target hybridization signal detected. However, as control experiments indicate (subtracted in Figure 5.5), this contribution is less than 5% of the probe signal, and therefore much less than 5% of the total hybridization signal. This non-specific contribution to assay signal is certainly a very minor component. Complete hybridization efficiency (e.g., 100% efficiency) dependence on probe density was in good agreement with values of $1.5\text{-}5x10^{12}$ probes/cm^2 reported by others immobilizing thiolated DNA on planar gold substrates from bulk solution adsorption.[21,54] The slightly lower values reported here could possibly be attributed to accessibility of probe DNA within the three-dimensional CodeLink™ gel matrix network compared to DNA –DNA duplex formation on planar gold surfaces.

Correlating XPS and radiometric results for DNA surface capture. To provide quantitative significance to relative fluorescence units shown in Figure 5.2, semi-quantitative XPS results and quantitative ^{32}P-labeling results were integrated into correlative DNA signal calibration plots versus RFUs, shown in Figure 5.6(A-C). With these data, semi-quantitative DNA surface density results collected from XPS can be calibrated against RFUs using absolute DNA surface densities obtained from radiometric ^{32}P labeling experiments. Results from the two quantitative approaches (Fig. 5.6A) correlate linearly to high reliability (correlation coefficient greater than 0.99), providing a reliable standard curve useful for routine determinations of DNA surface densities using

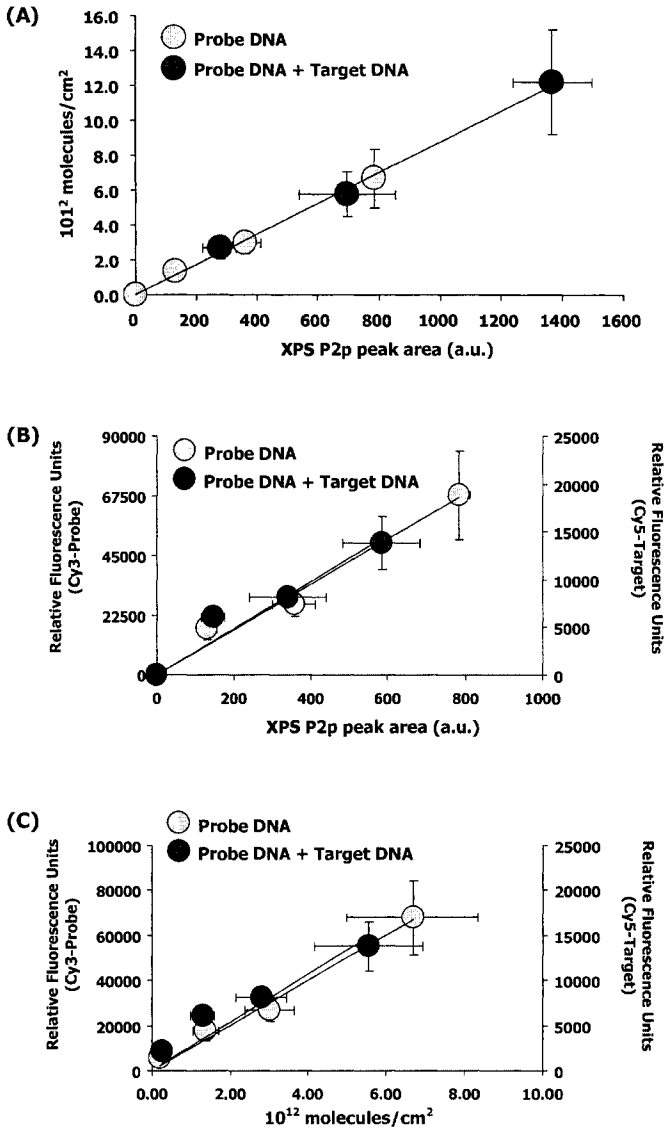

Figure 5.6 Cross-correlation of three different analytical methods for measuring DNA immobilization on commercial array slides: (A) semi-quantitative XPS P2p DNA surface density results (x-axis) correlated to molecular ^{32}P-DNA surface densities (from radiometric labeling experiments) (y-axis). Ordinary least squares regression produced a fit: y=0.0088x (R^2>0.99). (B) Cy3-DNA fluorescence probe (left) and Cy5-DNA target (right) RFU signals correlated to XPS P2p DNA surface signals (lines are best-fit linear regressions for each data set); and (C) Cy3-DNA fluorescence probe (left) and Cy5-DNA target (right) RFU signals correlated to ^{32}P-DNA surface densities from radiometric labeling experiments (lines are best-fit linear regressions for each data set). In all plots, gray disks represent data points from surface immobilized DNA probe samples (right y-axis); black disks represent data points from DNA hybridized samples (left y-axis).

convenient lower resolution XPS analysis methods. This linear "standard curve" is empirical, with an intrinsic dependence on the surfaces, assay conditions, and DNA, but provides a conceptual basis to correlate multiple surface techniques in microarray validation. XPS and ^{32}P data were then further correlated with observed RFUs on identical arrays to apply DNA densities to array RFU signals. Figure 5.6B shows RFU signal relationships to XPS P2p signals for both immobilized probe and hybridized target on these surfaces. Linear correlations are observed between the data, suggesting that XPS P2p and RFUs are measuring similar DNA surface density profiles, and that XPS validates RFU signals. Figure 5.6C makes this relationship quantitative, establishing a linear correlation between RFU signals for both immobilized probe and hybridized target signals on surfaces with DNA molecular density information from radioactive ^{32}P measurements. To our knowledge, this is the first such quantitative cross-correlation between conventional RFU measurements, XPS and radiometric approaches to yield molecular meaning to both XPS and RFUs, especially on a commercial arraying platform.

In such correlations, we note that RFU intensities are largely case-specific and variable, depending significantly on the dye label chemistry and photophysics, the DNA labeling efficiency (i.e., batch-batch variations in labeled DNA probe or target from PCR), vendor methods for DNA labeling, and quite possibly, oligonucleotide sequence and length, and array substrate chemistry (unpublished observations). Additionally, scanning and image analysis conditions also provide an intrinsic source of RFU variation, where different laser power PMT settings and collection optics from one scanner to another contribute to cross-platform RFU signal variation. A significant challenge in proving reliability and reproducibility for the bioanalytical metrics in microarray assays

will be to establish a quantitative understanding of the common RFU unit, its standardization and interpretation in absolute molecular terms capable of absolute quantitation (compared to relative abundance), implications to microarray data interpretation and, importantly, intrinsic limitations for applications in analyzing genetic assessments, disease diagnosis, and comparative expression assays.[9] We believe that this can currently be achieved by creating these cross-technique standard curves for nucleotide signals on surfaces and comparing information across these techniques.

5.5 Conclusions

Spotted, rapid-drying microarray DNA surface densities were successfully correlated with that of solution-phase macro-scale immobilized DNA densities using XPS, fluorescence scanning and radiometric methods. Fabrication of the 4.5 mm-diameter macro-scale array analogs required significantly higher buffer ionic strength and probe DNA concentrations to provide immobilized DNA densities roughly equivalent to spotted, dried microarray formats. This was attributed to differences in DNA bulk solution applications to surfaces and non-equilibrium dynamics of rapid micro-spot solvent evaporation. Typical probe densities obtained in microarray printing, using 20 μM 20mer aminated oligonucleotides in 0.15 M sodium phosphate spotting buffer, can be reproduced at macroscopic sizes using 125 μM DNA in 1 M spotting buffer. This DNA probe density was quantified using ^{32}P-radiometric assays to be 6.7×10^{12} probes/cm^2. Complete hybridization efficiency (100%) was achieved for lower DNA probe densities (e.g., at 10 μM probe concentration with resulting probe density of 2.1×10^{11} probes/cm^2). With increasing surface probe density, hybridization efficiency decreased slightly, maintaining a satisfactory efficiency of ~75-85% at the highest experimentally tested

probe density of $6.7x10^{12}$ molecules/cm^2. The proven immobilization density equivalence of macro-scale and micro-scale surface-immobilized DNA features allows molecular-level surface analysis by various quantitative, high-resolution surface analytical techniques that currently require features larger than a few hundred microns, such as XPS and FTIR methods.

Sensitive ^{32}P-DNA radiometric measurements accurately calibrate the DNA molecular densities from more routine XPS DNA analysis data, producing reproducible conversion of XPS signals into DNA molecular densities. This cross-comparison allows direct translation of high-resolution macro-scale DNA surface analysis to micro-spot arrays where DNA surface information is currently limited. Importantly, this also facilitates future routine DNA density determinations on this commercial arraying surface by use of routine methods (e.g., XPS) compared with standard curves, without the need for hazardous radioactive quantitation assays once standard curves for a given arraying surface are established. Ultimately, these quantitative aspects should be correlated to the often-reported fluorescence RFU signal unit for industry-standard and clinically relevant microarray assays, as a step toward standardizing, interpreting and directly quantifying this relative surface signal in this bioassay format. Absolute DNA molecular capture efficiencies as an assay endpoint should therefore be possible, in contrast to the relative data capabilities currently limiting the utility of the microarray assay technique. Lastly, such an approach demonstrated here for popular commercial arraying format can be applied to any microarraying surface, using multi-technique comparisons via surface-specific standard curves.

5.6 Acknowledgements

The authors are grateful for financial support from NIH EB001473. Technical assistance in fluorescence scanning from Dr. W. H. Hanneman (CSU) and insightful discussions with C. Greef, M. Lochhead, D. Castner, L. Gamble and C-Y. Lee are gratefully acknowledged.

5.7 References

(1) Ramsay, G. *Nat. Biotechnol.* **1998**, *16*, 40-44.

(2) Schena, M.; Heller, R. A.; Theriault, T. P.; Konrad, K.; Lachenmeier, E.; Davis, R. W. *Trends Biotechnol.* **1998**, *16*, 301-306.

(3) Sanchez-Carbayo, M.; Bornmann, W.; Cordon-Cardo, C. *Curr. Org. Chem.* **2000**, *4*, 945-971.

(4) Freeman, W. M.; Robertson, D. J.; Vrana, K. E. *BioTechniques* **2000**, *29*, 1042-1044, 1046, 1048-1055.

(5) van Hal, N. L. W.; Vorst, O.; van Houwelingen, A. M. M. L.; Kok, E. J.; Peijnenburg, A.; Aharoni, A.; van Tunen, A. J.; Keijer, J. *J. Biotechnol.* **2000**, *78*, 271-280.

(6) Helmberg, A. *Exp. Gerontol.* **2001**, *36*, 1189-1198.

(7) Beaucage, S. L. *Curr. Med. Chem.* **2001**, *8*, 1213-1244.

(8) Yang, Y. H.; Speed, T. *Nat. Rev. Genet.* **2002**, *3*, 579-588.

(9) Sherlock, G. *Nat. Methods* **2005**, *2*, 329-330.

(10) Kuo, W. P.; Jenssen, T.-K.; Butte, A. J.; Ohno-Machado, L.; Kohane, I. S. *Bioinformatics* **2002**, *18*, 405-412.

(11) Ross, D. T.; Scherf, U.; Eisen, M. B.; Perou, C. M.; Rees, C.; Spellman, P.; Iyer, V.; Jeffrey, S. S.; Van de Rijn, M.; Waltham, M.; Pergamenschikov, A.; Lee, J. C.; Lashkari, D.; Shalon, D.; Myers, T. G.; Weinstein, J. N.; Botstein, D.; Brown, P. O. *Nat. Genet.* **2000**, *24*, 227-235.

(12) Tan, P. K.; Downey, T. J.; Spitznagel, E. L., Jr.; Xu, P.; Fu, D.; Dimitrov, D. S.; Lempicki, R. A.; Raaka, B. M.; Cam, M. C. *Nucleic Acids Res.* **2003**, *31*, 5676-5684.

(13) Yauk Carole, L.; Berndt, M. L.; Williams, A.; Douglas George, R. *Nucleic Acids Res.* **2004**, *32*, e124.

(14) Larkin, J. E.; Frank, B. C.; Gavras, H.; Sultana, R.; Quackenbush, J. *Nat. Methods* **2005**, *2*, 337-343.

(15) Irizarry, R. A.; Warren, D.; Spencer, F.; Kim, I. F.; Biswal, S.; Frank, B. C.; Gabrielson, E.; Garcia, J. G. N.; Geoghegan, J.; Germino, G.; Griffin, C.; Hilmer, S. C.; Hoffman, E.; Jedlicka, A. E.; Kawasaki, E.; Martinez-Murillo, F.; Morsberger, L.; Lee, H.; Petersen, D.; Quackenbush, J.; Scott, A.; Wilson, M.; Yang, Y.; Ye, S. Q.; Yu, W. *Nat. Methods* **2005**, *2*, 477.

(16) Bammler, T.; Beyer Richard, P.; Bhattacharya, S.; Boorman Gary, A.; Boyles, A.; Bradford Blair, U.; Bumgarner Roger, E.; Bushel Pierre, R.; Chaturvedi, K.; Choi, D.; Cunningham Michael, L.; Deng, S.; Dressman Holly, K.; Fannin Rickie, D.; Farin Fredrico, M.; Freedman Jonathan, H.; Fry Rebecca, C.; Harper, A.; Humble Michael, C.; Hurban, P.; Kavanagh Terrance, J.; Kaufmann William, K.; Kerr Kathleen, F.; Jing, L.; Lapidus Jodi, A.; Lasarev Michael, R.; Li, J.; Li, Y.-J.; Lobenhofer Edward, K.; Lu, X.; Malek Renae, L.; Milton, S.; Nagalla Srinivasa, R.; O'Malley Jean, P.; Palmer Valerie, S.; Pattee, P.; Paules Richard, S.; Perou Charles, M.; Phillips, K.; Qin, L.-X.; Qiu, Y.; Quigley Sean, D.; Rodland, M.; Rusyn, I.; Samson Leona, D.; Schwartz David, A.; Shi, Y.; Shin, J.-L.; Sieber Stella, O.; Slifer, S.; Speer Marcy, C.; Spencer Peter, S.; Sproles Dean, I.; Swenberg James, A.; Suk William, A.; Sullivan Robert, C.; Tian, R.; Tennant Raymond, W.; Todd Signe, A.; Tucker Charles, J.; Van Houten, B.; Weis Brenda, K.; Xuan, S.; Zarbl, H. *Nat. Methods* **2005**, *2*, 351-356.

(17) http://www.roche-diagnostics.com/products_services/amplichip_cyp450.html.

(18) Grainger, D. W.; Greef, C. H.; Gong, P.; Lochhead, M. J. In *Microarrays: Methods and Protocols (Methods in Molecular Biology)* Rampal, J. B., Ed., 2006, in press.

(19) Petrovykh Dmitri, Y.; Kimura-Suda, H.; Whitman Lloyd, J.; Tarlov Michael, J. *J. Am. Chem. Soc.* **2003**, *125*, 5219-5226.

(20) Shen, G.; Anand, M. F. G.; Levicky, R. *Nucleic Acids Res.* **2004**, *32*, 5973-5980.

(21) Herne, T. M.; Tarlov, M. J. *J. Am. Chem. Soc.* **1997**, *119*, 8916-8920.

(22) Boland, T.; Ratner, B. D. *P. Natl. Acad. Sci.* **1995**, *92*, 5297-5301.

(23) Rabke, C. E.; Wenzler, L. A.; Beebe, T. P., Jr. *Scanning Microscopy* **1994**, *8*, 471-480.

(24) Patrick, J. S.; Cooks, R. G.; Pachuta, S. J. *Biological Mass Spectrometry* **1994**, *23*, 653-659.

(25) Boland, T.; Ratner, B. D. *Langmuir* **1994**, *10*, 3845-3852.

(26) Benninghoven, A. *J. Vac. Sci. Technol., A* **1985**, *3*, 451-460.

(27) Arlinghaus, H. F.; Kwoka, M. N.; Jacobson, K. B. *Anal. Chem.* **1997**, *69*, 3747-3753.

(28) Arlinghaus, H. F.; Hoppener, C.; Drexler, J. *Secondary Ion Mass Spectrometry, SIMS XII, Proceedings of the International Conference on Secondary Ion Mass Spectrometry, 12th, Brussels, Belgium, Sept. 5-10, 1999* **2000**, 951-954.

(29) Crain, J. N.; Kirakosian, A.; Lin, J. L.; Gu, Y.; Shah, R. R.; Abbott, N. L.; Himpsel, F. J. *J. Appl. Phys.* **2001**, *90*, 3291-3295.

(30) Cavic, B. A.; McGovern, M. E.; Nisman, R.; Thompson, M. *Analyst (Cambridge, U. K.)* **2001**, *126*, 485-490.

(31) Steel, A. B.; Levicky, R. L.; Herne, T. M.; Tarlov, M. J. *Biophys. J.* **2000**, *79*, 975-981.

(32) Zammatteo, N.; Jeanmart, L.; Hamels, S.; Courtois, S.; Louette, P.; Hevesi, L.; Remacle, J. *Anal. Biochem.* **2000**, *280*, 143-150.

(33) Balladur, V.; Theretz, A.; Mandrand, B. *J. Colloid Interf. Sci.* **1997**, *194*, 408-418.

(34) Halliwell, C. M.; Cass, A. E. G. *Anal. Chem.* **2001**, *73*, 2476-2483.

(35) Petrovykh, D. Y.; Kimura-Suda, H.; Tarlov, M. J.; Whitman, L. J. *Langmuir* **2004**, *20*, 429-440.

(36) Samuel, N. T.; Castner, D. G. *Appl. Surf. Sci.* **2004**, *231-232*, 397-401.

(37) May, C. J.; Canavan, H. E.; Castner, D. G. *Anal. Chem.* **2004**, *76*, 1114-1122.

(38) Gong, P.; Grainger, D. W. *Surf. Sci.* **2004**, *570*, 67-77.

(39) Lee, C.-Y.; Canavan, H. E.; Gamble, L. J.; Castner, D. G. *Langmuir* **2005**, *21*, 5134-5141.

(40) Mazzola, L. T.; Frank, C. W.; Fodor, S. P. A.; Mosher, C.; Lartius, R.; Henderson, E. *Biophys. J.* **1999**, *76*, 2922-2933.

(41) Forman, J. E.; Walton, I. D.; Stern, D.; Rava, R. P.; Trulson, M. O. *ACS Sym. Ser.* **1998**, *682*, 206-228.

(42) Ratner, B. D.; Castner, D. G. In *Surface Analysis - The Principal Techniques*; Vickerman, J. C., Ed.; John Wiley & Sons Ltd, 1997.

(43) Zhang, Y.; Tirrell, M.; Mays, J. W. *Macromolecules* **1996**, *29*, 7299-7301.

(44) Petrovykh, D. Y.; Kimura-Suda, H.; Whitman, L. J.; Tarlov, M. J. *J. Am. Chem. Soc.* **2003**, *125*, 5219-5226.

(45) Castelino, K.; Kannan, B.; Majumdar, A. *Langmuir* **2005**, *21*, 1956-1961.

(46) Huang, E.; Zhou, F.; Deng, L. *Langmuir* **2000**, *16*, 3272-3280.

(47) Ramakrishnanm, R.; Dorris, D.; Lublinsky, A.; Nguyen, A.; Domanus, M.; Prokhorova, A.; Gieser, L.; Touma, E.; Lockner, R.; Tata, M.; Zhu, X.; Patterson, M.; Shippy, R.; Sendera, T. J.; Mazumder, A. *Nucleic Acids Res.* **2002**, *30*, e30/31-e30/12.

(48) Garg, D. H.; Lenk, W.; Berwald, S.; Lunkwitz, K.; Simon, F.; Eichhorn, K. J. *J. Appl. Polym. Sci.* **1996**, *60*, 2087-2104.

(49) Vohrer, U.; Blomfield, C.; Page, S.; Roberts, A. *Appl. Surf. Sci.* **2005**, *252*, 61-65.

(50) Blomfield, C. J. *J. Electron Spectrosc. Relat. Phenom.* **2005**, *143*, 241-249.

(51) Heaton, R. J.; Georgiadis, R. M.; (Trustees of Boston University, USA; Heaton, Jonathan R.). Application: WOWO, 2002, pp 59 pp.

(52) Peterson, A. W.; Heaton, R. J.; Georgiadis, R. M. *Nucleic Acids Res.* **2001**, *29*, 5163-5168.

(53) Heaton, R. J.; Peterson, A. W.; Georgiadis, R. M. *P. Natl. Acad. Sci.* **2001**, *98*, 3701-3704.

(54) Peterson, A. W.; Wolf, L. K.; Georgiadis, R. M. *J. Am. Chem. Soc.* **2002**, *124*, 14601-14607.

Chapter 6 Complex Milieu and Non-specific Binding Influences on Microarray DNA Hybridization on Commercial Slides

This dissertation chapter was written by Ping Gong and edited by David W. Grainger. This chapter describes the preliminary research of microarray complex milieu hybridization performance on commercial slides and proposes future work required to complete the complex milieu hybridization study.

Complex Milieu and Non-specific Binding Influences on Microarray DNA Hybridization on Commercial Slides

Ping Gong, David Grainger

6.1 Abstract

Direct nucleic acid assay from complex samples (e.g., food, tissue, blood, serum, or PCR mix) is attractive but currently difficult and far from routine, especially in microarray assay format. In this study, DNA hybridization from cell lysate dilutions onto surface-immobilized printed DNA probe layers on commercial amine-reactive polymer-coated microarray slides is investigated using conventional fluorescence intensity measurements. Dynamic assay range of DNA oligomer target concentration is determined in hybridization buffer. Microarray DNA hybridization signal in buffer and cell lysate dilutions are compared, and no significant variations are observed. Target hybridization to probe microarrays printed onto both fresh (direct from supplier) and ethanolamine-blocked control slides are compared to assess hybridization fluorescence signal specificity. Notable amounts of microarray fluorescence are observed on ethanolamine-blocked control slides, indicating non-specific DNA attachment to substrate surfaces. A further series of control experiments are proposed to validate microarray hybridization results in order to complete this study.

6.2 Introduction

Nucleic acid assay is conducted almost exclusively from simple buffer solutions containing amplified target purified from PCR processes. DNA target capture cannot be conducted from complex biological milieu (e.g., tissue homogenates, cell lysate, PCR mix, food or environmental samples, or serum-based solutions) because assay surfaces are not capable of producing sufficient signal:noise without (1) high amplification of the target in the milieu, and (2) pre-purification of all competing, confounding and interfering co-adsorbates.[1] Literature reports for detection limits for various nucleic acid capture assays[2] range from nanomolar[3-5] (nM) to zeptomolar (zM)[6,7]. Almost all of these are conducted in simple buffer systems where only the target is present. Assays from PCR amplification without the two common ultracentrifugation steps to purify away confounding reagents, or from biologically complex samples are not often reported, and when they are, limits of detection are substantially reduced[8]. Surface capture assay systems will be incapable of point-of-care, direct sample-to-answer measurements without improvements in assays from complex milieu. Improved detection limits, assay methods that eliminate confounding noise intrinsic to most biological adsorbates, and reliable direct-from-sample reporting are goals that require further understanding of the current problems with surface-capture assay formats.

6.3 Experimental section

Materials. Phosphate, borate and Tris buffer components, 1-(3-dimethylaminopropyl)-3-ethlcarbodiimide hydrochloride (EDCI), N-hydroxysuccinimide (NHS), Tween 20, sarcosine, sodium citrate (SSC), sodium dodecyl sulfate (SDS) and ethanolamine were purchased from Sigma-Aldrich (St. Louis, MO) and used as received.

Commercial polymer-coated microarray slides were purchased from Amersham (Codelink™, Tempe, AZ) and are marketed as amine-reactive and three-dimensional (i.e., crosslinked polymer networks of thicknesses greater than a monolayer) hydrophilic polymer coatings on low-fluorescence glass substrates.

Cell culture and protein harvest. Murine monocyte-macrophage secondary cell line RAW 264.7 was obtained from the American Type Culture Collection (ATCC, Manassas, VA). Cells were cultured in RPMI 1640 (Mediatech) supplemented with 10% fetal bovine serum (FBS, HyClone) and 1% penicillin-streptomycin (Life Technologies). Cultures were maintained in T175 tissue culture polystyrene (TCPS) flasks (Nunc™) under standard conditions: incubation at 37°C, 98% humidity and 5% CO_2. Cells were dissociated from culture flasks by incubation with Ca^{2+}- and Mg^{2+}- free cell culture grade Hank's balanced salt solution (HBSS, Life Technologies). Cells were washed once with DPBS (HyClone) to remove residual media, and lysed with 0.5-1 ml of M-PER® (Pierce). Buffers were supplemented with protease inhibitors [1 μg/ml aprotinin, 1 μg/ml leupeptin and 1 mM final phenylmethylsulfonyl fluoride (PMSF)] just prior to use. Samples were collected in microcentrifuge tubes, vortexed briefly and placed on ice. Samples were then centrifuged at 16,000 xg for 15 minutes. The clarified supernatant (total lysate) was collected and transferred to a new tube. Samples were stored at -20° C until further dilution with hybridization buffer (v/v %) to obtain 1%, 10% and 50% cell lysate dilutions.

Oligonucleotide selection. DNA oligonucleotides were purchased from TriLink Biotechnologies (San Diego, CA); all oligonucleotides were HPLC-purified for highest purity.[9] The oligonucleotide sequence 5'-CTGAACGGTAGCATCTTGAC-NH_2-3'

(probe) was selected because it forms a stable duplex with its complement 5'-GTCAAGATGCTACCGTTCAG-Cy3-3' (target) at room temperature, with minimal interference due to self-complementarity or secondary structure.[10,11] All DNA sequences and abbreviations, both probes and targets, are written from the 5' end to the 3' end.

Commercial microarray slide treatments. Commercial polymer-coated amine-reactive slides from Amersham (Codelink™) were stored in vendor-sealed packaging per each vendor's recommendations. All slides were pre-treated prior to probe immobilization to ensure optimum surface amine-reactivity using an aqueous carbodiimide derivatization method previously described.[12] Reference control slides were immersed in blocking solution (50mM ethanolamine in 0.1M Tris, pH 9.0) at 50°C for 30 min before microarray printing to block the amine-reactive NHS groups on the slides, preventing amino-DNA probe covalent attachment.

Microarray printing. HPLC-purified oligonucleotides containing 3'-terminal hexylamine groups were spotted onto microarray slides using a Piezorray™ non-contact microarray printer (Perkin Elmer, Fremont, CA). PiezoTip™ dispensers were used for controlled non-contact DNA solution dispensing. Sub-nanoliter oligonucleotide solutions were spotted in replicates of 5 at concentrations of 20, 10, 5 and 1 μM DNA. These print conditions provide dried spots approximately 150-200 microns in diameter, depending on the substrate vendor (200μm for CodeLink™ slides). Print buffer was 150mM sodium phosphate (pH 8.5) with 0.001% Tween20 and 0.001% sarcosine. Humidity was set at 45%. Slide vendor's printing specifications were closely followed for handling, printing, buffer preparation and rinsing. Stable surface immobilization was attempted by incubating the printed slides overnight at room temperature and 75% relative humidity.

Post-print array treatment. Residual amine-reactive groups on slides post-printing were consumed using blocking solution (50mM ethanolamine in 0.1M Tris, pH 9.0) at 50°C for 30 min. Slides were then rinsed briefly with deionized water, then incubated in 4X saline sodium citrate (SSC, 1X saline-sodium citrate solution contains 15mM sodium citrate and 150mM NaCl) containing 0.1% sodium dodecyl sulfate at 50°C for 30 min, rinsed again with deionized water and finally blown dry with nitrogen.

Hybridization with target DNA. Target hybridization was performed unstirred with commercial silicone isolator gaskets (125 μl total volume per gasket, Grace-Bio Labs) in 4X SSC (with 0.1%SDS) solutions containing target solutions with various target concentrations and various milieu conditions. To determine the dynamic range of target hybridization, target solutions in buffer were prepared at concentrations of 1μM, 10nM, 1nM, 100pM, 10pM, 1pM, 100fM and 10fM. To investigate the influence of complex milieu on microarray target hybridization, target concentrations of 1nM, 100pM, 10pM and 1pM were each prepared in hybridization buffer, and 1%, 10% and 50% cell lysate solutions. Each target DNA solution was applied into single wells of the silicone isolators on slides to hybridize with identically printed probe microarrays. Hybridization proceeded at room temperature and 100% humidity for four hours. Slides were then rinsed with 4X SSC (0.1%SDS), followed by rinsing with 2X SSC/0.1%SDS for 5 min twice, then 0.2X SSC and 0.1X SSC each for 1 min. Slides were finally blown dry with nitrogen.

Fluorescence imaging and image analysis. Microarray slides were scanned using a Packard BioChip Imager. Laser power varied from 80-100%, PMT sensitivity varied from 70%-100% by experiments depending on specific fluorescence yields.

Scanning resolution was 10 microns for microarrays features. Excitation wavelength 543 nm and 633nm were selected for Cy3- and Cy5-labeled experiments, respectively. The microarray scanned fluorescence images were processed with ScanAlyze™ software written by Dr. Michael Eisen (University of California at Berkeley, USA, see http://rana.lbl.gov/EisenSoftware.htm). Arrays were first gridded with circles according to printing parameters, i.e., resolution of scanned images, location of spots and their position in the array. Grid parameters such as spot size and array tilt can be further fine-tuned according to the array image. Position of individual grid elements (circles) can be adjusted to fit each print spot image if necessary. ScanAlyze™ separates the image into pixels either contained within the identified spot or those that are not. Any pixel through which the spot circle passes is defined as being within the spot. Any pixels not within the spot but within a square, centered at the spot center, with side lengths of two-times the print spot radius (default value of 20) are defined as background pixels for this spot, excluding pixels contained within another spot. Pixel data intensities are imported into a spreadsheet program where background intensities are subtracted from corresponding spot intensities. Spots with defects that can be visually identified are excluded from replicate averaging (no more than 1 out of 5 replicates). Pixel intensities from replicates of 5 (or 4 in case of a defective spot) were averaged and standard deviations were calculated. Comparisons of relative fluorescence intensities were made on results normalized to identical laser/PMT settings in the Results and Discussion section below.

6.4 Results and Discussion

Dynamic range of target concentration in buffer hybridization. The dynamic range of target hybridization was studied by parallel hybridization of identically printed

probe microarrays at various target concentrations in vendor-specified hybridization buffer (4X SSC, 0.1% SDS). Target concentrations of 1μM, 10nM, 1nM, 100pM, 10pM, 1pM, 100fM and 10fM were studied. The highest target concentration (1μM) was chosen to be comparable with those reported in a number of model DNA hybridization studies.[13-16] The lower target concentrations were selected to compare with detection limits claimed in the literature.[17-21] Hybridization results shown in relative fluorescence units are plotted in Figure 6.1 for four different printed probe concentrations. Background

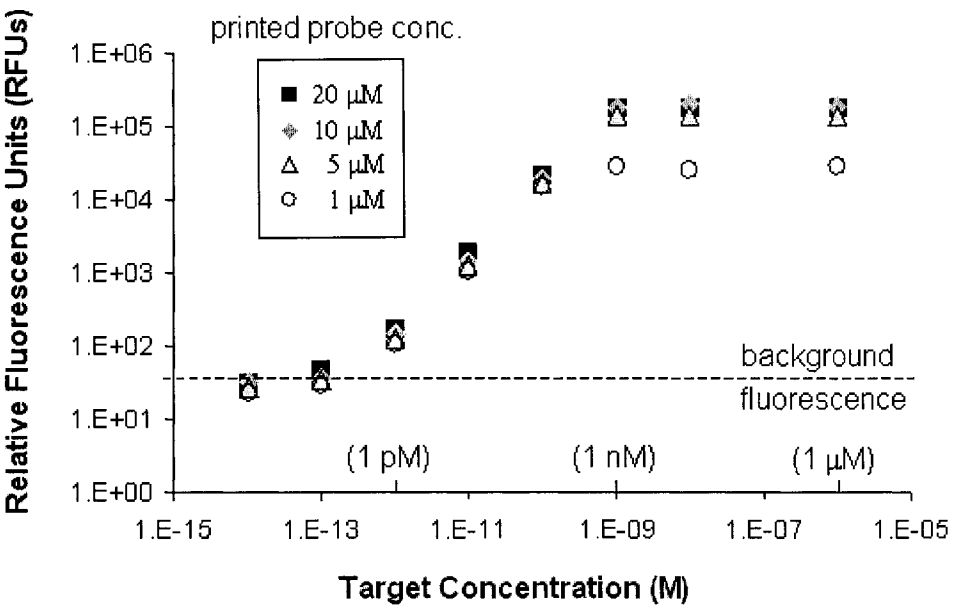

Figure 6.1 Dynamic range of microarray DNA target hybridization in hybridization buffer (4X SSC, 0.1% SDS)

fluorescence intensity is indicated with a dashed line. Each data point is the average of five replicate microarray spots. Error bars, representing standard deviation of the ten replicate spots, are smaller than the data point symbols, therefore not shown in the figure. As shown in Figure 6.1, the two lowest target concentrations, 100 fM and 10 fM, resulted

in hybridization fluorescence indistinguishable from background. Hence, these target concentrations are below the detection limit of this microarray assay method and not investigated further. From 1 nM to 1 pM target concentration, microarray DNA hybridization, indicated by relative fluorescence signals, shows a linear dependence on target concentration, and is affected little by the printed probe concentration. This likely indicates the dynamic range of the microarray hybridization experiment. At 1 pM, 10 pM and 100 pM target concentrations, given the 125 μl target solution volume, hypothetically, if all target molecules are hybridized to printed microarray probe spots (40 spots at 150 μm diameter), their resulting surface densities range from 1.1×10^{10}, 1.1×10^{11} to 1.1×10^{12} targets/cm^2, respectively. Surface-immobilized probe density has been previously quantified to be 4×10^{12} probes/cm^2 for printed 20μM probe spots,[15] therefore are likely in excess to the approaching target molecules for hybridization. As a result, hybridization signal represents relative amount of DNA target molecules in sample solutions. Above 1 nM target concentration, hybridization fluorescence intensity showed no further increase. This observation may come from two sources: (1) surface DNA probes sites are saturated with DNA target molecules, and (2) fluorescence self-quenching occurs and limits the observed fluorescence intensity. The second possible source could be confirmed or excluded by an experiment with diluted target-Cy3 (not performed). Since DNA target concentrations greater than 1nM are less relevant to DNA concentrations in real biological samples for diagnostic purposes, they were not studied. The apparently lower target hybridization on the 1 μM probe samples than the other three printed probe concentrations (5 μM, 10 μM and 20 μM) also indicates that probe density, not target bulk concentration, may be the limiting factor for the fluorescence intensities

observed in these hybridization experiments. At 1 nM target concentration and 125 μl sample volume, the amount of target molecules in solution is ~ 7.5 x 10^{10} per well. If all probe spots on these surfaces are assumed to be 150 μm in diameter, the total probe molecule-covered area for four probe concentrations in ten replicate spots at each concentration is 7.1 x 10^{-3} cm^2. If all target molecules hybridize to probe spots on this surface uniformly, the resulting target density on surface would be ~1.1 x 10^{13} targets/cm^2. Surface density of printed probe molecules was determined using ^{32}P methods in previous study to be ~ for the 20 μM probe solution,[15] and less than 4 x 10^{12} probes/cm^2 for the 10 μM, 5 μM and 1 μM probe solutions. Hence, target concentrations above 1 nM likely saturate the surface immobilized microarray probes under these experimental conditions. In addition to on-spot fluorescence signal representing specific target DNA binding, off-spot background fluorescence was also analyzed at various target concentrations. As shown in Figure 6.2, higher background fluorescence is

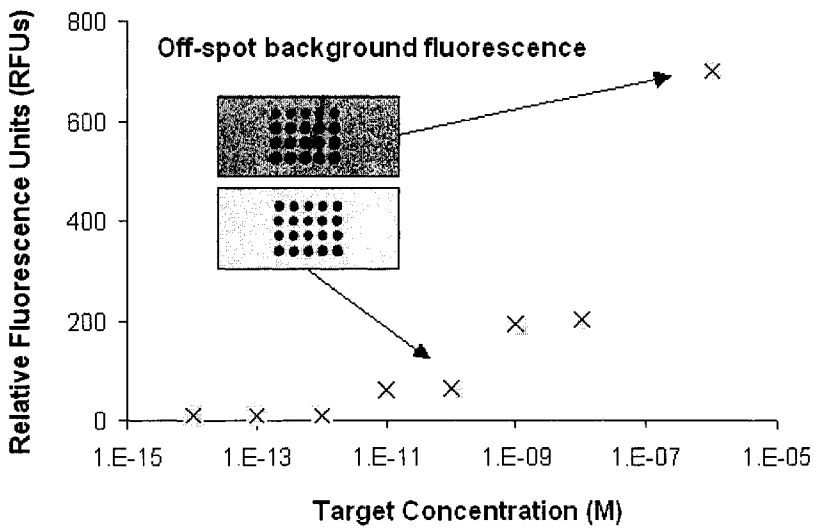

Figure 6.2 Off-spot background fluorescence at various target concentrations

observed for higher concentration target hybridization, possibly due to non-specific binding of the significant excess of fluorescently labeled target and physisorption of free dye contaminants commonly found in commercial target samples. Each background fluorescence value was the average of 40 individual off-spot intensity readings. The microarray images shown in Figure 6.2 were selected from a scanned full slide image collected at 80% laser power and 70% PMT efficiency. The contrast of the scanned image was adjusted in order to better visualize the difference in hybridization background fluorescence.

Comparison of target hybridization in buffer and cell lysate dilutions. 1 nM, 100 pM, 10 pM and 1 pM targets were chosen for cell lysate hybridization experiments to compare with the target concentration dynamic range studied in the previous section. Off-spot background fluorescence from 1nM target hybridization is compared for buffer and cell lysate hybridization conditions in Figure 6.3. The microarray images were selected from a scanned full slide image collected at 80% laser power and 70% PMT efficiency. The contrast of the scanned image was adjusted in order to better visualize

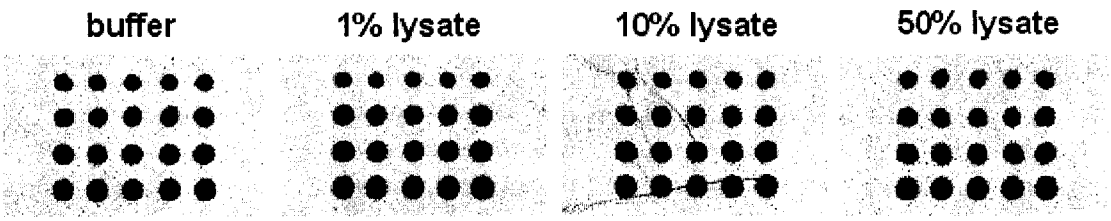

Figure 6.3 Background fluorescence comparison of 1 nM target hybridization in buffer and cell lysate dilutions

any difference in hybridization background fluorescence. As shown in Figure 6.3, the presence of cell lysate components (e.g., many different proteins and lipids) in microarray hybridization causes no significant increase in off-spot background

fluorescence. The same trend is also observed for 100 pM, 10 pM and 1 pM target hybridization (images not shown). Table 6.1 shows the off-spot background fluorescence intensities from microarray hybridization at the four milieu conditions and the four target concentrations. Each background fluorescence value was the average of 40 individual off-spot intensity readings.

Table 6.1 Microarray off-spot fluorescence under four different hybridization milieu conditions at four target concentrations.

	Hybridization Buffer	1% Cell Lysate	10% Cell Lysate	50% Cell Lysate
1 nM	42	44	45	45
100 pM	44	40	39	43
10 pM	39	38	39	44
1 pM	36	38	38	41

Hybridization fluorescence intensity of 20 μM printed probe spots in buffer and cell lysate dilutions are analyzed and shown in Figure 6.4. Each data point is the average of five replicate microarray spots. Error bars, representing standard deviation of the ten replicate spots, are smaller than the data point symbols, therefore not shown in this figure. Linear hybridization dependence on target concentration is observed for both buffer and the three complex milieu conditions (1% lysate, 10% lysate and 50% lysate). In addition, the relative fluorescence intensities from buffer and cell lysate hybridization experiments also agree with one another. The dashed line in Figure 6.4 is not intended as a linear trend line, but serves as guide for the eye in comparison with results in Figure 6.5 in the next section.

Specific versus non-specific target hybridization. Potential non-specific target binding (NSB) to microarray slide surfaces caused by physisorbed probes are discussed

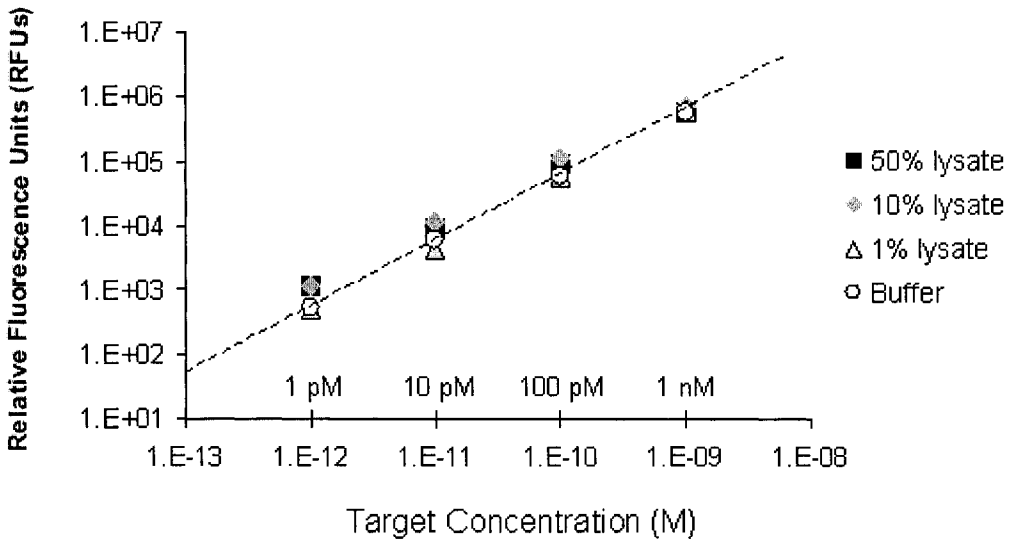

Figure 6.4 Target DNA hybridization of 20μM printed probe spots in buffer and cell lysate dilutions on NHS-activated polymer slides.

in this section. Other target NSB scenarios are included in the Future Work section of this chapter. Figure 6.5 shows the results for complex milieu hybridization from 20 μM probe spots printed onto slides pre-treated with ethanolamine. Since the NHS reactivity is removed from the surface prior to microarray DNA probe immobilization, it is assumed that DNA probe end-amine or nucleobase-amine covalent tethering to the surface is not possible in these experiments. As shown in Figure 6.5, the relative fluorescence intensity of target molecules from buffer and cell lysate dilutions overlap at each target concentration studied. This is in agreement with Figure 6.4, indicating minimum interference of cell lysate constituents with microarray DNA hybridization. Importantly, in Figure 6.5, data for the 1 pM and 10 pM target concentrations fall on the dashed line, indicating that amounts of target attached to printed probe microarray spots are identical to those in Figure 6.4 (probes tethered to slides through end-amine functionality). Slightly lower amounts of attached targets and significantly lower

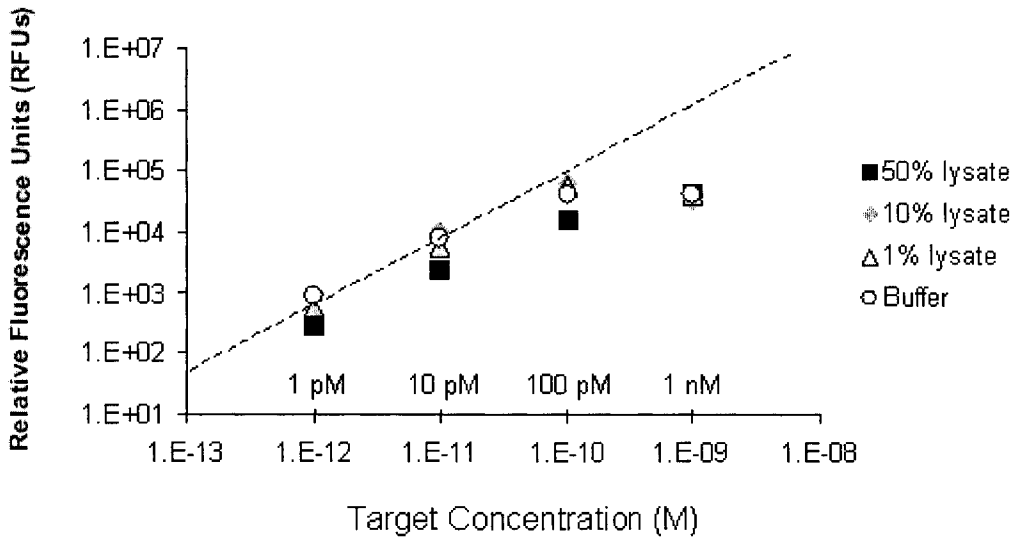

Figure 6.5 Target DNA hybridization of 20μM printed probe spots in buffer and cell lysate dilutions on ethanolamine-deactivated polymer control slides.

amounts of attached targets are observed for the 100 pM and 1 nM target samples, respectively. These observations indicate potential target binding to physisorbed probe molecules through hybridization, a type of specific recognition binding, although the resulting duplex stability is compromised by restricted probe conformations. Physisorption, as one possible route for microarray DNA probe immobilization, requires less probe and surface functionalization, but is more susceptible to probe loss during hybridization and post-hybridization stringency wash steps due to the weaker nature of the attachment.

As reported in previous studies,[12,15] DNA oligonucleotides lacking end-amine functionality may attach to amine-reactive polymer slides through nucleobase amines or by physisorption. These sideways-attached DNA probes may still be capable of DNA target hybridization, but their duplex stability is reduced from that of end-tethered probes. Their ability to differentiate a perfectly matched target from a mismatched target is also compromised by the restraints in probe surface conformational freedom. Probe density

of a 20 μM printed microarray probe spot is estimated to be $4.5x10^{12}$ probes/cm^2.[15] Assuming that 5% of the probe molecules are physisorbed,[22] their surface density is approximately $0.9x10^{12}$ probes/cm^2. If the probe spots are uniform in density and size, forty such probe spots provides 6.4 x 10^9 probes, equivalent to ~85 pM in a 125 μl hybridization solution volume. Depending on their ability to form a duplex with perfectly matched or mismatched targets, and the stringency in post-hybridization wash steps, these physisorbed probe molecules, together with other sideways-attached (e.g., nucleobase amine-tethered) probe molecules, may be critical factors in determining the sensitivity and selectivity performance of a DNA microarray. Therefore, this contribution needs to be systematically investigated.

6.5 Future work

Optimization of target hybridization conditions. Target pre-treatment (heating), sample surface mixing (static vs. dynamic assay), hybridization and post-hybridization wash temperatures and durations are factors that have potential effects on the kinetics and efficiencies of surface DNA hybridization. Optimization of these conditions needs to be performed based on the specific surface-DNA systems. As a general rule, hybridization temperature 10-25°C below the melting temperature (T_m) of a DNA duplex is recommended. While a lower hybridization temperature allows the formation of more stable DNA duplexes, a higher temperature hybridization more efficiently differentiate perfect matched duplexes from mismatched duplexes. The probe-target pair in this study, a 20mer oligonucleotide sequence with 50% GC content, has a T_m approximating 53°C[23] and forms stable duplexes at room temperature[10, 11].

Validation of hybridization signal with complementary control experiments. As mentioned in "specific versus non-specific target hybridization" of the Results and Discussion section, probe, target, and dye contaminant molecules could attach to substrate slide surfaces non-specifically and interfere with microarray DNA hybridization. Aside from the previously mentioned probe physisorption NSB, several other NSB mechanisms should be analyzed in order to validate target hybridization signals in microarray experiments. These NSBs include probe nucleobase amine NSB, non-complementary target binding, and target and dye contaminant surface physisorption.

To systematically study DNA probe NSBs, aminated and non-aminated DNA probes will be printed onto fresh (amine-reactive) slides and blocked (ethanolamine-deactivated) slides. Four attachment scenarios result from these printings: (1) amine-probe onto amine-reactive slides (the ideal immobilization scheme: probe end tethering), (2) amine-probe onto deactivated slide (physisorption), (3) non-amine probe onto amine-reactive slide (nucleobase attachment) and (4) non-amine probe onto deactivated slide (physisorption).

Target and dye contaminant molecules could possibly attach to probe-modified surface by physisorption. Micro-printed nanoliter drops of probe solutions printed onto substrate surfaces commonly result in rapidly dried DNA films as spots. The rapid drying of buffer salt and DNA probe molecules onto the polymer matrices may change the surface properties of the printed areas (spots) and cause subsequent target and dye contaminant physisorption, although the mechanism is not clear. To investigate this possibility, print buffer solutions will be spotted onto polymer slides in microarray format without the presence of probe DNAs and allowed to "hybridize" with target DNA

solutions. Without any probe molecules on surface, any fluorescence observed after "hybridization" can only be explained by target or dye physisorption to the surface. If any microarray patterns are revealed in fluorescence imaging, the on-spot and off-spot fluorescence must be different, indicating a change of surface property caused by microarray printing and on-spot drying. The magnitude of this fluorescence is indicative of the impact of surface property change on DNA microarray detection limit.

Absence of non-specific target binding to non-complementary microarray DNA probes (cross-hybridization) is critical for the selectivity performance of a DNA microarray. This is especially important when two DNA sequences of significantly different abundance are to be analyzed from a single sample solution (i.e., if sequence A is abundant and it cross-hybridizes with the probe DNA of sequence B, this "hybridization" results as a false positive. Hence, the presence of substantial amount of sequence A excludes confident detection of trace amount of sequence B). To investigate this type of NSB, aminated DNA probes will be printed onto amine-reactive polymer slides, and "hybridized" with its non-complementary target sequences (e.g., itself, since the probe sequence is free of self-complementarity) at various concentrations. On-spot fluorescence at different concentrations is indicative of the selectivity threshold of this method under the specified assay conditions.

Hybridization in serum dilutions. Complex milieu performance of the amine-reactive polymer slides in microarray hybridization has been challenged using cell lysate dilutions. The polymer arraying slides demonstrated excellent resistance to lysate component interference due to the nature of their polymer matrices (polyacrylamide for CodeLink™ and polyethylene glycol for OptArray™). The relevance of this study to

other biosensing and microarraying surface performance studies will be improved if the same microarray hybridization strategy is challenged using serum, a better characterized and commonly studied biological milieu.

6.6 Summary

In this work, microarray DNA hybridization performance in buffer and various cell lysate dilutions were compared on commercial amine-reactive polymer slides using fluorescence intensity measurements. Preliminary results suggested strong impedance of hybridization assay detection limit by non-specific probe, target and dye contaminant bindings to microarray assay surfaces. Insignificant complex milieu influence was observed for the model oligonucleotide microarray hybridization assay. To the best of our knowledge, DNA target surface capture from cell lysate dilutions or relatively concentrated protein media has not been previously reported, particularly not on commercial microarraying surfaces. While substantial attention has been directed to the construction and performance of potential microarraying and biosensing surfaces assaying in simple systems (e.g., single component buffers), less effort has been directed to developing surfaces capable of more practical applications (e.g., direct assay from complex sample milieu). To remove the long-standing barriers and to improve clinical sensing applications, assessment of microarray assay performance in complex milieu and extensive microarray data validation are necessary for all capture assay surface development.

6.7 Acknowledgements

The authors are grateful for financial support from NIH EB001473. M. Godek, L. Chamberlain and A. Winterbower are thanked for providing the cell lysate solutions for this study. Technical assistance in fluorescence scanning from Dr. W. H. Hanneman (CSU) and insightful discussions with C. Greef, M. Lochhead, P. Wu and G. Harbers are gratefully acknowledged.

6.8 References

(1) Grainger, D. W.; Greef, C. H.; Gong, P.; Lochhead, M. J. In *Microarrays: Methods and Protocols (Method in Molecular Biology),* 2nd ed.; Rampal, J. B., Ed.; Humana Press: Totowa, New Jersey, 2006, in press.

(2) Rosi, N. L.; Mirkin, C. A. *Chem. Rev.* **2005**, *105*, 1547-1562.

(3) Elghanian, R.; Storhoff, J. J.; Mucic, R. C.; Letsinger, R. L.; Mirkin, C. A. *Science* **1997**, *277*, 1078-1081.

(4) Gerion, D.; Chen, F.; Kannan, B.; Fu, A.; Parak, W. J.; Chen, D. J.; Majumdar, A.; Alivisatos, A. P. *Anal. Chem.* **2003**, *75*, 4766-4772.

(5) Sato, K.; Hosokawa, K.; Maeda, M. *J. Am. Chem. Soc.* **2003**, *125*, 8102-8103.

(6) Nam, J. M.; Stoeva, S. I.; Mirkin, C. A. *J. Am. Chem. Soc.* **2004**, *126*, 5932-5933.

(7) Ho, H. A.; Dore, K.; Boissinot, M.; Bergeron, M. G.; Tanguay, R. M.; Boudreau, D.; Leclerc, M. *J. Am. Chem. Soc.* **2005**, *127*, 12673-12676.

(8) Lee, C.-Y.; Gong, P.; Harbers, G. M.; Grainger, D. W.; Castner, D. G.; Gamble, L. J. *Anal. Chem.* **2006**, *in press*.

(9) Lee, C.-Y.; Canavan, H. E.; Gamble, L. J.; Castner, D. G. *Langmuir* **2005**, *21*, 5134-5141.

(10) Forman, J. E.; Walton, I. D.; Stern, D.; Rava, R. P.; Trulson, M. O. *ACS Symp. Ser.* **1998**, *682*, 206-228.

(11) Mazzola, L. T.; Frank, C. W.; Fodor, S. P. A.; Mosher, C.; Lartius, R.; Henderson, E. *Biophys. J.* **1999**, *76*, 2922-2933.

(12) Gong, P.; Grainger, D. W. *Surf. Sci.* **2004**, *570*, 67-77.

(13) Peterson, A. W.; Wolf, L. K.; Georgiadis, R. M. *J. Am. Chem. Soc.* **2002**, *124*, 14601-14607.

(14) Shen, G.; Anand, M. F. G.; Levicky, R. *Nucleic Acids Res.* **2004**, *32*, 5973-5980.

(15) Gong, P.; Harbers, G. M.; Grainger, D. W. *Anal. Chem.* **2006**, *in press*.

(16) Gong, P.; Lee, C.-Y.; Gamble, L. J.; Castner, D. G.; Grainger, D. W. *Anal. Chem.* **2006**, *in press*.

(17) Lee, H. J.; Li, Y.; Wark, A. W.; Corn, R. M. *Anal. Chem.* **2005**, *77*, 5096-5100.

(18) Ferguson, J. A.; Steemers, F. J.; Walt, D. R. *Anal. Chem.* **2000**, *72*, 5618-5624.

(19) Zhou, X.; Zhou, J. *Anal. Chem.* **2004**, *76*, 5302-5312.

(20) Le Berre, V.; Trevisiol, E.; Dagkessamanskaia, A.; Sokol, S.; Caminade, A. M.; Majoral, J. P.; Meunier, B.; Francois, J. *Nucleic Acids Res.* **2003**, *31*, e88.

(21) Kuhn, K.; Baker, S. C.; Chudin, E.; Lieu, M. H.; Oeser, S.; Bennett, H.; Rigault, P.; Barker, D.; McDaniel, T. K.; Chee, M. S. *Genome Res.* **2004**, *14*, 2347-2356.

(22) The amount of physisorbed and sideway-attached probe DNA molecules (and potential physisorbed dye contaminants), as indicated by the relative fluorescence intensity of non-aminated DNA probes, is less than 5% of the total DNA probes immobilized in a microarray printing experiment. .

(23) Melting temperature of known oligonucleotide sequences can be calculated at http://www.idtdna.com/analyzer/Applications/OligoAnalyzer/.

Chapter 7 Quenching and Steric Influences of Fluorescent Dye Labels on DNA Microarray Hybridization Signal

This dissertation chapter was written by Ping Gong and edited by David W. Grainger. This chapter describes how fluorescent quenching and dye label position influence microarray DNA hybridization efficiency and signal generation.

Quenching and Steric Influences of Fluorescent Dye Labels on DNA Microarray Hybridization Signal

Ping Gong, David W. Grainger

7.1 Abstract

Fluorescent dye end labeling of nucleic acids is widely employed as a DNA microarray detection method because it is straightforward and easy to implement. In this work, self-quenching of end-labeled fluorescent dyes (Cy3 and Cy5) on densely immobilized and hybridized DNA surfaces were studied. Dilution of fluorescently labeled DNA by unlabeled DNA counterparts was found necessary for reliable fluorescence quantification of surface DNA density. Steric effects of bulky dye labels on DNA hybridization were investigated. Dye location on captured target after hybridization to unlabeled probe, either at the surface or buried within the DNA duplex layer, has negligible influence on hybridization efficiency. Hybridization of two ssDNA oligomers, with their respective dye molecules forced to co-locate in close proximity upon duplex formation, was sterically hindered on short 20-mer duplex pairs. Fluorescence labeling, as a detection method commonly used in microarray technology, requires thorough understanding for both qualitative and quantitative purposes.

7.2 Introduction

Microarrays are a powerful tool for high-throughput analysis of nucleic acids due to their miniaturized, parallel detection capabilities.[1-8] Reduction of the surface-capture array feature to micron scales enables simultaneous detection of thousands of genes from a single analyte sample. The technique exploits hybridization base pairing specificity of two single stranded DNA (ssDNA) molecules, one with a known sequence and immobilized on a solid substrate surface in a microscopic format (probe), the other present in sample milieu whose identity and abundance are to be determined (target).[9] The presence of target DNA sequences, after hybridization with probe DNAs immobilized at pre-determined microarray locations, is commonly detected by a signaling reagent often covalently attached to the target, such as fluorescent dyes[10,11], radioisotopes[12-15], chemiluminescent labels[16] and electrochemically active complexes[17-19]. Label free detection methods based on mass spectroscopy[20-23] and surface plasmon resonance (SPR)[24-26] are also under development without their microarray forms yet realized.

Although the fluorescent labelling approach requires lengthy, expensive sample preparation as well as highly sophisticated optical scanners and laser excitation sources, this method remains a powerful and entrenched means for DNA microarray detection.[10,11] It is straightforward and easy to implement, and is widely used in both research and clinical formats. In order to improve microarray assay performance based on fluorescence signal detection, a thorough understanding of the potential effects of the fluorescent label on microarray DNA-DNA interactions, hybridization and ultimate assay performance is necessary. Oligonucleotide-based DNA microarrays, including various

research platforms and commercially available Affymetrix (DNA 25-mer immobilized oligos)[27], Amersham (30-mer)[28] and Agilent (60-mer)[29] arrays, often contain oligonucleotides (20 to 60 nucleotides in length), estimated to be 7 - 20 nm long if fully extended. Fluorescent dyes routinely used in DNA labeling, such as Cy3 and Cy5, are highly conjugated planar molecules ~2 nm in diameters (see structures in Figure 7.1). As the size of these fluorescent dye labels is approximately 10-25% of the size of the analyte molecules, labeling may present significant steric influences on their hybridization activities at surfaces, and hence signal reliability in microarray formats.

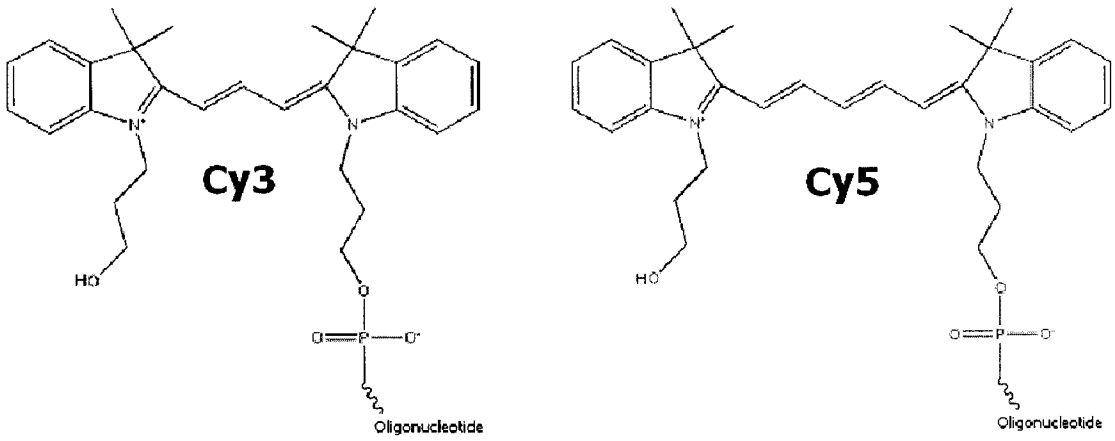

Figure 7.1 Cyanine dye structures (adapted from http://www.trilinkbiotech.com/)

Fluorescent dye labels have been used for abundance quantification of surface-bound oligonucleotide molecules.[10,11] When present on surfaces at high density, their close proximity to the surface chemistry and to each other (e.g., in microarray features) may induce altered fluorescence generation and self-quenching, resulting in altered molecular fluorescence intensity compared to isolated dyes.[30,31] Dilution of dye labeled DNAs with their un-diluted counterparts may be an alternative for surface DNA density quantification as it excludes concerns of dye self-quenching. Dye molecules are

generally known to exhibit different fluorescence quantum yields depending on their molecular structures.[32] Even when the same type of dye is labeled onto DNA sequences at different conditions, because the labeling efficiency varies (i.e., not 100% yield), the fluorescence yield of the final DNA products varies. In order to study steric effects of a dye label on DNA hybridization based solely on fluorescence response, fluorescence self-quenching and the different quantum yields in various DNAs must be considered. Two scenarios are proposed with possible dye label steric influence on DNA hybridization (1), probe-target hybridization is compromised by molecular crowding within the DNA layer due to the presence of dye labels on the target alone; (2), hybridization is hindered by unfavorable duplex formation when two dye labels are forced into close proximity (i.e., dye on probe 3' end, dye on target 5' end) by hybridization. Both scenarios are systematically investigated and discussed in detail for the case of short oligomer DNA pairs.

7.3 Experimental section

Materials. Phosphate, borate, and Tris buffer components, 1-(3-dimethylaminopropyl)-3-ethlcarbodiimide hydrochloride (EDCI), N-hydroxysuccinimide (NHS), Tween 20, sarcosine, sodium citrate (SSC), sodium dodecyl sulfate (SDS) and ethanolamine were purchased from Sigma-Aldrich (St. Louis, MO) and used as received. Commercial polymer-coated microarray slides were purchased from Amersham (Codelink™, Tempe, AZ) and Accelr8 Technology Corp. (OptArray™, Denver, CO). Both microarray surfaces are marketed as amine-reactive and three-dimensional (i.e., crosslinked polymer networks of thicknesses greater than a monolayer) hydrophilic polymer coatings on low-fluorescence glass substrates. All slides were pre-treated prior

to probe immobilization to ensure optimum surface amine-reactivity using an aqueous carbodiimide derivatization method previously described.[33]

Oligonucleotide selection. DNA oligonucleotides were purchased from TriLink Biotechnologies (San Diego, CA); all oligonucleotides were HPLC-purified for highest purity.[34] The oligonucleotide sequence 5'-CTGAACGGTAGCATCTTGAC-3' (probe) was selected because it forms a stable duplex with its complement GTCAAGATGCTACCGTTCAG (target) at room temperature, with minimal interference due to self-complementarity or secondary structure.[35,36] Table 7.1 lists all oligonucleotide sequences and modifications involved in this work (upper three as probe sequences, bottom three as target sequences). All DNA sequences and abbreviations, both probes and targets, are written from the 5' end to the 3' end.

Table 7.1 Oligonucleotide Sequences

Description	**5' modification**	**Oligonucleotide Sequence**	**3' modification**
probe sequence for surface immobilization		CTGAACGGTAGC-ATCTTGAC	$-NH_2$
probe sequence as reference	NH_2-	CTGAACGGTAGC-ATCTTGAC	
probe sequence for fluorescence detection	Cy3-	CTGAACGGTAGC-ATCTTGAC	$-NH_2$
target sequence for hybridization		GTCAAGATGCTA-CCGTTCAG	
target sequence 1 for fluorescence detection		GTCAAGATGCTA-CCGTTCAG	-Cy5
target sequence 2 for fluorescence detection	Cy5-	GTCAAGATGCTA-CCGTTCAG	

Probe and target set design. Four types of terminally-hexylaminated DNA probes were designed for microarray printing as listed in the upper half of Table 7.2. P-NH_2 (3' hexylamine functionality) is selected as the main probe. NH_2-P is the reference probe (5' hexylamine functionality). Probe Cy3(1%)-P-NH_2 comprises 1% Cy3-labeled P-NH_2 and 99% unlabeled P-NH_2. Presence of 1% Cy3-P-NH_2 allows fluorescence

Table 7.2 Probe and Target Sets

	Description	**Denotation**
Probe Set 1	NH_2-Probe (reference)	NH_2-P
Probe Set 2	Probe-NH_2 (probe)	P-NH_2
Probe Set 3	1% Cy3-Probe-NH_2 + 99% Probe-NH_2	Cy3(1%)-P-NH_2
Probe Set 4	Cy3-Probe-NH_2	Cy3(100%)-P-NH_2
Target Set i	1% Cy5-Target + 99% Target	Cy5(1%)-T
Target Set ii	1% Target-Cy5 + 99% Target	T-Cy5(1%)
Target Set iii	Cy5-Target	Cy5(100%)-T
Target Set iv	Target-Cy5	T-Cy5(100%)

visualization and quantification of surface-immobilized probe species. Cy3-P-NH_2 contains 100% Cy3-P-NH_2, which at high surface density, may cause fluorescence quenching. Each set of probe arrays includes four sub-arrays generated from the four types of terminally aminated DNA probes. Each sub-array is dedicated to one type of probe with four DNA concentrations (20 μM, 10 μM, 5 μM and 1 μM), each printed as five replicate spots as shown in Figure 7.2. Four replicate array sets were printed onto one microarray glass slide, later hybridized with four types of DNA targets. In order to perform target hybridization and quantify relative amounts of target hybridized from four

different target types, the initial probe surfaces must first be analyzed and confirmed to be identical.

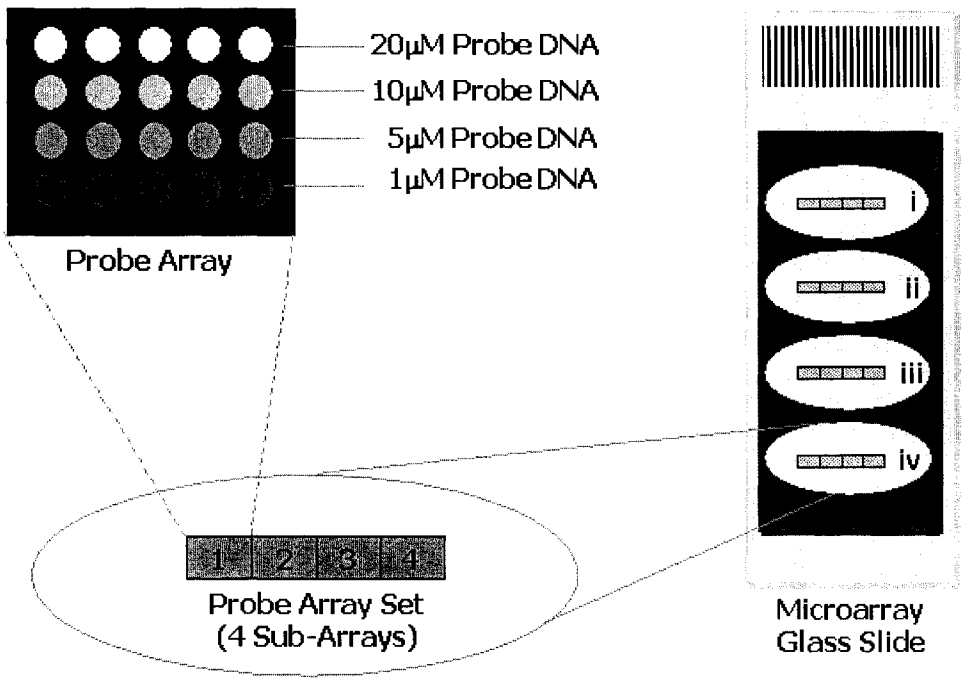

Figure 7.2 Microarray Outlay

Four types of DNA targets were designed for microarray hybridization as listed in the bottom half of Table 7.2. T-Cy5 and Cy5-T contain the Cy5 dye label on the 3' end and 5' end, respectively. Because of the anti-parallel hybridization mechanism between two complementary ssDNA molecules, when hybridized to a surface-immobilized DNA probe, these two labeled targets will present the two scenarios of interest: target capture to the surface will results in Cy5 fluorescent dye labels residing either at the top or bottom of the formed duplex layer, depending on immobilized probe orientation. T-Cy5(1%) and Cy5(1%)-T each contain 1% fluorescent-labeled DNA target diluted with identical unlabeled DNA target. The 100-fold fluorescent target dilution by unlabeled

target seeks to minimize effects of self-quenching and fluorescence energy transfer within the duplex capture layer in the microarray.

Microarray printing. Commercial polymer-coated amine-reactive slides from Amersham (Codelink™) and Accelr8 Technologies (OptArray™) were stored in vendor-sealed packaging per each vendor's recommendations. HPLC-purified oligonucleotides containing 3' or 5' -terminal hexylamine group were spotted onto microarray slides using a Piezorray™ non-contact microarray printer (Perkin Elmer, Fremont, CA). PiezoTip™ dispensers were used for controlled non-contact DNA solution dispensing. Sub-nanoliter oligonucleotide solutions were spotted in replicates of 5 at concentrations of 20, 10, 5 and 1 μM DNA. These print conditions provide dried spots approximately 150-200 microns in diameter, depending on the substrate vendor (150 μm for OptArray™ and 200μm for CodeLink™). Print buffer was 150mM sodium phosphate (pH 8.5) with 0.001% Tween20 and 0.001% sarcosine. Humidity was set at 45%. Slide vendor's printing specifications were closely followed for handling, printing, buffer preparation and rinsing. Stable surface immobilization was attempted by incubating the printed slides overnight at room temperature and 75% relative humidity.

Post-print array treatment. Residual amine-reactive groups on slides post-printing were consumed using blocking solution (50mM ethanolamine in 0.1M Tris, pH 9.0) at 50°C for 30 min. Slides were then rinsed briefly with deionized water, then incubated in 4X saline sodium citrate (SSC, 1X saline-sodium citrate solution contains 15mM sodium citrate and 150mM NaCl) containing 0.1% sodium dodecyl sulfate (SDS) for 30 min., rinsed again with deionized water and finally blown dry with nitrogen.

Hybridization with target DNA. Target hybridization was performed unstirred with commercial silicone isolator gaskets (125 μl per gasket, Grace-Bio Labs) in 4X SSC (with 0.1%SDS) solutions containing 1μM DNA target. Four types of DNA targets were applied separately into four wells of silicone isolators on each slide. Hybridization proceeded at room temperature and 100% humidity for four hours. The slides were then rinsed with 4X SSC (0.1%SDS), followed by rinsing with 2X SSC/0.1%SDS for 5 min twice, then 0.2X SSC and 0.1X SSC each for 1 min. Slides were finally blown dry with nitrogen.

Fluorescence imaging and image analysis. Microarray slides were scanned using a ScanArray® Express Microarray Imager (Perkin Elmer, Fremont, CA). Laser power was set to 90% for all measurements. PMT sensitivity varied from 35%-70% by experiments depending on specific fluorescence yields. Scanning resolution was 10 microns for microarrays features. Excitation wavelength 543 nm and 633nm were selected for Cy3- and Cy5-labeled experiments, respectively. Scanned microarray fluorescence images were processed with QuantArray® (Perkin Elmer) software using the adaptive circle segmentation technique[37]. Each fluorescence intensity value was averaged from five replicate spots. Comparisons of relative fluorescence intensities were made on results normalized to identical Laser/PMT settings in the Results and Discussion section below.

7.4 Results and Discussion

Dye self-quenching on surface-immobilized DNA probes. Cyanine dyes, including those used for DNA labeling in this study, are highly conjugated planar molecules that are not only fluorescently active but also subject to self-quenching when

present in close proximity to each other.[30] When excitation and emission spectra of different cyanine dyes exhibit substantial overlap, fluorescence resonance energy transfer (FRET) may also occur, depending on intermolecular distances and relative orientation of the molecular excitation and emission dipoles.[38] When an excited donor molecule and an acceptor molecule are within the Förster radius, typically several nanometers, and oriented favorably, fluorescence energy transfer is observed as molecular fluorescence loss, termed self-quenching.[30] Given the quasi-three-dimensional nature of the polymer slides and the hydrophilic nature of the polymers, a combined effect of molecular distance and orientation makes the limiting density of self-quenching difficult to predict by calculation.

To assess the presence of Cy3-P-NH_2 self-quenching in surface-immobilized DNA layers, pure and 100-fold diluted Cy3-P-NH_2 (shown as schematic in Figure 7.3a) were printed onto CodeLink™ and OptArray™ microarraying slides at concentrations 1, 5, 10 and 20μM. Fluorescence intensities from both types of probes were collected and normalized using a home-generated standard curve to the same laser/PMT efficiency. Intensities from the pure Cy3-P-NH_2 printed array samples were adjusted with a factor of 1/100 for comparison with the 100-fold diluted probe samples. The normalized and adjusted intensities from both probes were quantified and plotted in Figure 7.3b and 7.3c. Black diamonds represent pure Cy3-P-NH_2 probe, gray diamonds represent Cy3(1%)-P-NH_2 probe. All intensity values were averaged from 8 replicate sets of arrays with 5 replicate spot of each concentration condition. Error bars represent standard deviation. As shown in Figure 7.3b and 7.3c, fluorescence intensities per molecule for pure Cy3-P-NH_2 are significantly lower than that for the Cy3(1%)-P-NH_2, indicating dye self-

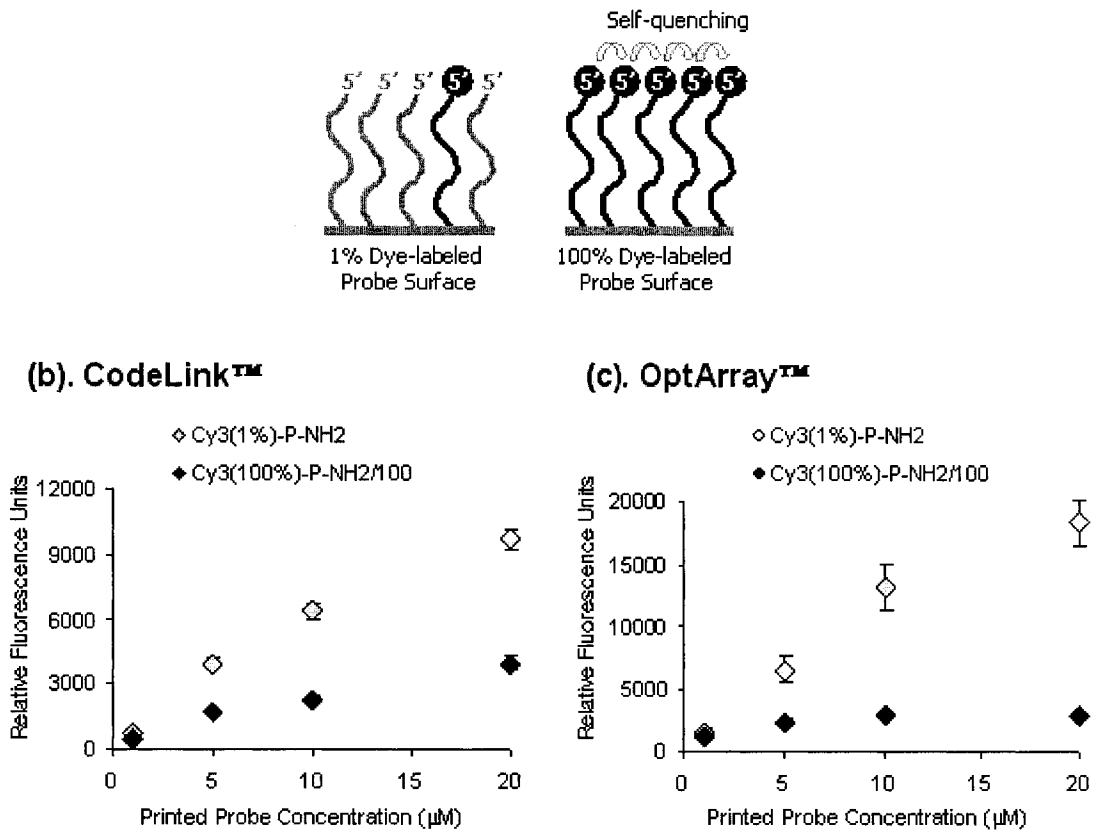

Figure 7.3 Dye self-quenching on 3'-surface immobilized 5'-dye labeled DNA probes

quenching of the undiluted probe dye on the printed array surface. Dye molecules tethered to the ends of each DNA probe molecule in densely print-immobilized probe arrangements allows fluorophore lateral self-quenching. Pure and undiluted Cy3-P-NH_2 probes, as a result, are not suitable for microarray probe density quantification. The Cy3(1%)-P-NH_2 probe, prepared by 100-fold dilution of the Cy3-P-NH_2 probe with unlabeled P-NH_2, allows relative fluorescence intensity quantification of surface-immobilized DNA probes excluding the effect of dye self-quenching. The absence of dye self-quenching with the Cy3(1%)-P-NH_2 probe is also confirmed by comparing resulting molecular fluorescence with that of even further diluted Cy3(0.1%)-P-NH_2 (data

not shown). In order to perform target hybridization and quantify relative amounts of target hybridized from four different target types, the initial probe surface densities should be nearly identical. The quality of replicate arrays, indicated by tight error bars, ensures the following hybridization comparisons to be valid based on nearly identical immobilized probe systems.

Effect of target dye location on hybridization. Dye labels are introduced into DNA molecules for microarray analysis commonly by use of specific base-dye conjugates positioned at terminal 5' or 3' ends. Complimentary single stranded DNAs (ssDNA) hybridize into duplexes following an anti-parallel mechanism, with one molecule orienting 5' to 3' while the other one orienting in the opposite direction (3' to 5'). As a result, when 5' and 3' dye-labeled target DNAs are hybridized to respective complementary surface-immobilized probes, their dye labels may reside at the top or be buried inside the resulting DNA double-strand layer, depending on the direction of the immobilized probe (i.e., surface tethering from either the aminated 3' or 5' end). Four hybridization scenarios are schematically shown in Figure 7.4a with 5' and 3' dye-labeled targets hybridized to both probe surface (P-NH_2, 3' ends attached to surface, 5' ends pointing away from surface) and reference probe surface (NH_2-P, 5' ends attached to surface, 3' ends pointing away from surface). When targets are hybridized to the probe surface following the anti-parallel duplex forming mechanism, the 5' dye on successfully hybridized target Cy5-T is buried inside the DNA layer (Figure 7.4a, 1st scenario from left) while the 3'-dye on target T-Cy5 extends out of the DNA layer (2nd scenario from left). The opposite is intended for experiments using the reference probe surface. Upon hybridization, the 5' dye on target Cy5-T extends out of the duplex DNA

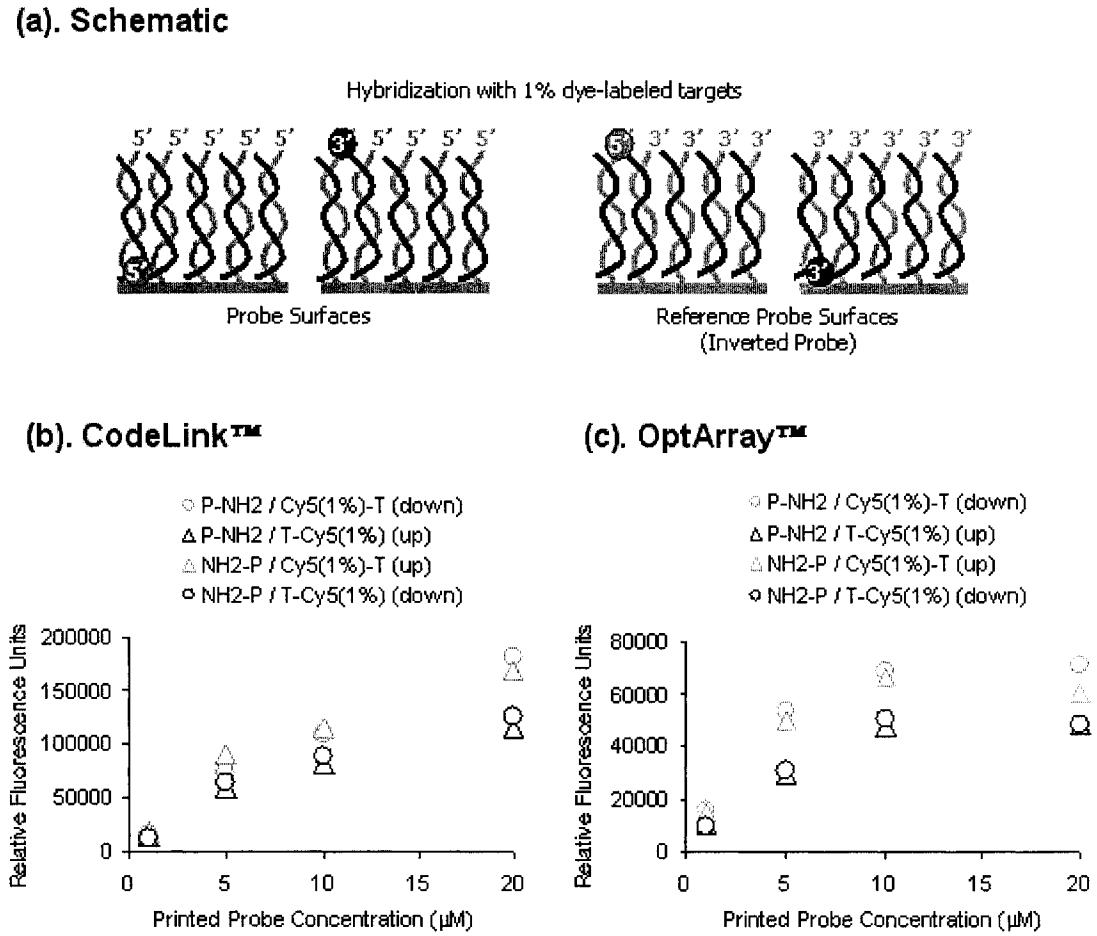

Figure 7.4 Steric influences of dye labels on opposite ends (5' vs. 3') of DNA targets

layer (3rd scenario from left), while the 3' dye on target T-Cy5 is buried inside the DNA layer (4th scenario from left). Since the dye labels are relatively large in size (planar diameter ~2nm, 20mer DNAs commonly used in microarray work are ~7nm in length when fully extended), their steric effect on DNA hybridization can be significant, especially when they are buried within the DNA layer, causing surface crowding that could compromise further hybridization efficiency. This effect, if indeed present, becomes more significant when surface probes are more densely packed and access of

solution target to surface probe is hindered by increased probe density and duplex surface crowding.

To exclude the problem of dye self-quenching from the fluorescence intensity measurements, 100-fold diluted dye labeled DNA targets (T-Cy5(1%) and Cy5(1%)-T) were used instead of pure dye labeled targets(T-Cy5(100%) and Cy5(100%)-T). Although both targets were labeled with Cy5 dyes, labeling efficiencies on 3' and 5' ends and their fluorescence quantum yields cannot be assumed to be identical. The labeling efficiencies likely depend on the dyes, the DNA sequences and conditions of individual labeling reactions, with variations between labeling reactions. Relative fluorescence intensities observed from two DNA targets are not directly comparable. Reference probe surface intensities, with DNA probes inversely oriented via 5' ends on array surfaces, are included in attempts to account for quantum yield and labeling efficiency variations. Any hybridization trend (target 3' dye vs. 5' dye) observed on these probe surfaces, if derived from steric influences of the dye label, should inverse on the reversed reference probe surface.

Fluorescence intensity results of dye location differences (on top or buried within of the DNA layer) study are shown in Figure 7.4b and 7.4c. Open triangles represent intensities for target-bound dye labels ideally extending out of the DNA layer and open circles represent results for identical hybridization experiments for target dye labels buried inside the DNA layer, using T-Cy5(1%) in black and Cy5(1%)-T in gray as shown schematically in Figure 7.4a. Black triangles and circles in Figure 7.4b and 7.4c representing the same target DNA (T-Cy5(1%)), overlap well with each other, indicating negligible hybridization efficiency influence from target dye locations on the 5' versus 3'

ends. This conclusion is further supported by the same signal overlap observed for the gray triangles and circles. The data points in black (T-Cy5(1%)) are consistently higher than the data points in gray (1% Cy5(1%)-T), indicating higher fluorescence quantum yield from the T-Cy5 target molecules used in this study.

Effect of 1% probe dye labeling on hybridization. To quantify or compare relative amounts of target hybridized from the four different target types, immobilized probe densities should best be identical on the initial probe surfaces prior to hybridization. For this purpose, 100-diluted dye-labeled probe (Cy3(1%)-P-NH_2) was used to quantify the amount of surface-immobilized probe. The presence of dye label allows fluorescence intensity measurements while the 100-fold dilution ensures the absence of fluorescence self-quenching. Introduction of 1% dye label on the probes could lead to biased hybridization results. To investigate this possibility, a set of hybridization experiments was conducted following the schematic shown in Figure 7.5a. In this study, 1% dye-labeled targets (Cy5(1%)-T and T-Cy5(1%)) were hybridized onto either pure DNA probe surfaces (P-NH_2) or 1% dye-labeled probe surfaces (Cy3(1%)-P-NH_2). Fluorescence intensities from these hybridization scenarios are quantified and plotted in Figure 7.5b and 7.5c. Open circles and triangles represent hybridization results on pure DNA probe surfaces, gray colored filled circles and triangles represent hybridization results on the 1% dye-labeled probe surfaces. As shown in Figure 7.5b and 7.5c, filled circles overlap with open circles while filled triangles overlap with open triangles, indicating that 1% dye labeling on probe DNA does not affect the hybridization performance of the probe surfaces.

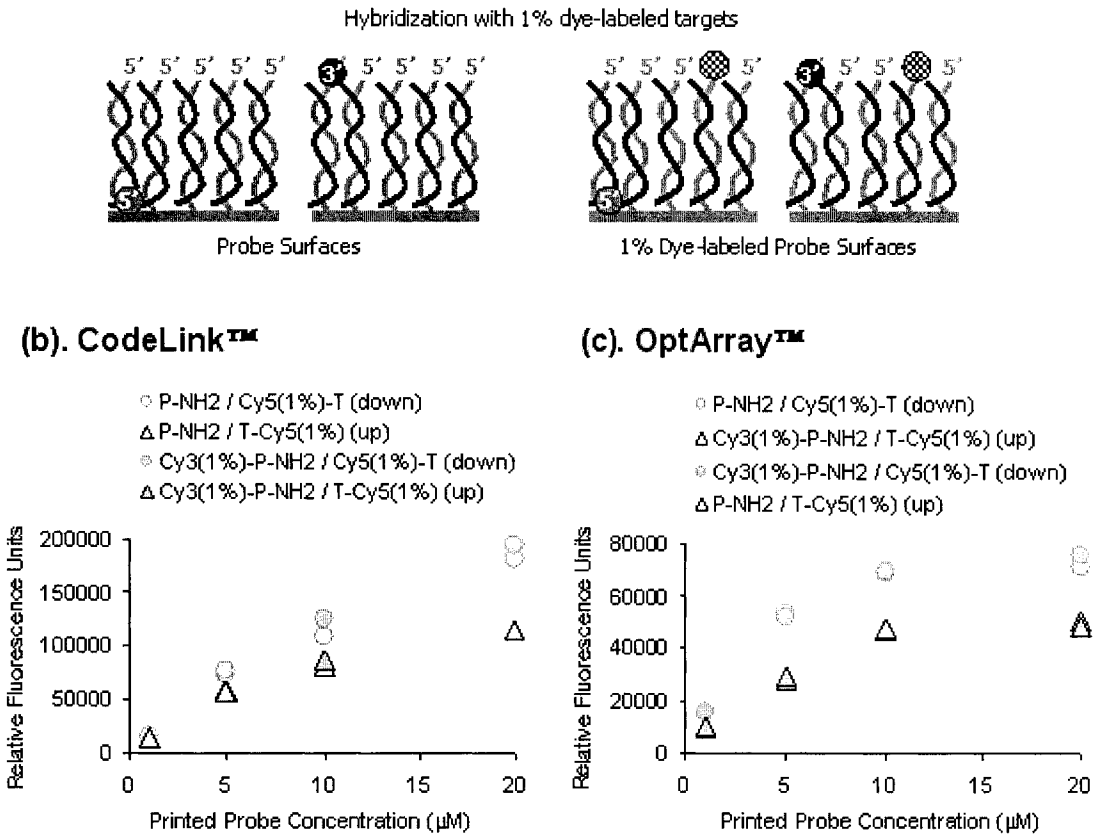

Figure 7.5 Effect of 1% probe dye label on hybridization

Effect of same-end dyes on hybridization efficiency to immobilized DNA. With 100-fold dilution of dye-labeled probes and targets, fluorescence self-quenching is excluded. The spatially isolated (100-fold diluted) dye molecules do not show significant influence on DNA hybridization performance on various surfaces. However, in a scenario of two dye molecules close together (one from probe, the other from target, as shown schematically in Figure 7.6a, farthest right scenario) a combined steric effect may hinder probe-target hybridization. To study this possible steric influence of same-end

dye location on DNA hybridization, surface-immobilized probes with and without dye labels (P-NH_2 and Cy3(100%)-P-NH_2) are hybridized with 1% dye-labeled targets.

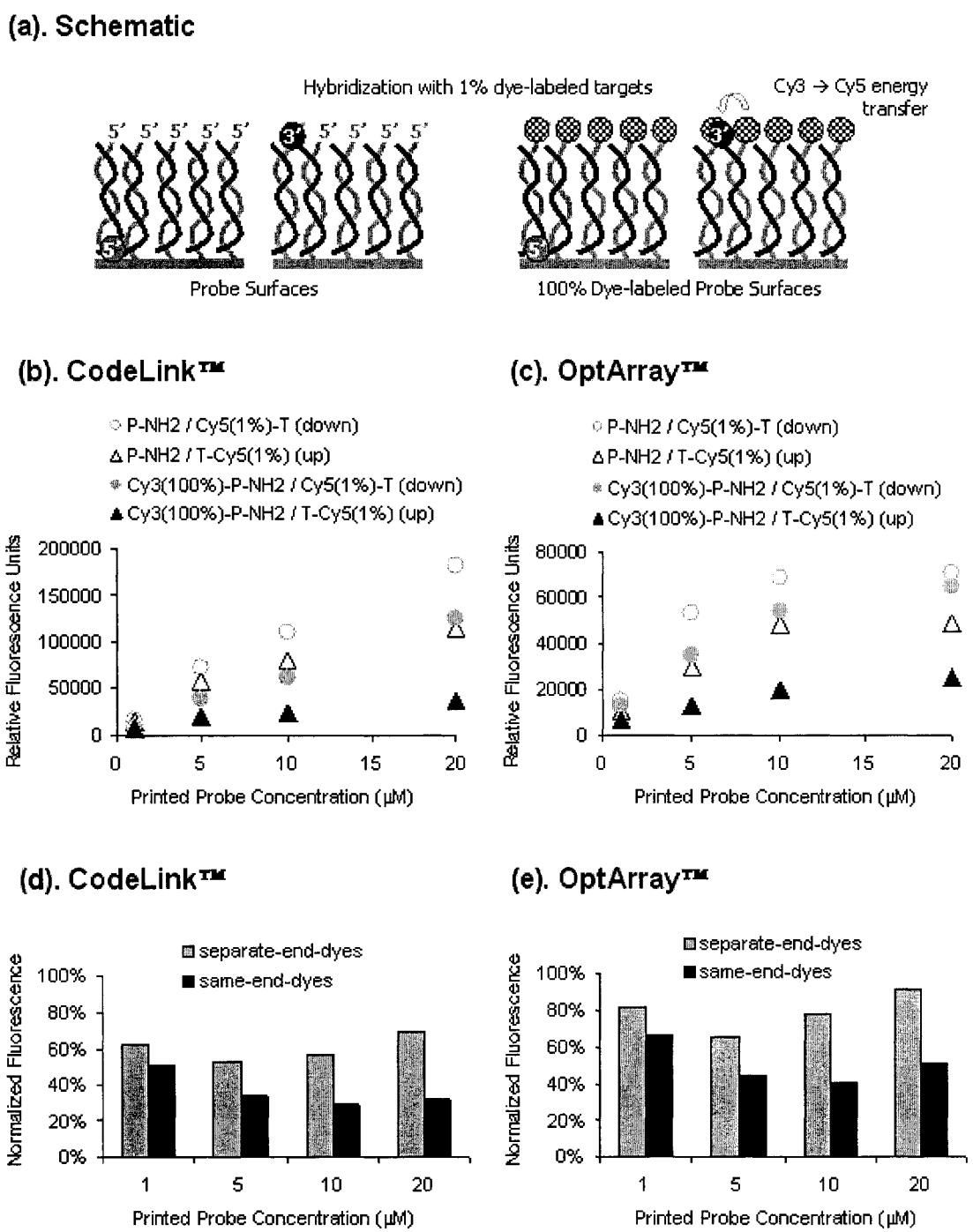

Figure 7.6 Effect of same-end dyes on hybridization efficiency

Although only 1% of the target molecules are Cy5-labeled, Cy3(100%)-P-NH_2 provides one Cy3 per probe molecule, ensuring that Cy5-labeled targets must hybridize to probe molecules with a Cy3 label. Fluorescence intensity results from these experiments are plotted in Figure 7.6b and 7.6c. Open circles and triangles represent hybridization to the unlabeled probe surfaces, filled circles and triangles represent hybridization to the dye-labeled probe surfaces. As shown in Figure 7.6b and 7.6c, the filled black circles are at consistently lower intensities than the open black circles, as are the filled gray triangles to the open gray triangles. This indicates that 100% Cy3 dye label (1 Cy3 label per probe) on surface-immobilized probe reduces target Cy5 fluorescence intensities from hybridization. This decrease in intensity could come from two sources: (1) dye quenching by fluorescence energy transfer upon hybridization, Cy5 to Cy3; or (2) reduced hybridization amount by steric hindrance (same-end dyes, farthest right scenario in Figure 7.6a). Given that the Cy3 emission spectrum overlaps with the Cy5 excitation spectrum, fluorescence energy transfer could only occur in one direction (from Cy3 to Cy5, not reverse). The presence of Cy3 dyes may increase the Cy5 fluorescence, but not lower it. Therefore, dye-quenching contributions to the Cy5 fluorescence drop are not possible. Any fluorescence decrease must come from reduced target hybridization.

Lower target hybridization observed on the Cy3(100%)-P-NH_2 probe surfaces could come from two sources: (1) lower probe density, and (2) lower hybridization efficiency caused by steric hindrance. The contribution from each source cannot be determined unless DNA density on the surface is confirmed using complimentary techniques, such as XPS and radiometric assay.[39,40]

To explore the effect of same-end labels on hybridization efficiency at surfaces, Cy5 target fluorescence hybridized on the Cy3(100%)-P-NH_2 probe surfaces was normalized to that on the P-NH_2 probe surfaces. Normalized fluorescence results are organized as bar charts in Figures 7.6d and 7.6e. Lower fluorescence observed for the Cy3(100%)-P-NH2 probe hybridized with the T-Cy5(1%) target, shown in black, consistent with steric hindrance produced by same-end dyes upon surface DNA hybridization.

Dye self-quenching on surface-hybridized DNA targets. Dye self-quenching is not limited to the Cy3 dye on the surface-immobilized probe upon printing (i.e., Cy3(100%)-P-NH_2), but is also possible for Cy5 dyes on surface-hybridized targets. The magnitude of target Cy5 self-quenching in various hybridization assays is analyzed using dye-labeled targets (Cy5(1%)-T, T-Cy5(1%), Cy5(100%)-T and T-Cy5(100%)) on the same P-NH_2 probe surface, as schematically shown in Figure 7.7a. Fluorescence intensities from all targets were collected and normalized to the same laser/PMT efficiency. Intensities from the 100% dye labeled targets (Cy5(100%)-T and T-Cy5(100%)) were adjusted using a factor of 1/100 for comparison to the 100-fold diluted targets (Cy5(1%)-T, T-Cy5(1%)). The normalized and adjusted fluorescence intensities from all targets were quantified and plotted in Figure 7.7b and 7.7c. Open squares and diamonds represent the 100-fold diluted targets, filled squares and diamonds represent the 100% dye-labeled targets. As shown in Figure 7.7b and 7.7c, molecular fluorescence intensities for 100% dye-labeled targets (filled symbols) are an order of magnitude lower than that of the diluted targets (open symbols), indicating strong dye self-quenching at the

100% labeled target surfaces. Pure, undiluted dye-labeled targets are therefore not suitable for microarray target density quantification. The fluorescence intensity of the

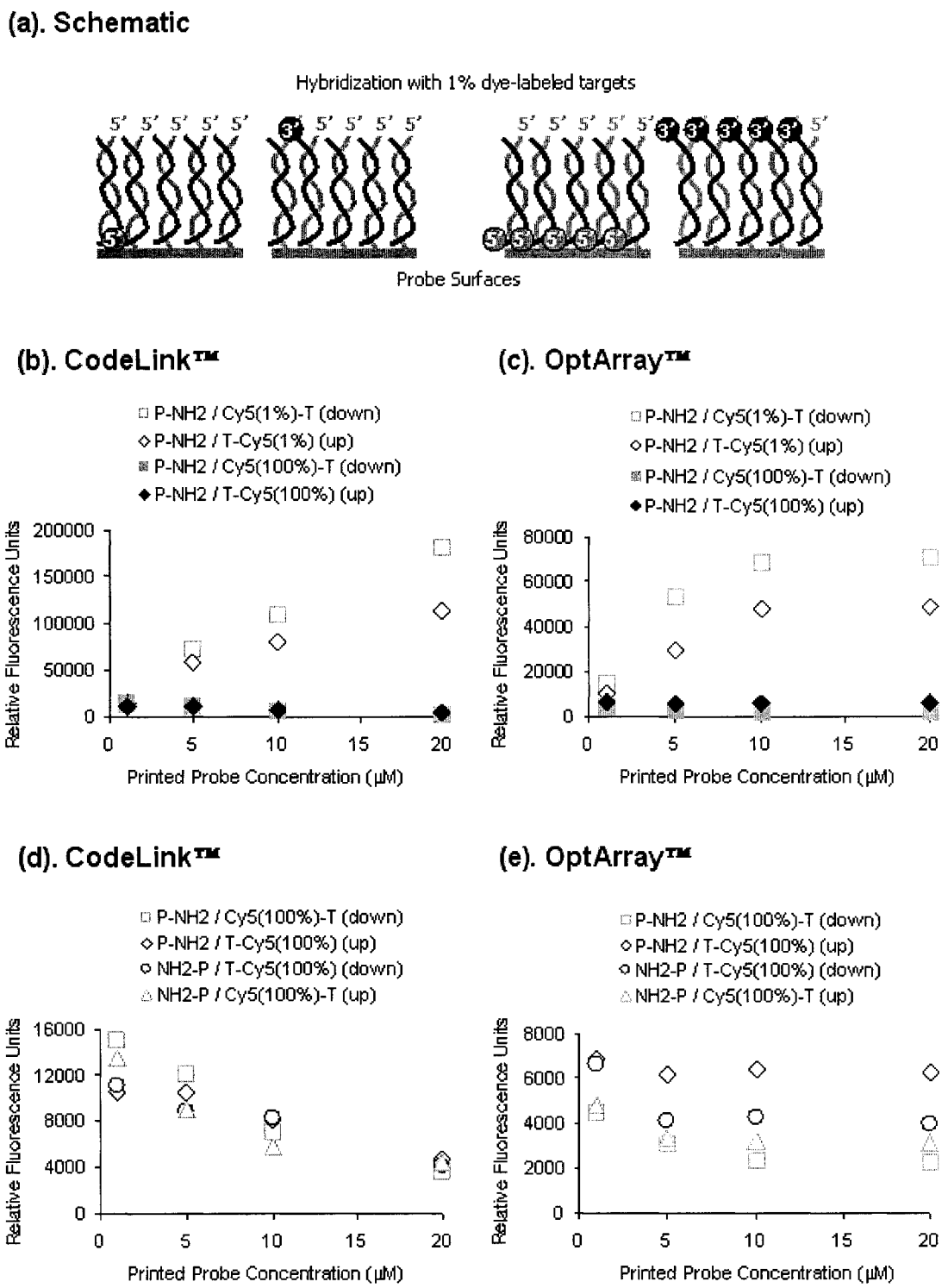

Figure 7.7 Self-quenching of dye-labeled target molecules

100% dye-labeled targets is plotted with a smaller intensity range and shown in Figure 7.7d and 7.7e. A general trend of target fluorescence decrease is observed as surface probe density increases, indicating combined effects of target dye quenching and possibly lower hybridization efficiency at higher probe density. Because the magnitude of quenching is overwhelming, changes in hybridization efficiency are difficult to analyze without further quantifying surface DNA densities using complimentary analytical techniques (XPS, ^{32}P assay).[39,40]

7.5 Conclusions

Fluorescence intensities of two dye-labeled DNAs, even when identical dye and DNA sequence were involved, are not directly comparable for quantification purposes. As shown in results (Figures 7.4, 7.5, 7.6), consistently higher fluorescence quantum yield were observed for the T-Cy5 target molecules than the Cy5-T target molecules used in this study. In order to compare fluorescence signals coming from two dye-labeled DNAs, effect of their intrinsic dye quantum efficiencies, predetermined by individual DNA dye labeling reactions, must be considered. Dye self-quenching and fluorescence energy transfer play important roles in fluorescence quantification of surface DNA. Terminal dye label on DNA may affect both surface immobilization density and distribution. The steric influence of dye label on hybridization is not significant when compared with the effects of dye quenching and the influence of surface probe density. Alternative, complimentary quantification techniques are necessary to determine the effect of dye label on both DNA probe immobilization and target hybridization efficiencies.

7.6 Acknowledgements

The authors are grateful for financial support from NIH EB001473. Technical assistance in fluorescence scanning from Dr. W. H. Hanneman (CSU) and insightful discussions with P. Wu, Drs. G. Harbers, C. Greef and M. Lochhead are gratefully acknowledged.

7.7 References

(1) Ramsay, G. *Nat. Biotechnol.* **1998**, *16*, 40-44.

(2) Schena, M.; Heller, R. A.; Theriault, T. P.; Konrad, K.; Lachenmeier, E.; Davis, R. W. *Trends Biotechnol.* **1998**, *16*, 301-306.

(3) Sanchez-Carbayo, M.; Bornmann, W.; Cordon-Cardo, C. *Curr. Org. Chem.* **2000**, *4*, 945-971.

(4) Freeman, W. M.; Robertson, D. J.; Vrana, K. E. *BioTechniques* **2000**, *29*, 1042-1044, 1046, 1048-1055.

(5) van Hal, N. L. W.; Vorst, O.; van Houwelingen, A. M. M. L.; Kok, E. J.; Peijnenburg, A.; Aharoni, A.; van Tunen, A. J.; Keijer, J. *J. Biotechnol.* **2000**, *78*, 271-280.

(6) Helmberg, A. *Exp. Gerontology* **2001**, *36*, 1189-1198.

(7) Beaucage, S. L. *Curr. Med. Chem.* **2001**, *8*, 1213-1244.

(8) Yang, Y. H.; Speed, T. *Nat. Rev. Genet.* **2002**, *3*, 579-588.

(9) Phimister, B. *Nat. Genet.* **1999**, *21*, 1.

(10) Park, H. G.; Song, J. Y.; Park, K. H.; Kim, M. H. *Chem. Eng. Sci.* **2006**, *61*, 954-965.

(11) Epstein, J. R.; Biran, I.; Walt, D. R. *Anal. Chim. Acta* **2002**, *469*, 3?6.

(12) El Atifi, M.; Dupre, I.; Rostaing, B.; Benabid, A. L.; Berger, F. *BioTechniques* **2003**, *35*, 262,264,266.

(13) Marx, V. *Genomics & Proteomics* **2004**, *4*, 37-40.

(14) Querec, T. D.; Stoyanova, R.; Ross, E.; Patriotis, C. *Bioinformatics* **2004**, *20*, 1955-1961.

(15) Garcia, N.; Salamanca, F.; Astudillo-de la Vega, H.; Curiel-Quesada, E.; Alvarado, I.; Penaloza, R.; Arenas, D. *BMC Cancer* **2005**, *5*, No pp given.

(16) Gershon, D. *Nat. Methods* **2004**, *1*, 263-270.

(17) Li, X.; Zhou, Y.; Sutherland, T. C.; Baker, B.; Lee, J. S.; Kraatz, H.-B. *Anal. Chem.* **2005**, *77*, 5766-5769.

(18) Liepold, P.; Wieder, H.; Hillebrandt, H.; Friebel, A.; Hartwich, G. *Bioelectrochemistry* **2005**, *67*, 143-150.

(19) Marchand, G.; Delattre, C.; Campagnolo, R.; Pouteau, P.; Ginot, F. *Anal. Chem.* **2005**, *77*, 5189-5195.

(20) Ross, P.; Hall, L.; Smirnov, I.; Haff, L. *Nat. Biotechnol.* **1998**, *16*, 1347-1351.

(21) Yang, H.; Wang, H.; Wang, J.; Cai, Y.; Zhou, G.; He, F.; Qian, X. *Anal. Chem.* **2003**, *314*, 54-62.

(22) Samuel, N. T.; Castner, D. G. *Appl. Surf. Sci.* **2004**, *231-232*, 397-401.

(23) May, C. J.; Canavan, H. E.; Castner, D. G. *Anal. Chem.* **2004**, *76*, 1114-1122.

(24) Wegner, G. J.; Wark, A. W.; Lee, H. J.; Codner, E.; Saeki, T.; Fang, S.; Corn, R. M. *Anal. Chem.* **2004**, *76*, 5677-5684.

(25) Smith, E. A.; Wanat, M. J.; Cheng, Y.; Barreira, S. V. P.; Frutos, A. G.; Corn, R. M. *Langmuir* **2001**, *17*, 2502-2507.

(26) Nelson, B. P.; Grimsrud, T. E.; Liles, M. R.; Goodman, R. M.; Corn, R. M. *Anal. Chem.* **2001**, *73*, 1-7.

(27) http://www.affymetrix.com/technology/design/index.affx.

(28) http://www4.amershambiosciences.com/APTRIX/upp01077.nsf/Content/codelink_human_bioarrays?OpenDocument&hometitle=codelink.

(29) http://www.chem.agilent.com/scripts/generic.asp?lpage=11617&indcol=N&prodcol=Y.

(30) Lakowicz, J. R. In *Principles of Fluorescence Spectroscopy*, 1999.

(31) Schmitt, F. J.; Meller, P.; Ringsdorf, H.; Knoll, W. *Progress in Colloid & Polymer Science* **1990**, *83*, 136-145.

(32) http://probes.invitrogen.com/handbook/sections/0001.html.

(33) Gong, P.; Grainger, D. W. *Surf. Sci.* **2004**, *570*, 67-77.

(34) Lee, C.-Y.; Canavan, H. E.; Gamble, L. J.; Castner, D. G. *Langmuir* **2005**, *21*, 5134-5141.

(35) Forman, J. E.; Walton, I. D.; Stern, D.; Rava, R. P.; Trulson, M. O. *ACS Symp. Ser.* **1998**, *682*, 206-228.

(36) Mazzola, L. T.; Frank, C. W.; Fodor, S. P. A.; Mosher, C.; Lartius, R.; Henderson, E. *Biophys. J.* **1999**, *76*, 2922-2933.

(37) Li, Q.; Luis, R.; Adnan, A.; Alioune, N. *Appl. Bioinformatics* **2005**, *4*, 1-11.

(38) $K^2 = (\cos qt - 3\cos qD \cos qA)^2$, where q = the angle between a fluorophore emission dipole and another fluorophore's excitation dipole: K=0 for orthogonal alignment (no energy transfer), K=4 for perfectly aligned dipoles (high probability of FRET, and K=0.667 for random isotropic dye orientation.

(39) Gong, P.; Harbers, G. M.; Grainger, D. W. *Anal. Chem.* **2006**, *in press*.

(40) Lee, C.-Y.; Gong, P.; Harbers, G. M.; Grainger, D. W.; Castner, D. G.; Gamble, L. J. *Anal. Chem.* **2006**, *in press*.

Chapter 8 SUMMARY

This dissertation research focuses on understanding the surface chemistry influences on DNA probe environments that affect the efficiency of target capture from solution in order to improve microarray assay performance. Assay surface reliability, DNA density, hybridization efficiency and the influence of fluorescent dye label and complex milieu (serum dilutions, cell lysate) on hybridization were assessed on both model gold surfaces and commercial microarraying slides using XPS, SPR as well as more traditional biological and microarray analysis techniques (^{32}P-radiometric assay and fluorescence intensity measurements).

Probe DNA/mercaptoundecanol (MCU) mixed adlayers on gold served as a model system for conducting surface and DNA analyte capture assays. The multi-technique characterization of the model systems showed clear dependence of hybridization performance (efficiency and kinetics) on probe density [$(1.7 \sim 4.4)\times10^{13}$ probes/cm^2] and orientation, with optimum target hybridization (8.9×10^{12} targets/cm^2) observed at intermediate probe density (3.6×10^{13} probes/cm^2) backfilled with MCU diluent for improved probe orientation. The probe DNA surfaces with optimum target hybridization performance were challenged with complex milieu hybridization. Serum protein adsorption onto the sensor surfaces was found to significantly affect the SPR curve shape, impeding hybridization detection beyond 30% serum.

Following surface characterization and DNA hybridization studies on gold, surface and analyte capture assays were performed on commercial microarraying slides. The commercial slides were noted to lose reactivity over time due to intrinsic hydrolytic instability of NHS, resulting in poor DNA probe immobilization efficiency with accompanying reliability and variability between assays. A straightforward one-step reaction was developed to regenerate microarray slide reactivity *in situ* to provide improved reactivity towards DNA probe immobilization and more consistent assay to assay results. Using the more consistent microarraying substrate, efforts were made to establish a quantitative understanding of the correlation between immobilized DNA probe density and target hybridization efficiency on the microarray slides. Macroscopic analogs of DNA microarray spots were created and successfully utilized as a new platform for the study of DNA surface chemistry using highly sensitive, quantitative surface analytical techniques (e.g., XPS) that are currently incompatible with microarray dimensions (100-200μm). Surface densities of immobilized DNA probes ($2x10^{11}$ ~ $6.7x10^{12}$ probes cm^2) and hybridized DNA targets (and $2x10^{11}$ ~ $5.6x10^{12}$ targets/cm^2) on commercial slides were quantified using sensitive ^{32}P-DNA radiometric measurements. Complete hybridization (100% efficiency) occurred at lower probe densities while decreased hybridization efficiencies were observed at higher probe densities. The more sensitive ^{32}P-DNA radiometric measurements are now calibrated with more routine XPS DNA signals, facilitating future routine DNA density determinations without the use of hazardous radioactive assays. Furthermore, complex milieu and fluorescence dye label influences on microarray DNA hybridization were investigated. Contrary to the complex

milieu hybridization results on the gold model system, preliminary results on commercial slides showed minimum complex milieu influence on microarray DNA hybridization.

In summary, surface chemistry influences on DNA probe environments affect target capture efficiency from solution and propose itself as a research focus for optimization of microarray assay performance. The combination of a variety of surface analytical, biological and microarray assay techniques reveals molecular disposition of microarray DNA on surfaces, facilitating a better understanding of DNA microarrays for improved assay performance.

Appendix A Surface Coverage and Structure of Mixed DNA/Alkylthiol Monolayers on Gold: Characterization by XPS, NEXAFS, and Fluorescence Intensity Measurements

Reprinted with permission from: C.-Y. Lee, P. Gong, G.M. Harbers, D.W. Grainger, D.G. Caster and L.J. Gamble, Analytical Chemistry **2006**, *in press*

Appendix A is a companion journal article of Chapter 3 of this dissertation. It contains the manuscript of a full paper published in *Analytical Chemistry*. The manuscript was written by Chi-Ying Lee and Ping Gong, and edited by David W. Grainger, David G. Castner and Lara J. Gamble. This chapter describes the fabrication and surface characterization of thiol-DNA/MCU mixed adlayers on gold using XPS, NEXAFS and fluorescence intensity measurements.

Surface Coverage and Structure of Mixed DNA/Alkylthiol Monolayers on Gold: Characterization by XPS, NEXAFS, and Fluorescence Intensity Measurements

Chi-Ying Lee, Ping Gong, Greg Harbers, David W. Grainger, David G. Castner, and Lara J. Gamble

A.1 Abstract

Self-assembly of thiol-terminated single-stranded DNA (HS-ssDNA) on gold has served as an important model system for DNA immobilization at surfaces. Here, we report a detailed study of the surface composition and structure of mixed self-assembled DNA monolayers containing a short alkylthiol surface diluent [11-mercapto-1-undecanol (MCU)] on gold supports. These mixed DNA monolayers were studied with X-ray photoelectron spectroscopy (XPS), near-edge X-ray absorption fine structure spectroscopy (NEXAFS), and fluorescence intensity measurements. XPS results on sequentially adsorbed DNA/MCU monolayers on gold indicated that adsorbed MCU molecules first incorporate into the HS-ssDNA monolayer, and, upon longer MCU exposures, displace adsorbed HS-ssDNA molecules from the surface. Thus, HS-ssDNA surface coverage steadily decreased with MCU exposure time. Polarization-dependent NEXAFS and fluorescence results both show changes in signals consistent with changes in DNA orientation after only 30 min of MCU exposure. NEXAFS polarization dependence (followed by monitoring the N 1s $\rightarrow$ π^* transition) of the mixed DNA monolayers indicated that the DNA nucleotide base ring structures are oriented more

parallel to the gold surface compared to DNA bases in pure HS-ssDNA monolayers. This indicates that HS-ssDNA oligomers reorient toward a more-upright position upon MCU incorporation. Fluorescence intensity results using end-labeled DNA probes on gold show little observable fluorescence on pure HS-ssDNA monolayers, likely due to substrate quenching effects between the fluorophore and the gold. MCU diluent incorporation into HS-ssDNA monolayers initially increases DNA fluorescence signal by densifying the chemisorbed monolayer, prompting an upright orientation of the DNA, and moving the terminal fluorophore away from the substrate. Immobilized DNA probe density and DNA target hybridization in these mixed DNA monolayers, as well as effects of MCU diluent on DNA hybridization in complex milieu (i.e., serum) as characterized by ^{32}P-labeling and surface plasmon resonance (SPR) reported in a related study (*Gong et al., Anal. Chem., 2006, in press*) were used for comparison and supporting data.

A.2 Introduction

Methods for surface-immobilizing single-strand nucleic acids that preserve their original hybridization specificity with minimized non-specific interactions remain an important goal for improving the performance of DNA microarray and biosensor applications. As summarized in a recent review,[1] nucleic acid hybridization behavior observed between complementary probe and target DNA molecules in bulk solution differ from identical hybridization at a solid-liquid interface. In surface hybridization, non-specific probe-surface interactions, electrostatic forces and steric issues between adjacent DNA probes influence DNA target hybridization efficiency and capacity. For example, nucleotide primary amines on non-hybridized DNA segments can interact (e.g., covalently,[2] or by acid-base adsorption) with the surface, becoming unavailable to

hybridize with target DNA molecules. Effects of immobilized DNA probe density, charge density, and orientation on target capture and methods to reliably control these surface states remain poorly characterized on most surfaces. Therefore, before the full potential of DNA microarrays can be realized, many fundamental issues must be better understood, including how the crowding, conformation and orientation of immobilized DNA impacts DNA target hybridization efficiency.

Tarlov and co-workers pioneered a technique for DNA immobilization that utilizes the chemisorptive self-assembly of thiol-terminated single-stranded DNA (HS-ssDNA) monolayers onto gold surfaces, mixed with a short hydroxyl-terminated alkylthiol surface diluent [e.g., mercaptohexanol (MCH)].[3-5] Based on X-ray photoelectron spectroscopy (XPS),[4,6] neutron reflectivity,[3] and surface plasmon resonance (SPR)[5] studies of this mixed self-assembled monolayer (SAM) system, the MCH has been proposed to prevent the non-specific attachment of DNA to the surface by nucleotide amine groups and enhance specific attachment by the thiolated group.

Chemisorbed adlayers of alkylthiols on gold provide a high degree of control over surface physical properties, providing useful model systems for examining relationships between HS-ssDNA surface composition and orientation, as well as subsequent hybridization behavior with solution-phase targets. These previous studies have provided some important quantitative information on possible HS-ssDNA conformational changes in self-assembled mixed monolayers resulting from addition of the MCH surface diluent. However, HS-ssDNA oligomers may behave differently when the packing density or other properties (e.g., DNA length) of the film is varied. To develop a fuller understanding of surface properties in these mixed DNA monolayers at the molecular

level, the packing density of the HS-ssDNA was systematically changed by backfilling the pure HS-ssDNA monolayer with a short alkylthiol surface diluent [11-mercapto-1-undecanol (MCU)], similar to those used in the original reports.[3-5] The effect of diluent backfill time on mixed adlayer surface composition, density, and orientation of HS-ssDNA oligomers was evaluated with XPS, near-edge X-ray absorption fine structure spectroscopy (NEXAFS), and fluorescence intensity measurements.

To the best of our knowledge, relatively few DNA characterization experiments using high-resolution surface analytical techniques[3,4,6-8] have been directed at immobilized DNA molecules in mixed monolayer systems. In previous investigations, we reported XPS quantitation of the chemical composition of individual DNA nucleobases, nucleotides, and oligomers,[9] and identified contaminants in thiolated ssDNA monolayer films on gold.[10] In this work, we have used complementary XPS, NEXAFS and fluorescence intensity measurements to characterize monolayer composition, density, and orientational changes as a function of MCU backfill-time and DNA surface displacement. Quantitative atomic compositions of the mixed DNA monolayers were obtained and compared using XPS. Polarization-dependent NEXAFS, also known as X-ray absorption near-edge structure (XANES), a technique used to determine molecular orientation and ordering of surface-bound molecules,[11] was used to probe surface orientation and order in pure DNA and mixed DNA/MCU monolayers. NEXAFS has been used to examine the surface molecular orientation and ordering for a variety of materials including SAMs on gold[12] and polymers.[13-16] In our previous DNA studies, NEXAFS has been used to characterize DNA nucleobases and nucleotides, as well as the orientation of polydA and polydT oligomers on gold.[17] Finally, end-labeled DNA

fluorescence intensity measurements were used to obtain information about the interaction between the DNA oligomers and the gold substrate by comparing the normalized fluorescence intensities from DNA monolayers with varied MCU-backfill time.

In a companion article,[18] we have used ^{32}P-radiometric measurements of DNA immobilized densities (e.g. molecules/cm^2) to calibrate the XPS nitrogen and phosphorus signals from identical DNA monolayers to those reported here, creating a convenient basis for XPS-based DNA surface density determinations. Furthermore, the molecular densities of these same DNA monolayers were then correlated with their DNA hybridization efficiencies using both radiometric ^{32}P-labeling and SPR real-time assays. DNA hybridization and target capture efficiencies from complex milieu (i.e., serum dilutions) were further evaluated for an optimized DNA/MCU mixed monolayer surface using SPR. Corroboration of results between these two studies on identical DNA-gold monolayer surfaces provides a new, more comprehensive picture of HS-ssDNA "molecular disposition" immobilized on a surface that influences hybridization events relevant to microarray capture assays and other biotechnological manipulations on surfaces.

A.3 Experimental section

Preparation of Mixed DNA/MCU Self-Assembled Monolayers for XPS and NEXAFS Analysis. Silicon wafers (Silicon Valley Microelectronics, Inc., San Jose), coated with 10 nm Cr and 80 nm Au (99.99%) by electron beam evaporation at pressures below 1 x 10^{-6} Torr, were used as substrates. DNA oligomers [5'-HS-$(CH_2)_6$-CTGAACGGTAGCATCTTGAC-3'] were purchased from TriLink Biotechnologies

(HPLC-purified for highest purity,[10] San Diego, CA). Mixed DNA/MCU monolayers of varying DNA surface coverage were assembled by a known, sequential two-step process. First, pure DNA monolayers were prepared by immersing freshly gold-coated substrates in 1 μM HS-ssDNA solutions in 1 M NaCl-TE buffer (1 M NaCl, 10 mM Tris-HCl, 1 mM EDTA, pH 7.4, Fisher, Fair Lawn, NJ) for 5 hours. After HS-ssDNA assembly, samples were rinsed thoroughly with buffer for 30 seconds and Millipore grade water for 1 minute to remove loosely bound HS-ssDNA. These DNA-adsorbed samples were then immersed in 10 μM MCU (97% purity, Sigma-Aldrich) diluent thiol solution (in water) for backfill times ranging from 30 minutes to 18 hours. After the specified MCU backfill-time, samples were removed from the solutions and rinsed thoroughly in Millipore grade water for 1 minute. Samples were then blown dry with N_2 and stored under N_2 until analysis.

X-ray Photoelectron Spectroscopy. XPS is a quantitative, surface analytical tool sensitive to the atomic composition of the outermost 100 Å of a sample surface. XPS measurements were performed on a Kratos AXIS Ultra DLD instrument using a monochromatic Al-Kα X-ray source and a 0^{o} take-off-angle. The take-off angle is defined as the angle between the sample surface normal and the axis of the XPS analyzer lens. Compositional survey and detailed scans (P2p, C1s, N1s, O1s, and S2p) were acquired using a pass energy of 80 eV. High-resolution spectra (P2p, C1s, N1s, O1s, S2p, and Au4f) were acquired for the DNA samples using a pass energy of 20 eV. For the high-resolution spectra, peak binding energies were referenced to the Au 4f peak at 84.0 eV. Three spots on two or more replicates of each DNA sample were analyzed.

Reported compositional data were averages of values determined at each spot. Data analysis was performed with Vision Processing data reduction software.

Near-Edge X-ray Absorption Fine Structure Spectroscopy. NEXAFS spectra were taken at the National Synchrotron Light Source (NSLS) U7A beamline at Brookhaven National Laboratory, using an ~85% polarized, high intensity beam.[19] This beam line uses a monochromator and 600 l/mm grating that provides a full-width at half-maximum (FWHM) resolution of ~0.15 eV at the carbon K-edge (~285 eV). The monochromator energy scale was calibrated using the 285.35 eV C 1s $\rightarrow \pi^*$ transition of adventitious hydrocarbon on a gold coated 90% transmission grid placed in the path of the X-rays. To eliminate the effect of incident beam intensity fluctuations and monochromator absorption features, all NEXAFS spectra were normalized by the signal from a pure gold (gold deposited *in situ*) control sample (I_0) and the beam flux (I_{ring}). Partial electron yield (PEY) was monitored by a detector with the bias voltage maintained at –150 V for the carbon K-edge spectrum and –350 V for the nitrogen K-edge spectrum. Samples were mounted to allow rotation about the vertical axis to change the angle between the sample surface and the incident X-ray beam. The NEXAFS angle is defined as the angle between the incident X-ray beam and the sample surface. The incident beam normal to the surface is defined as 90° while a glancing incident beam is generally 20° from the surface plane. The electric field vector (**E**) is perpendicular to the X-ray beam; therefore, when the beam is at normal incidence, the **E** vector lies parallel to the surface. A disordered system on the sample surface does not show any polarization dependence because of random distribution in molecular orientation. Polarization dependence is indicative of directional alignment of the molecules in the overlayer.[11]

Fluorescence Intensity Measurements of DNA-Cy3 Layers on Gold. The 3'-thiolated DNA probe bearing a 5'-fluorescent-Cy3 label [5'-Cy3-CTGAACGGTAGCATCTTGAC-$(CH_2)_6$-SH-3'] was custom synthesized and HPLC-purified (TriLink Biotechnologies, San Diego, CA). Gold substrates were prepared by thermal evaporation of 100 nm of Au onto a 10 nm Cr adhesion layer using an Auto306 coating system (Edwards, Wilmington, MA) on low-fluorescence glass slides (OptArray, Accelr8, Denver, CO). The gold substrates were then cleaned with O_2 plasma (5 min, 100 Watts, 0.1 torr) just prior to immersion into DNA probe solutions. DNA probe surface immobilization was performed at room temperature using 1 μM thiolated DNA probe in 1 M NaCl-TE buffer at pH 7.0 for 5 hours, followed immediately by various timed exposures of 10μM MCU backfilling diluent solutions as described above. Probe samples were then rinsed with Millipore grade water for 15 seconds and dried with N_2. Fluorescence intensity images of the resulting surfaces were collected using a ScanArray Express scanner (Perkin Elmer, Fremont, CA) and analyzed using ImageQuant software (Amersham Biosciences).

A.4 Results and Discussion

XPS Analysis of Pure DNA and Mixed DNA/MCU Monolayer Compositions. XPS was used to obtain detailed information about the chemical composition of mixed monolayers of HS-ssDNA and MCU. Adlayer compositional change was followed as pure DNA monolayers formed from the first assembly step on gold were exposed to MCU diluent thiol for varied lengths of time (0.5 – 18 h). Table A.1 summarizes the XPS elemental compositions from pure HS-ssDNA and mixed DNA/MCU monolayers. Only those elements expected from the HS-ssDNA (P, C, N, O, and S), MCU (C, O, and

S), and substrate (Au) are detected in XPS survey scans. Elements P and N are unique to DNA and are therefore good indicators of relative amounts of HS-ssDNA present on the surface under each condition.

Surfaces of pure HS-ssDNA on gold, in the absence of MCU diluent thiol, exhibited a composition of 1.4% P, 7.6% N, 15.4% O, 41.9% C, and 33.6% Au (as

Table A.1 XPS compositional data for pure DNA and mixed DNA/MCU monolayers on gold.[α]

Time in HS-ssDNA	Time in MCU	Atomic percent						Atomic ratio		
		P 2p	**N 1s**	**O 1s**	**C 1s**	**S 2p**	**Au 4f**	**P/N**	**O/N**	**C/N**
HS-ssDNA theoretical		-	-	-	-	-	-	0.3	1.7	2.8
5h	0 h	1.4	7.6	15.4	41.9	-	33.6	0.2	2.0	5.5
5h	0.5 h	1.1	5.7	12.5	52.0	1.0	27.8	0.2	2.3	9.8
5h	1 h	1.2	5.2	11.9	52.1	1.3	28.2	0.2	2.3	10.4
5h	2 h	0.8	5.3	11.8	53.9	1.2	26.8	0.2	2.3	10.4
5h	5 h	0.8	3.9	10.4	53.7	1.4	29.8	0.2	2.8	14.6
5h	18 h	0.6	3.2	9.7	55.0	1.5	30.1	0.2	3.1	17.4
0h	18 h	0.0	0.0	7.9	57.6	2.6	31.9	-	-	-

[α]All standard deviations < 2%.

summarized in Table A.1). The experimental atomic ratios calculated from the atomic percentages (P/N = 0.2, O/N = 2.0, and C/N = 5.5) are similar to those predicted by the stoichiometry of the DNA molecule (P/N = 0.3, O/N = 1.7, and C/N = 2.8) with the exception of excess carbon. This is likely due to the presence of adventitious hydrocarbon contamination, a presumption supported by the accuracy of the P/N and O/N atomic ratios. After short-term exposure of the DNA monolayer to the MCU diluent thiol (< 2 hr), relative atomic percents of C and S increased, while relative atomic percents of Au, P, N, and O all decreased (see Table A.1). The increased atomic percent of C and S

is consistent with the presence of MCU, as the smaller MCU diluent thiols take up unoccupied gold sites surrounding the loosely-packed DNA on the surface. The corresponding Au signal decreased during this same short-term exposure of the DNA monolayer to MCU consistent with this interpretation. MCU surface reactions could also displace other weaker, non-specific interactions between nitrogen-containing DNA bases and gold, promoting single-point tethering of DNA oligomers on gold via thiolate bonds, with greater tendency to orient away from the surface. NEXAFS and fluorescence data further support this contention.

For longer MCU exposure times (> 2 h), relative Au substrate atomic percent increased, while the relative atomic percent of P and N decreased further. These results indicate that after gold site-filling, further MCU exposure promotes displacement of DNA molecules from the surface by the more competitive MCU diluent thiols. In a companion article,[18] we present radiolabeling evidence which supports the hypothesis that the DNA is displaced by MCU at longer backfill times in identical adlayer systems.

In addition to elemental composition changes, significant differences in the high-resolution XPS spectra between the pure DNA and mixed DNA/MCU monolayers were also observed. Figure A.1 compares high-resolution C1s, N1s, P2p, O1s, S2p and Au4f spectra for a pure DNA monolayer to that after a 1 h MCU backfill. The pure HS-ssDNA adlayer has a C1s high-resolution spectrum (Figure A.1a) with four peaks attributed to DNA, as previously described.[9,10] The relative concentrations of the different carbon species were 54% C-C and C-H (285 eV), 31% C-N and C-O (287 eV), 11% N-C(=O)-C, N-C(=N)-N, N=C-N and N-C-O (288 eV), and 4% N-C(=O)-N (289 eV), as summarized in Table A.2. When compared with theoretically expected values (Table A.2), XPS

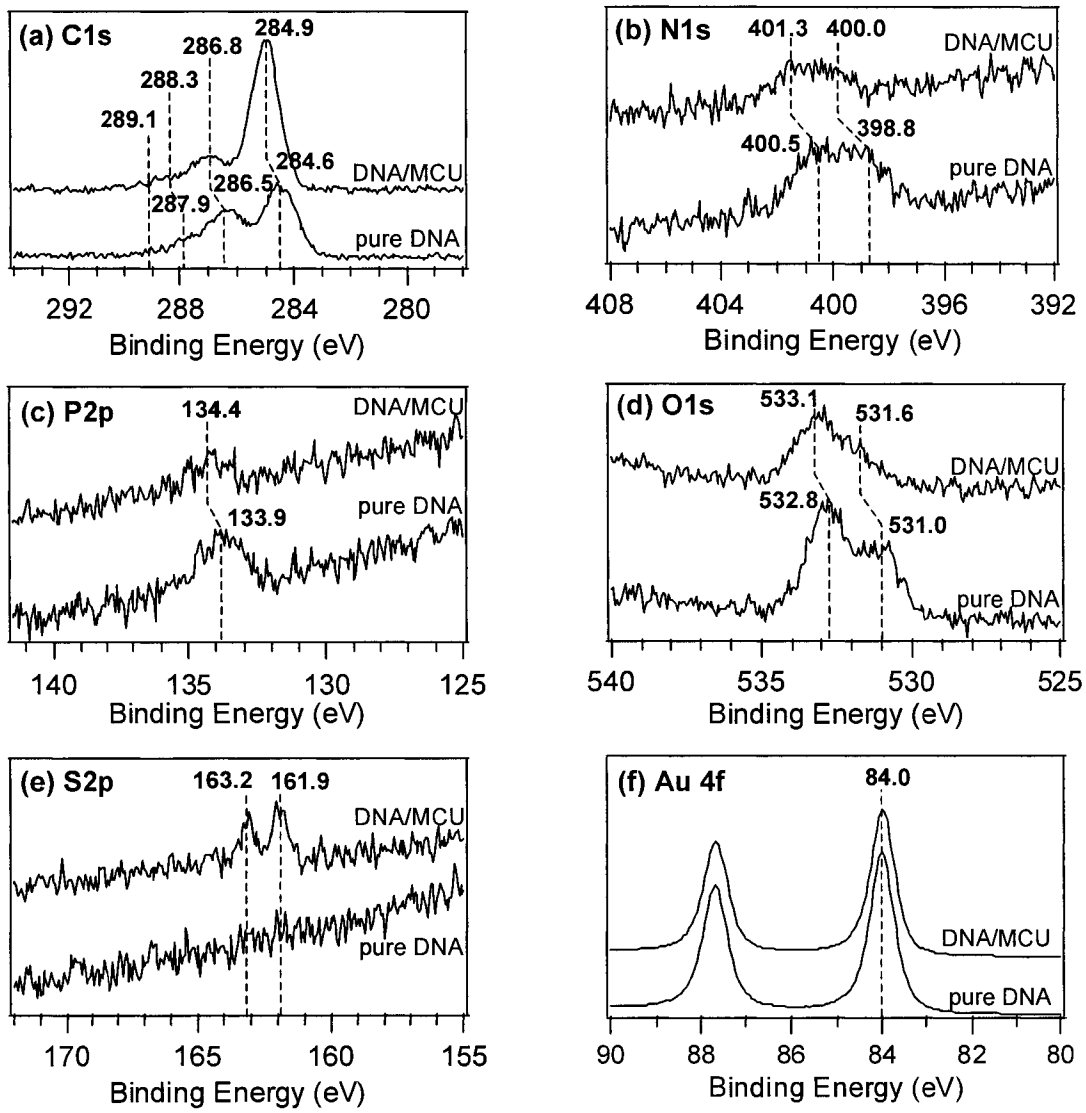

Figure A.1 High-resolution XPS (a) C1s, (b) N1s, (c) P2p, (d) O1s, (e) S2p and (f) Au4f spectra from pure DNA and mixed DNA/MCU (1 h MCU backfill) monolayers on gold. Peak binding energies for high-resolution spectra were referenced to the Au 4f peak (f) at 84.0 eV. Decreases in the N1s, P2p, and O1s peak intensities are also observed after MCU backfill (b-d). S2p peaks are observed only after MCU backfill. The binding energy (BE) of the $S_{2p3/2}$ peak (e, 161.9 eV) is consistent with the sulfur bound to the gold surface as a thiolate species.[22]

experimental values exhibit higher C-H species concentrations, supporting the same conclusion *(vida infra)* that excess %C is from adventitious hydrocarbon contamination. After 1 h exposure of the HS-ssDNA monolayer to the MCU diluent thiol, the

hydrocarbon peak (C-C and C-H) intensity at 285 eV increased, supporting the conclusion that the increase in carbon composition (summarized in Table A.1) is due primarily to increased hydrocarbon species from the MCU (for high-resolution XPS C1s spectrum, see Figure A.1a; for compiled high-resolution XPS C1s results, see Table A.2). Increased C-H species (due to increased MCU exposure), produced a corresponding decrease in peak intensities for the other DNA-related carbon peaks for species at ~287 eV, ~288 eV, and ~289 eV (see Table A.2).

Table A.2 XPS C1s high-resolution data for pure DNA and mixed DNA/MCU monolayers on gold.[α]

Time in HS-ssDNA	Time in MCU	Percentage			
		C-C, **C**-H	**C**-N, **C**-O	N-**C**(=O)-C, N-**C**(=N)-N, N=**C**-N, N-**C**-O	N-**C**(=O)-N
		(284.7 eV)	(286.6 eV)	(288.1 eV)	(289.1 eV)
HS-ssDNA theoretical		20.0	45.0	27.0	8.0
5 h	0 h	54.3	30.9	10.7	4.1
5 h	0.5 h	61.5	25.8	9.0	3.7
5 h	1 h	67.7	22.0	7.3	3.0
5 h	2 h	70.6	20.2	7.2	1.9
5 h	5 h	72.2	20.0	7.0	0.8
5 h	18 h	80.5	16.2	3.3	-
0 h	18 h	88.5	11.5	-	-
MCU theoretical		90.9	9.1	-	-

[α]All standard deviations < 2%.

While the presence of an S2p doublet structure at 161.9 eV in mixed DNA/MCU monolayers (Figure A.1e) is clear evidence of sulfur bound to gold as a thiolate,[20] no such features were observed in the S2p region for the pure HS-ssDNA monolayers. This was expected as the stoichiometric sulfur concentration in the HS-ssDNA molecule (0.2 atomic percent) was close to the XPS detection limit (~0.1%) and the S signal was likely

attenuated by the overlying DNA film. Backfill of MCU molecules, with higher sulfur concentration (7.9 atomic percent), increased relative percentages of sulfur species on the surface, allowing unambiguous thiolate assignment of the sulfur doublet in mixed DNA/MCU films near 162 eV.

Figure A.1 also shows that addition of MCU diluent shifts the binding energies (BE) in all XPS high-resolution spectra. Peak binding energies for all high-resolution spectra were referenced to the Au 4f peak at 84.0 eV (see Figure A.1f). As seen in Figures A.1a-d, the C1s, N1s, P2p, and O1s XPS peaks, from pure HS-ssDNA monolayers shift to lower BEs than those from mixed DNA/MCU films. While the BE shifts for the C1s, P2p, and O1s peaks were small (~0.3 – 0.5 eV), the BE shift for the N1s peaks were of larger magnitude (~1.0 eV). These XPS peak shifts seen in pure DNA monolayers are proposed to arise from non-thiol interactions of the DNA polyanions with the gold substrate. Furthermore, the larger BE shift observed for the N1s spectrum in pure DNA monolayers indicates that these DNA interactions with the surface may also occur through the nitrogen atoms in the DNA bases, producing the observed shift in pure HS-ssDNA adlayers that is removed when MCU diluent out-competes these interactions to force DNA into a more upright position.[4,8]

NEXAFS Orientation Studies of Pure DNA and Mixed DNA/MCU Monolayers. Polarization-dependent NEXAFS was used to further probe the surface orientation and order of the pure DNA and mixed DNA/MCU monolayers. X-ray absorption by molecular orbitals is strongly dependent on the favorable overlap of antibonding orbitals with the electric field (**E**) vector of the incident X-rays. As a result, the polarized X-ray absorption spectra will show differences with differing incident X-ray angles for oriented

and ordered molecules at surfaces. For little long-range alignment in the structure of the surface-bound DNA, the X-ray absorption spectra will not vary with angle of incidence. Polarization dependence observed in the NEXAFS spectrum is therefore indicative of both the orientation and the long range ordering of the molecules in the overlayer. In this study, C K-edge and N K-edge NEXAFS spectra of DNA monolayers were collected at normal (incident X-ray beam 90° to the surface) and glancing (20°) angles to examine the effect of MCU backfill on the orientation of gold-bound DNA oligomers.

NEXAFS Orientation Studies: N K-edge. Figure A.2a presents the NEXAFS N K-edge spectra for the pure DNA and mixed DNA/MCU (0 – 18h MCU backfill) monolayers measured at normal and glancing X-ray incident angles. All NEXAFS N K-edge spectra from pure DNA and mixed DNA/MCU monolayers contained a doublet feature in the 399-402 eV region. Previous studies on nucleobases,[17,21-24] DNA oligomers,[17,25] and other polymers with similar nitrogen-containing ring structures[26-28] found similar splitting of the two π^* orbitals (ΔE = 1.7 eV). We hypothesize that the π^* doublet observed in the nitrogen region represents an average signal over the four different nucleotide bases. While the higher energy π^* peak around 401 eV is attributed to the nitrogen atoms in the nucleobases located next to carbonyl groups,[17,25] the lower energy π^* peak near 399 to 400 eV is consistent with the location of the "aromatic" nitrogen π^* peak in molecules that have nitrogen atoms present in a ring structure.[26,28] The broader peak above 405 eV is attributed to the N 1s $\rightarrow \sigma^*$ transition.[17,25]

For the pure HS-ssDNA monolayer (Figure A.2a, t = 0), the intensity of the π^* peaks was slightly higher when the X-ray beam was at a glancing angle of incidence compared to that at normal incidence. At glancing incidence, the **E** vector of the

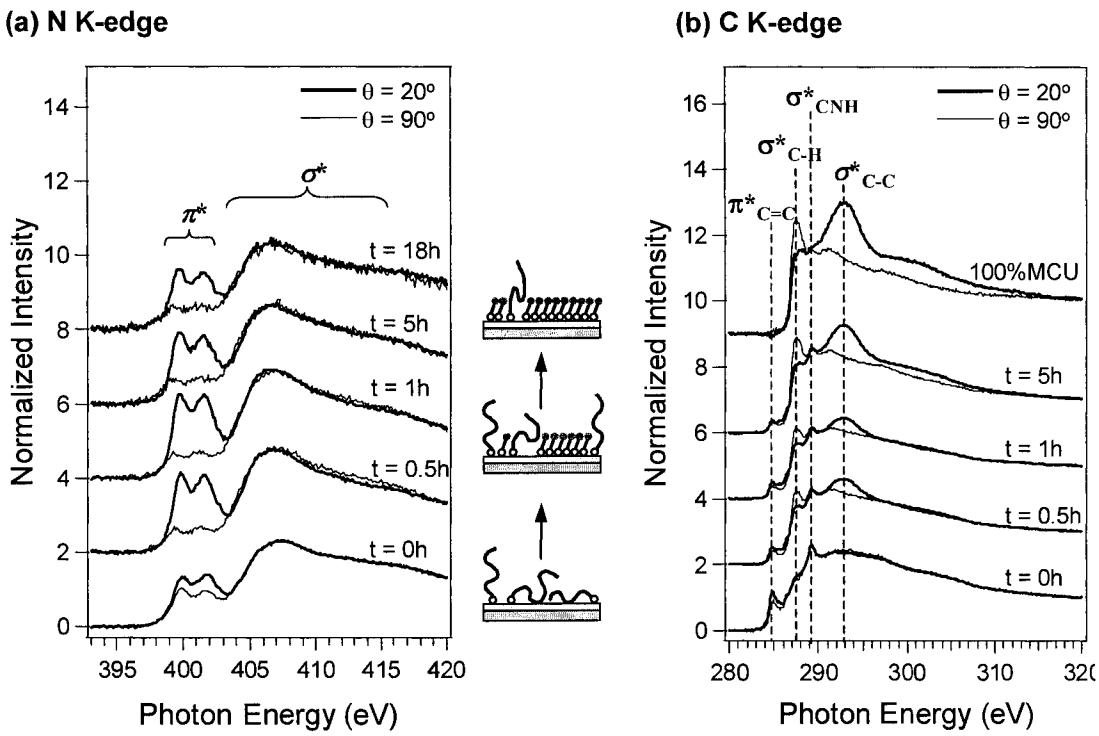

Figure A.2 Nitrogen (a) and carbon (b) K-edge NEXAFS spectra from pure DNA and mixed DNA/MCU monolayers on gold at normal (90°) and glancing (20°) incident X-ray angles (t = MCU backfill time in hours). The increase in polarization dependence of nitrogen K-edge NEXAFS spectra (a) indicates that DNA bases are oriented more parallel to the surface than bases in the pure DNA monolayer, and that ssDNA oligomers reorient on average towards a more upright orientation on the surface upon MCU addition. The decrease in intensity of the $\pi^*_{C=C}$ and σ^*_{C-NH} peaks in the carbon K-edge NEXAFS spectra (b) with longer MCU backfill time is consistent with DNA displacement from the surface. From the polarization dependence of the mixed monolayer spectra (t > 0), MCU alkyl chains orient in an upright position away from the surface. The increase in σ^*_{C-H} and σ^*_{C-C} peak intensities with increasing MCU backfill time is consistent with increasing MCU surface density with prolonged exposure to the DNA monolayer.

polarized X-ray source is nearly perpendicular to the surface; therefore, the overlap of this **E** vector with the aromatic nitrogen bonds that cause the 1s → π^* transition indicates that the DNA bases in a pure DNA film were, on average, oriented parallel to the surface. Similar trends were observed with surface-bound double-stranded DNA oligomers on gold.[25] This indicates that on average the HS-ssDNA chains had a slightly perpendicular

orientation to the substrate. It is believed that the electrostatic repulsive forces between the ssDNA chains may cause the chains to stand on average slightly upright on the surface, although it is likely they remain disordered overall. Upon incorporation of the MCU diluent thiol into the DNA monolayer, this polarization dependence increased significantly (also Figure A.2a, $t \geq 0.5$), indicating that MCU induced changes to the ssDNA oligomers forces some degree of reorientation, on average more towards an upright conformation on the surface, with DNA bases oriented more parallel to the surface. This change in orientation is further evidence that the MCU diluent thiol removes unintended nucleobase amine groups from interactions with the gold surface.

To compare the change in orientation of these DNA monolayers as a function of backfill time, the dichroic ratio, ΔN_{π^*},[29,30]

$$\Delta N_{\pi^*} = \frac{N_{\pi^*, 20^\circ} - N_{\pi^*, 90^\circ}}{N_{\pi^*, 20^\circ} + N_{\pi^*, 90^\circ}}$$

was calculated. These ΔN_{π^*} values are summarized in Figure A.3. Note that the dichroic ratios calculated here are relative and cannot be directly compared to the values from different experimental setups. Comparison of dichroic ratios derived from different experiments requires a correction factor 1/(2P-1), where P is the polarization degree of the synchrotron light.[29,30] ΔN_{π^*} initially increased rapidly with MCU backfill time, reaching a maximum at 0.5 to 1 h. Beyond 1 h of MCU backfill, ΔN_{π^*} began to decrease slightly. All ΔN_{π^*} values for the mixed DNA/MCU monolayers were greater than the ΔN_{π^*} value for the pure HS-ssDNA monolayer, indicating that, on average, the DNA chains in the MCU backfilled surfaces are more perpendicular to the surface than those in pure DNA adlayers. The trend towards ΔN_{π^*} decreasing at longer MCU backfill times

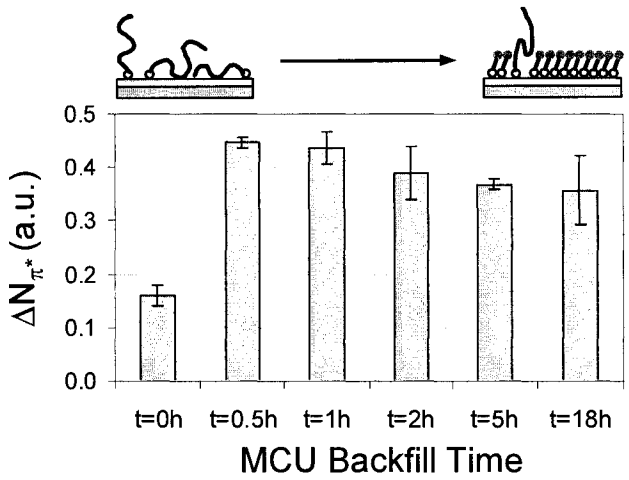

Figure A.3 Dichroic ratio (ΔN_{π^*}) for pure DNA and mixed DNA/MCU monolayers on gold as a function of MCU backfill time. ΔN_{π^*} reaches its maximum at ~0.5 to 1 h of MCU exposure, after which ΔN_{π^*} decreases due to the loss of DNA from surface.

may be due to loss of ssDNA (seen with the XPS results shown above as well as ^{32}P-labeling results in Chapter 3, companion paper[18]). With less DNA on the surface, the electrostatic repulsive interactions between ssDNA chains would be less effective at holding the DNA molecules perpendicular to the surface, permit more disorder among the DNA chains, and facilitate some nucleotide-surface re-engagement. Despite the reduction in N1s nitrogen signal at longer MCU backfill times, ΔN_{π^*} at t = 18 h was still greater than that of the pure HS-ssDNA surface, leading to the conclusion that the change in polarization dependence was due to relative orientational changes in the DNA layer. For MCU-backfilled DNA samples where the greatest polarization dependence was observed for the N 1s $\rightarrow \pi^*$ peaks (i.e., 0.5 to 1 h MCU backfill times), the N 1s $\rightarrow \sigma^*$ peak also showed a slight polarization dependence (Figure A.2a).

NEXAFS Orientation Studies: C K-edge. The C K-edge spectra contained a series of features originating from 1s $\rightarrow \pi^*$ and 1s $\rightarrow \sigma^*$ transitions in organic molecules (see Figure A.2b). The major peaks in the C K-edge NEXAFS spectra were assigned to

functional groups present in HS-ssDNA and MCU using results from previous studies of alkylthiol monolayers, amino acids, and polymers. For example, the peak at 285 eV was assigned to $\pi^*_{C=C}$ species in DNA based on the features found in NEXAFS spectra of polymers[11] and amino acids[31] containing double-bonded and aromatic carbon atoms. Upon addition of MCU diluent thiols to the DNA adlayer surface, the $\pi^*_{C=C}$ peak intensity decreased due to displacement of DNA oligomers by MCU molecules. The peak at ~289 eV was attributed to the π^*_{CNH} peak in DNA, based on previous assignments for amino acids.[31] The π^*_{CNH} peak was also more pronounced in the C K-edge spectra of pure HS-ssDNA than that in mixed DNA/MCU (0 – 18 h MCU backfill) monolayers due to the higher concentration of C-N species in pure DNA, as shown by XPS analysis in the previous section. The peak at 287.4 eV was attributed to a transition to anti-bonding orbitals involving the C-H group.[12,32] With the addition of MCU diluent thiol, this peak was enhanced when the X-ray beam was at normal (90°) incidence to the sample surface, indicating that the C-H bonds in the MCU molecules were oriented nominally parallel to the surface. Meanwhile, the peak at 293 eV, assigned to the C-C species (σ^*_{C-C}),[12,32] was enhanced when the X-rays were at glancing (20°) incidence. This indicates that the C-C σ^* orbital had more of a perpendicular orientation. The polarization dependences of the σ^*_{C-H} and σ^*_{C-H} peaks were similar to those for spectra previously reported for hydrocarbon adlayers[12] and Langmuir-Blodgett films.[32] These results indicate that the MCU alkyl chain is oriented in an upright position away from the surface, further suggesting that the MCU diluent thiol structurally orders the mixed DNA/MCU surface.

Fluorescence Studies of Pure DNA and Mixed DNA/MCU Monolayers. Fluorescence signal intensities of analogous, fluorophore-labeled HS-ssDNA probes on gold were used to study orientation changes in pure DNA and mixed DNA/MCU monolayers on gold of known densities of $1.7x10^{13}$ to $4.4x10^{13}$ probes/cm^2 based on ^{32}P-DNA radio-label work (see Table 3.2 in the Chapter 3, companion paper[18]). Normalized relative fluorescence intensity of surface-bound Cy3-labeled DNA probes as a function of MCU backfilling time is shown in Figure A.4a. Very little fluorescence signal was observed from pure fluorophore HS-ssDNA adlayers when MCU diluent molecules were absent. The DNA planar adlayer arrangement could allow fluorophore lateral self quenching, but this will likely be insignificant when compared to quenching due to Cy3-gold interactions since self quenching does not typically occur until much higher fluorophore densities (molecules/cm^2).[33-35] Tsukanova and coworkers showed that fluorescence quenching from 7-nitro-2-1,3-benzoxadiazol-4-yl (NBD) dye aggregate stacking in compressed dye-lipid monolayers at the air-water interface did not occur at surface density of $1.1x10^{14}$ molecules/cm^2 (0.9nm^2/molecule), but was eventually observed at $2.5x10^{14}$ molecules/cm^2 (0.4nm^2/molecule) upon further lateral monolayer compression and the resulting in-plane molecular ordering.[33] Schmitt, et. al. showed that for two cyanine dyes studied as adsorbed planar films on fatty acid monolayers at the air-water interface, the first evidence for optical transition associated with monomer → dimer → aggregate in-plane in these compressed films occurs between 0.6 and 0.7nm^2 per molecule. This translates to the requirement for dye densities of 1.4 to 1.7 x 10^{14} molecules/cm^2 in these compressed but initially fluid monolayer systems to produce consistent, observable energy transfer effects.[34] These molecular density estimates are an

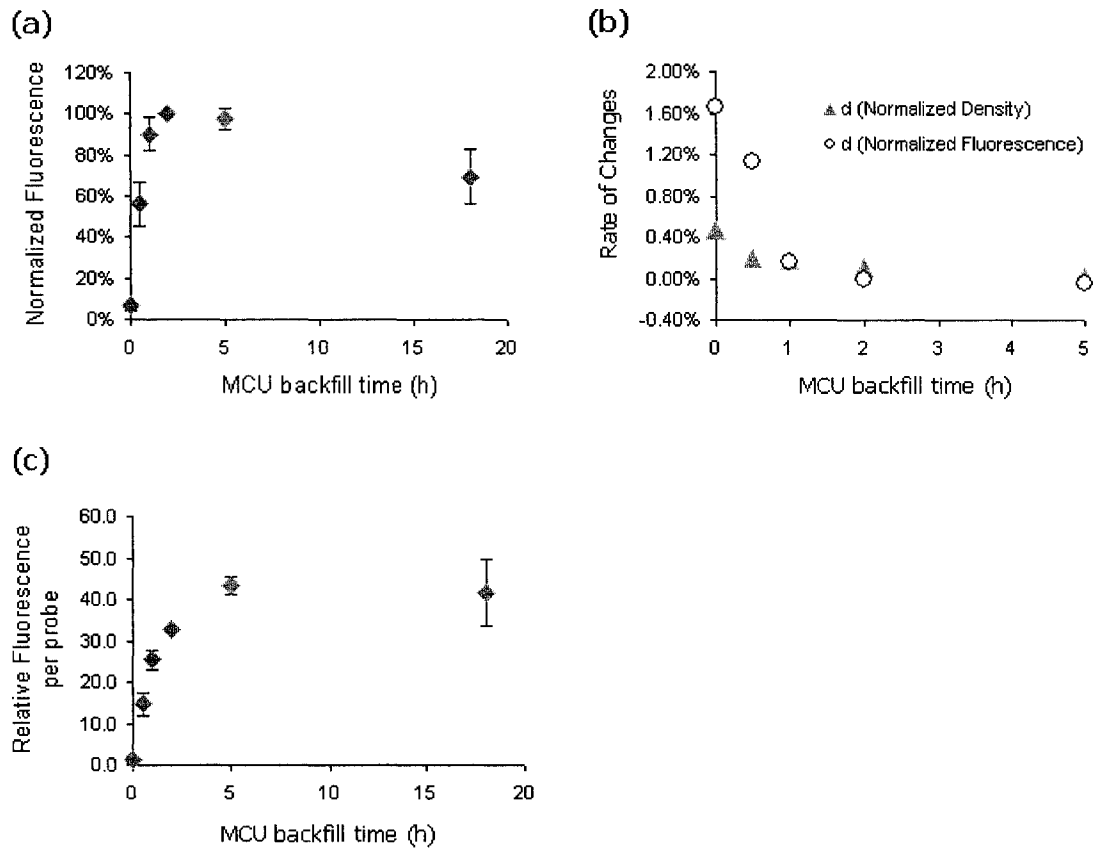

Figure A.4 3'-Thiol-DNA-Cy3-5' 20mer probe surface fluorescence intensity in pure DNA and mixed DNA/MCU adlayers on gold: (a) normalized immobilized DNA fluorescence signal relative to the 2 h MCU backfill data point (100%). Little fluorescence is observed from the pure DNA layer indicating a "lying down" conformation producing Cy3 fluorophore-gold non-radiant quenching without MCU diluent. Relative adlayer DNA-Cy3 fluorescence increases as MCU diluent molecules were incorporated into the adlayer, reaching a maximum at the 2 h MCU backfill condition, then decreasing as additional MCU molecules are assembled into the adlayer, resulting in displacement of DNA-Cy3 from the surface. (b) Rates of change in normalized fluorescence intensity, and normalized DNA surface probe densities (data taken from ^{32}P DNA probe density results in reference 18), are plotted against MCU backfill time. More dramatic rate change is observed for the normalized fluorescence signal, indicating the initial fluorescence intensity increase is a result of change in DNA probe conformation, not surface displacement. (c) Relative fluorescence per probe DNA molecule is derived by dividing the normalized fluorescence signal by corresponding DNA surface probe densities. Fluorescence signal increases dramatically as soon as MCU diluent is introduced into the DNA monolayer, reaching a maximum near 5 h of MCU backfill (density = 2.3×10^{13} probes/cm^2).

order of magnitude greater than the planar immobilized HS-ssDNA Cy3 surface densities produced in this study ($1.7x10^{13}$ to $4.4x10^{13}$ molecules/cm^2), underscoring the limited probability that Cy3-Cy3 quenching is the major cause for the low fluorescence signals observed for the pure DNA monolayers. Cy3 dye quenching is therefore not significant under desiccated, DNA surface-immobilized conditions that limit effective dynamic chain motion, rearrangement or dye mobility (e.g., rotational, translational) within each layer except possibly during MCU diluent addition. Hence, the low fluorescence intensity observed for pure HS-ssDNA adlayers on gold is primarily attributed to the substantial fraction of non-upright probe DNA molecules at these lower surface packing densities. Lack of vertical DNA chain orientation permits sufficient Cy3-gold surface contact as an energy transfer and dye quenching mechanism in these adlayers. This is consistent both with poor fluorescence yield from these surfaces and the relatively poor hybridization efficiency observed for this pure DNA adlayer as well (i.e., Figure 3.3 in Chapter 3, companion paper[18]). Additionally, consistent with both the XPS and NEXAFS results, the DNA fluorescence intensity increases dramatically upon MCU exposure, reflecting alteration of either DNA surface density, or adlayer conformational or orientational changes that remove the terminal Cy3 dye away from the gold, reducing non-radiant energy transfer, increasing signal (Figure A.4b). Importantly, like the NEXAFS results, most of the fluorescence signal increase occurs at relatively short MCU backfill times when only moderate changes in DNA molecular density are occurring (i.e., low displacement). These results indicate that DNA conformational and orientational changes in the layer are the major reason for the observed significant increase in fluorescence signal at short MCU backfill times.

To explicitly test the proposed effect of MCU diluent on the changes of probe DNA orientation and lateral spacing, identical experiments were conducted using 10- and 100-fold diluted Cy3-probe-HS-ssDNA (i.e., diluted with identical thiolated probe DNA lacking a dye label). At a 10-fold dye probe DNA dilution, the identical trend of increasing fluorescence with MCU exposure observed in Figure A.4a for pure dye probe DNA layers was observed for the MCU backfill series, although the absolute fluorescence intensity was reduced by the dilution. At a 100-fold dye probe dilution, fluorescence was indistinguishable from background (dilution data not shown).

Dye self-quenching via fluorescence resonance energy transfer (FRET) is a viable mechanism for decreased fluorescence intensity in high density systems with highly oriented fluorophores.[36] The fluorophore orientational dependence of FRET quenching, as described by the orientation factor, K^2, indicates the significance of fluorophore dipole orientation in efficient energy transfer quenching.[37] However, given the nearly random orientation of the immobilized DNA probes observed in the pure HS-ssDNA monolayer (c.f., NEXAFS evidence), their low lateral densities compared to known fluorophore Förster distance dependence[37,41] shown in other systems,[33-35] and results from the lateral spacing fluorophore dilution experiments, self-quenching is not perceived to be a major cause of the low DNA Cy3 fluorescence intensity emanating from the pure DNA monolayer. Instead, the observed non-linear florescence signal trends with increasing MCU backfill time can be explained by DNA conformational changes produced by MCU adlayer addition that increase the distance between the fluorescent label and the underlying gold substrate. Gold surfaces in close proximity to a fluorophore are well-known to strongly quench fluorescence from excited dipoles, primarily from nonradiative

energy transfer of dye to metal.[38-40] This quenching efficiency decreases as the gold-fluorophore separation distance (Förster distance, generally up to a few nanometers) increases, diminishing to zero beyond this radius.[41] Additionally, orientational effects between proximal fluorophores also contribute to quenching probability within the Förster distance.[42] A fully extended 20mer DNA molecule measures approximately 6-7 nm in length, comparable to the largest effective quenching distance. At highest molecular densities (pure DNA monolayers, 4.4×10^{13} probes/cm^2), average probe-probe separation distance is approximately 1.5 nm, increasing to 2.5 nm as MCU diluent concentration increases. As all of the DNA densities in this study are well-below the value for an ideally close-packed layer[43] (estimated to be 8×10^{13} probes/cm^2, 1.1nm average lateral spacing), fluorophore Cy3 dye labels on 5'-ends of 3'-thiol gold-immobilized DNA molecules have sufficient spacing to reside in close proximity to the substrate gold surface, allowing fluorescence energy transfer resulting in fluorescence quenching of the dye labels. XPS evidence (*vida infra*) also shows some DNA-gold interactions with nucleobases that might also stabilize such interactions. Thus, the lack of fluorescence intensity from the pure DNA monolayer is consistent with an average lying-down conformational tendency of the thiol-DNA on the gold surface at lower surface densities. As MCU backfill molecules increase, the relative adlayer fluorescence increases, reaching a maximum at the 2 h backfill condition, then decreasing as even more MCU molecules are assembled into the adlayer (see Figure A.4a). This relative fluorescence signal observed is a combined result of both fluorophore surface density and the distance between dye and gold substrate. MCU addition to the DNA monolayer initially increases the fluorescence intensity by reorienting the DNA chains to a more

upright configuration, removing the fluorophore from gold quenching interactions, and eventually decreases the fluorescence intensity as MCU displaces DNA molecules from the surface at longer MCU backfill times. This interpretation is consistent with the XPS and NEXAFS data presented above.

Relative fluorescence signal per probe DNA molecule was derived by dividing the normalized fluorescence signal by the corresponding surface DNA probe density derived from ^{32}P measurements on identical systems (from Table 3.2 in Chapter 3, companion paper[18]). As shown in Figure A.4c, a large increase in fluorescence intensity was observed as soon as the diluent MCU molecules were introduced into the adlayer, even at low concentrations (0.5 h MCU backfill), suggesting that adsorbed DNA conformation changes readily under this influence, displacing dye away from the surface as MCU occupies space between probe molecules. In Figure 4c, the normalized fluorescence curve reaches a maximum near 5 h of MCU backfill (corresponding to $2.3x10^{13}$ probes/cm^2 from reference 18). With increased MCU backfill times (1 – 5h), the MCU displaces some of the probe HS-ssDNA from the adlayer as seen by XPS. The small increase in fluorescence intensity in this time period is likely due to the loss of Cy3-Cy3 quenching. Beyond 5 h of MCU backfill, relative fluorescence signal remained constant. Relative rates of change in fluorescence intensity as a function of MCU exposure and loss of probe DNA from the surface as a function of MCU exposure support this interpretation (Figure A.4b).

A.5 Conclusions

In this work, the composition and orientation of mixed self-assembled DNA/MCU monolayers designed for the specific capture of DNA targets have been

characterized in detail using several high-resolution surface analytical methods. XPS results indicate that initially backfill of MCU diluent thiols become incorporated into the unoccupied gold surface sites surrounding the loosely-packed low-density HS-ssDNA surface assembled first. While DNA displacement by MCU is initially slow (vacant site filling preferred), upon extended MCU backfill time, the HS-ssDNA surface coverage steadily decreased. The observed increase in NEXAFS polarization-dependence with MCU diluent addition into DNA monolayers indicates that the immobilized ssDNA oligomers reorient towards a more upright orientation on the surface. MCU addition, yielding a strong thiol-gold bond (XPS evidence) displaces weaker nucleobase nitrogen-gold interactions, producing an overall change in ssDNA chain orientation. The NEXFAS nitrogen polarization dependence reaches a maximum at ~0.5 to 1 h of MCU exposure, beyond which the polarization dependence decreases slightly due to DNA displacement. Despite reduction in HS-ssDNA surface density with longer MCU backfill times, evidence suggests that the upright orientation of remaining ssDNA is generally retained. Fluorescence intensity results show little fluorescence signal in pure fluorophore-labeled DNA monolayers. This is mainly attributed to substantial interactions between DNA oligomers and the gold substrate, resulting in fluorescence quenching of the terminal fluorophore. Addition of MCU surface diluent into the DNA adlayers initially increases the relative fluorescence signal due to MCU-induced reorientation of the DNA and relocation of the terminal fluorophore away from the gold substrate. At longer MCU backfill times fluorescence intensity decreases due to DNA probe displacement from the gold surface and some loss of Cy3-Cy3 interactions. Experimental differences observed in kinetics of maximum HS-ssDNA orientational

changes determined from fluorescence compared to NEXAFS measurements could be explained by the different measurement reporting capabilities of these two methods. NEXAFS measures average bond orientation throughout the oligonucleotide chain ensemble, while fluorescence intensity measurements are simply indicative of the local environment around the fluorophore. In this case, the fluorescence intensity measurements are primarily affected by the position of the end-labeled fluorescent molecule relative to the gold substrate. In the fluorescence measurements, Cy3-gold quenching is rapidly eliminated at short MCU backfill times, in agreement with the NEXAFS results. The Cy3-gold quenching explains the majority of the MCU response detected by fluorescence intensity increase. At longer MCU backfill times, MCU displaces HS-ssDNA chains from the gold substrate, diluting the surface immobilized florescent labeled DNA molecules, thereby reducing the dye-dye interactions in any sub-populations on the surface capable of proximity (within Forster radius) Cy3-Cy3 interactions. Supporting evidence from a different set of methods analyzing identical DNA adlayers in Chapter 3 as a companion paper[18] suggests that immobilized DNA molecular orientations are correlated with their surface densities, and can be changed using MCU diluent addition to affect hybridization efficiencies with complementary target. Hence, full understanding and control of both DNA probe density and orientation on surfaces seems very significant to DNA's capture efficiency and capture assay performance in buffer and complex milieu.

A.6 Acknowledgements

The authors gratefully acknowledge support from NESAC/BIO (NIH Grant No. EB-002027) and also NIH Grant EB-001473. H. Canavan and J.Apte are thanked for

their assistance with discussions and experiments involved in this study. We also thank D. Fischer for his expert technical assistance with the NEXAFS experiments. NEXAFS studies were performed at the NSLS, Brookhaven National Laboratory, which is supported by the U.S. Department of Energy, Division of Materials Science and Division of Chemical Sciences.

A.7 References

(1) Levicky, R.; Horgan, A. *Trends Biotechnol.* **2005**, *23*, 143-149.

(2) Huang, E.; Zhou, F.; Deng, L. *Langmuir* **2000**, *16*, 3272-3280.

(3) Levicky, R.; Herne, T. M.; Tarlov, M. J.; Satija, S. K. *J. Am. Chem. Soc.* **1998**, *120*, 9787-9792.

(4) Herne, T. M.; Tarlov, M. J. *J. Am. Chem. Soc.* **1997**, *119*, 8916-8920.

(5) Peterlinz, K. A.; Georgiadis, R. M.; Herne, T. M.; Tarlov, M. J. *J. Am. Chem. Soc.* **1997**, *119*, 3401-3402.

(6) Moses, S.; Brewer, S. H.; Lowe, L. B.; Lappi, S. E.; Gilvey, L. B. G.; Sauthier, M.; Tenent, R. C.; Feldheim, D. L.; Franzen, S. *Langmuir* **2004**, *20*, 11134-11140.

(7) Petrovykh, D. Y.; Kimura-Suda, H.; Whitman, L. J.; Tarlov, M. J. *J. Am. Chem. Soc.* **2003**, *125*, 5219-5226.

(8) Petrovykh, D. Y.; Kimura-Suda, H.; Tarlov, M. J.; Whitman, L. J. *Langmuir* **2004**, *20*, 429-440.

(9) May, C. J.; Canavan, H. E.; Castner, D. G. *Anal. Chem.* **2004**, *76*, 1114-1122.

(10) Lee, C. Y.; Canavan, H. E.; Gamble, L. J.; Castner, D. G. *Langmuir* **2005**, *21*, 5134-5141.

(11) Stohr, J. *NEXAFS Spectroscopy*; Springer-Verlag: New York, 1992.

(12) Hahner, G.; Kinzler, M.; Thummler, C.; Woll, C.; Grunze, M. *J. Vac. Sci. Technol., A* **1992**, *10*, 2758-2763.

(13) Gamble, L. J.; Ravel, B.; Fischer, D. A.; Castner, D. G. *Langmuir* **2002**, *18*, 2183-2189.

(14) Nagayama, K.; Sei, M.; Mitsumoto, R.; Ito, E.; Araki, T.; Ishii, H.; Ouchi, Y.; Seki, K.; Kondo, K. *J. Electron. Spectrosc. Relat. Phenom.* **1996**, *78*, 375-378.

(15) Ziegler, C.; Schedelniedrig, T.; Beamson, G.; Clark, D. T.; Salaneck, W. R.; Sotobayashi, H.; Bradshaw, A. M. *Langmuir* **1994**, *10*, 4399-4402.

(16) Castner, D. G.; Lewis, K. B.; Fischer, D. A.; Ratner, B. D.; Gland, J. L. *Langmuir* **1993**, *9*, 537-542.

(17) Samuel, N. T.; Lee, C.-Y. L.; Gamble, L. J.; Fisher, D. A.; Castner, D. G. *J. Electron. Spectrosc. Relat. Phenom., submitted.*

(18) Gong, P.; Lee, C.-Y.; Harbers, G. M.; Gamble, L. J.; Grainger, D. W.; Castner, D. G. *Anal. Chem.*,**2006**, *in press*.

(19) Lenhart, J. L.; Jones, R. L.; Lin, E. K.; Soles, C. L.; Wu, W. L.; Fischer, D. A.; Sambasivan, S.; Goldfarb, D. L.; Angelopoulos, M. *J. Vac. Sci. Technol., B* **2002**, *20*, 2920-2926.

(20) Castner, D. G.; Hinds, K.; Grainger, D. W. *Langmuir* **1996**, *12*, 5083-5086.

(21) Fujii, K.; Akamatsu, K.; Yokoya, A. *J. Phys. Chem. B* **2004**, *108*, 8031-8035.

(22) Furukawa, M.; Fujisawa, H.; Katano, S.; Ogasawara, H.; Kim, Y.; Komeda, T.; Nilsson, A.; Kawai, M. *Surf. Sci.* **2003**, *532*, 261-266.

(23) Fujii, K.; Akamatsu, K.; Muramatsu, Y.; Yokoya, A. *Nucl. Instrum. Methods Phys. Res., Sect. B* **2003**, *199*, 249-254.

(24) Kirtley, S. M.; Mullins, O. C.; Chen, J.; Vanelp, J.; George, S. J.; Chen, C. T.; Ohalloran, T.; Cramer, S. P. *Biochim. Biophys. Acta* **1992**, *1132*, 249-254.

(25) Crain, J. N.; Kirakosian, A.; Lin, J. L.; Gu, Y. D.; Shah, R. R.; Abbott, N. L.; Himpsel, F. J. *J. Appl. Phys.* **2001**, *90*, 3291-3295.

(26) Zwahlen, M.; Brovelli, D.; Caseri, W.; Hahner, G. *J. Colloid Interface Sci.* **2002**, *256*, 262-267.

(27) Sakai, T.; Ishikawa, K.; Takezoe, H.; Matsuie, N.; Yamamoto, Y.; Ishii, H.; Ouchi, Y.; Oji, H.; Seki, K. *J. Phys. Chem. B* **2001**, *105*, 9191-9195.

(28) Shard, A. G.; Whittle, J. D.; Beck, A. J.; Brookes, P. N.; Bullett, N. A.; Talib, R. A.; Mistry, A.; Barton, D.; McArthur, S. L. *J. Phys. Chem. B* **2004**, *108*, 12472-12480.

(29) Zharnikov, M.; Ouchi, Y.; Hasegawa, M.; Scholl, A. *J. Phys. Chem. B* **2004**, *108*, 859-863.

(30) Samant, M. G.; Stohr, J.; Brown, H. R.; Russell, T. P.; Sands, J. M.; Kumar, S. K. *Macromol.* **1996**, *29*, 8334-8342.

(31) Kaznacheyev, K.; Osanna, A.; Jacobsen, C.; Plashkevych, O.; Vahtras, O.; Agren, H.; Caravetta, V.; Hitchcock, A. *J. Phys. Chem. A* **2002**, *106*, 3153-3168.

(32) Outka, D. A.; Stohr, J.; Rabe, J. P.; Swalen, J. D. *J. Chem. Phys.* **1988**, *88*, 4076-4087.

(33) Tsukanova, V.; Grainger, D. W.; Salesse, C. *Langmuir* **2002**, *18*, 5539-5550.

(34) Schmitt, F. J.; Meller, P.; Ringsdorf, H.; Knoll, W. *Prog. Colloid & Polym. Sci.* **1990**, *83*, 136-145.

(35) Vranken, N.; Van der Auweraer, M.; De Schryver, F. C.; Lavoie, H.; Salesse, C. *Langmuir* **2002**, *18*, 1641-1648.

(36) Lakowicz, J. R. In *Principles of Fluorescence Spectroscopy*; Kluwer Academic/Plenum: New York, 1999, pp 237-265.

(37) $K^2 = (\cos \theta_t - 3 \cos \theta_D \cos \theta_A)^2$, where θ = the angle between a fluorophore emission dipole and another fluorophore's excitation dipole: K = 0 for orthogonal alignment (no energy transfer), K = 4 for perfectly aligned dipoles (high probability of FRET), and K = 0.667 for random isotropic dye orientation.

(38) Dubertret, B.; Calame, M.; Libchaber, A. J. *Nat. Biotechnol.* **2001**, *19*, 365-370.

(39) Dulkeith, E.; Morteani, A. C.; Niedereichholz, T.; Klar, T. A.; Feldmann, J.; Levi, S. A.; van Veggel, F. C. J. M.; Reinhoudt, D. N.; Moller, M.; Gittins, D. I. *Phys. Rev. Lett.* **2002**, *89*, 203002/203001-203002/203004.

(40) Gryczynski, I.; Malicka, J.; Gryczynski, Z.; Lakowicz, J. R. *J. Phys. Chem. B* **2004**, *108*, 12568-12574.

(41) Chance, R. R.; Prock, A.; Silbey, R. *Adv. Chem. Phys.* **1978**, *37*, 1-65.

(42) http://www.anatomy.usyd.edu.au/mru/fret/abot.html.

(43) Steel, A. B.; Levicky, R. L.; Herne, T. M.; Tarlov, M. J. *Biophys. J.* **2000**, *79*, 975-981.

List of Abbreviations

α- ^{32}P-ddATP	α position ^{32}P-substituted dideoxy-adnosine triphosphate
γ- ^{32}P-ATP	γ position ^{32}P-substituted adnosine triphosphate
a.u.	arbitrary units
BSA	bovine serum albumin
DCC	dicyclohexylcarbodiimide
DNA	deoxyribonucleic acid
cDNA	complementary DNA
ssDNA	single-stranded DNA
dsDNA	double-stranded DNA
DMF	dimethylformamide
EDCI	1-(3-dimethylaminopropyl)-3-ethlcarbodiimide hydrochloride
EDTA	ethylenediaminetetraacetic acid
ELISA	enzyme-linked immunosorbent assay
FBS	fetal bovine serum
FTIR	Fourier transform infrared
HPSF	high purity salt free
MCH	Mercaptohexanol
MCU	mercaptoundecanol
MS	mass spectrometry
NBD	7-nitro-2-1,3-benzoxadiazol-4-yl
NEXAFS	near edge x-ray adsorption fine structure

NHS	N-hydroxy succinimide
NSB	non-specific binding
OEG	oligo ethylene glycol
OWLS	optical waveguide lightmode spectroscopy
PCR	polymerase chain reaction
PEG	polyethylene glycol
PEO	polyethylene oxide
PLL	poly-L-lysine
PMT	photomultiplier tube
RFUs	relative fluorescence units
RIUs	relative intensity units
RP-HPLC	reverse phase – high performance liquid chromotography
SAM	self-assembled monolayer
SDS	sodium dodecyl sulfate
SIMS	secondary ion mass spectrometry
SPR	surface plasmon resonance
SSC	saline sodium citrate
ToF-SIMS	time-of-flight secondary ion mass spectrometry
TE-NaCl	tris-EDTA-sodium chloride (NaCl) buffer
XANES	x-ray absorption near-edge structure
XPS	x-ray photoelectron spectroscopy